

Sexually Dimorphic Impacts of Placental Endocrine Function:  
Unraveling Cerebellar Development and Inflammation Through Allopregnanolone Loss

Jacquelyn Moriya Salzbank

Submitted in partial fulfillment of the  
requirements for the degree of  
Doctor of Philosophy  
under the Executive Committee  
of the Graduate School of Arts and Sciences

COLUMBIA UNIVERSITY

2024

© 2024

Jacquelyn Moriya Salzbank

All Rights Reserved

## Abstract

Sexually Dimorphic Impacts of Placental Endocrine Function:  
Unraveling Cerebellar Development and Inflammation Through Allopregnanolone Loss

Jacquelyn Moriya Salzbank

The placenta plays a vital role in a healthy pregnancy by supporting the intricacies of fetal development. Over 10% of pregnancies experience impaired placental function, resulting in the loss of critical neuroactive steroids the fetal brain cannot yet make, thus leaving them vulnerable to perinatal brain injury and abnormal neurodevelopment. However, this vulnerability is not always equal. Many neurodevelopmental disorders exhibit a sex bias in incidence and severity. I hypothesize that loss of placental support during pregnancy results in sex differences in both behavioral presentation as well as on the cellular and transcriptomic levels. Utilizing the *akr1c14<sup>cyp19a</sup>* KO (plKO) mouse model, which features placenta-specific allopregnanolone (ALLO) knockdown, I investigated the sex specific impact of placental hormones on cerebellar development. Here I show that placental ALLO is essential for cerebellar white matter development and inflammatory regulation via microglial function. Male mice without placental ALLO exhibit signs of placental inflammation, accelerated postnatal myelination, and defects in microglial phagocytosis of excess myelin. Alternatively, females seem to be more resilient with a progressive anti-inflammatory profile across development and reduced myelination. Additionally male plKO show autism-like behaviors such as deficits in social behavior and increased stereotyped behavior. The females do not exhibit this phenotype. My main goals were threefold; to investigate how male and female inflammatory profiles differ and where this difference originates, to investigate how this inflammation impacts microglia and thereby oligodendrocytes,

and how I can alter microglial function in a way to improve pIKO outcomes. Mechanistically, these changes appear to be in part due to baseline sex differences in response to inflammatory stimuli which prime microglia to differentially support the surrounding white matter. Together, this work supports a novel link between placental ALLO loss, microglial function, and sex specific presentation of neurodevelopmental disorders.

## Table of Contents

List of Figures.....	v
Acknowledgments.....	vii
Chapter 1: Introduction .....	1
1.1 Neuroplacentology, the Cerebellum, and Microglial Regulation of Myelination .....	1
1.2 Placenta-Brain Axis.....	3
1.2a Placenta Anatomy and Function.....	3
1.2b Placenta Function and Brain Development.....	4
1.2c Biosynthesis of Neurosteroids.....	6
1.2d Placenta and Neuroactive Steroids .....	10
1.2 Allopregnanolone .....	11
1.2e ALLO and GABA <sub>A</sub> R Signaling.....	11
1.2f ALLO and Myelination .....	14
1.2g ALLO and Inflammation .....	17
1.2h ALLO and Microglia .....	18
1.3 Neurodevelopment and Sex Differences .....	19
1.3a Sources of Sex Differences .....	20
1.3b Microglia and Sex Differences.....	23
1.3c Microglia and Myelination.....	24
1.4 Cerebellum and Prenatal Insult .....	29
1.4a Cerebellar Development.....	29

1.4b Cerebellar Sex Differences .....	32
1.4c Cerebellar Microglia .....	33
Conclusions.....	34
Chapter 2: Materials and Methods.....	37
2.1 Mice.....	37
2.2 Human Samples.....	37
2.3 Drug Injections.....	38
2.4 Mass Spectrometry .....	38
2.4a Steroid extraction.....	39
2.4b GC–MS/MS analysis .....	40
2.5 RNA-sequencing .....	41
2.5a 3' mRNA sequencing .....	41
2.5b Time-Course RNA-sequencing .....	42
2.6 RT-PCR/ Biomark.....	43
2.7 Histology.....	45
2.8 Fluorescence imaging and cell counting.....	46
2.9 Electron Microscopy .....	47
2.9a Sample preparation .....	47
2.9b Image acquisition.....	48
2.9c Myelin thickness measurement .....	48
2.10 Proteins .....	49
2.10a Western Blots .....	49

2.10b Protein extraction and cytokine assay .....	50
2.10c ELISA assays.....	50
2.11 Flow Cytometry.....	51
2.11a Cell Suspension .....	51
2.11b Image Stream.....	52
2.12 Animal behavior .....	53
2.12a Pup ultrasonic vocalizations .....	53
2.12b Spontaneous behavior/ stereotypies.....	53
2.12c Marble Burying.....	53
2.12d Socialization test.....	54
2.12e Autism severity score.....	54
Statistics.....	54
 Chapter 3: Placental endocrine function shapes cerebellar development and social behavior .....	57
Abstract.....	57
Introduction.....	58
Results .....	60
Deletion of <i>Akr1c14</i> in Cyp19+ cells disrupts the production of placental ALLO .....	60
OPC proliferation and differentiation rate diverges in pIKO males and females .....	62
Placental ALLO loss alters postnatal cerebellar myelination.....	66
Placental ALLO insufficiency leads to autism spectrum disorder-like behaviors in males..	69
ASD-like symptom severity correlates with cerebellar MBP level .....	72
Myelin genes show similar sex divergence in preterm infants and pIKO mice.....	73

ALLO or GABA <sub>A</sub> agonist rescues cerebellar and behavioral impairments .....	75
Discussion.....	77
Chapter 4: Microglia Alter Sex-linked Cerebellar Myelination following Placental	
Allopregnanolone Loss .....	80
Abstract.....	80
Introduction.....	81
Results .....	82
Placental ALLO loss alters inflammatory pathways in the postnatal brain .....	82
The pKO cerebellum shows sexually divergent inflammatory profiles across the lifespan	84
Placental inflammatory response to ALLO loss differs by sex. ....	87
pKO mice show sex- and age-specific alterations in cerebellar white matter microglia. ....	89
pKO mice show sex and genotype linked differences in microglial phagocytosis machinery.	
.....	93
Male pKO microglia engulf fewer myelin components. ....	95
Cerebellar PGE <sub>2</sub> contributes to the sex-linked pKO ASD-like behaviors. ....	98
Discussion.....	101
Chapter 5: General Discussion .....	104
Future directions for WM differences in pKO .....	104
Bridging the gap between prenatal insult and postnatal phenotype.....	106
Contribution of sex differences to pKO WM defects .....	107
Teasing out the many roles of ALLO in the developing brain .....	109

References .....	112
Appendix A: Chemical validation of the pIKO model by mass spectrometry .....	128
Appendix B: Molecular validation of the RNA sequencing cutoffs. ....	130
Appendix C: Long-term impact of placental ALLO insufficiency on brain transcriptome: highlight on the myelin-associated genes in the cerebellum .....	132
Appendix D: Appendix D: List of Donors .....	135
Appendix E: Cerebellar WM and behavioral impairments in male pIKO mice can be prevented by pharmacological treatments at E15.5. ....	136
Appendix F: The pIKO brain transcriptome landscape shows dysregulated inflammation-related pathways across postnatal development.....	137
Appendix G: pIKO cytokine panels show sex-specific developmental trajectories .....	138
Appendix H: Postnatal pIKO cerebellum shows transcriptional differences in microglia-enriched genes starting the first week of life .....	140
Appendix I: The contents in myelin-enriched transcripts are altered in the pIKO microglia in a sex-linked manner. ....	141
Appendix J: EP4 agonist treatment does not alter female behaviors.....	142

## **List of Figures**

[Figure 1. Loss of placental support during pregnancy results in sex differences in behavioral presentation and at the cellular and transcriptomic levels.](#)

[Figure 2. Conditional deletion of \*akr1c14\* in \*Cyp19a\*-expressing trophoblasts results in reduced ALLO levels in the fetal brain.](#)

[Figure 3: Oligodendrocyte lineage progression during the postnatal period.](#)

[Figure 4: Placental ALLO insufficiency results in sex-linked cerebellar WM abnormalities at P30.](#)

[Figure 5: Male pIKO mice exhibit ASD-like behavior.](#)

[Figure 6: Myelin proteins are dysregulated in a sex-linked manner in the cerebellar vermis of preterm infants](#)

[Figure 7: ALLO or muscimol administration during late gestation rescues MBP expression and abnormal behaviors in pIKO males at P30](#)

[Figure 8: The postnatal pIKO cerebellum shows a distinct inflammatory signature](#)

[Figure 9: The pIKO cerebellum shows a progressive anti-inflammatory cytokine signature in females but not in males](#)

[Figure 10: Embryonic inflammation is more predominant in male pIKO placentas](#)

[Figure 11: pIKO microglia exhibit sex-linked functional differences in the postnatal cerebellum](#)

[Figure 12: pIKO males exhibit altered cerebellar phagocytosis machinery](#)

[Figure 13: MBP phagocytosis is altered in the pIKO microglia in a sex-linked manner](#)

[Figure 14: Cerebellar PGE2 contributes to the sex-linked pIKO ASD-like behaviors](#)

[\*\*Figure 15: Schematic of how the \*akr1c14\*<sup>cyp19a</sup>KO diverges from normal myelin development due to microglial functional alterations.\*\*](#)

## Acknowledgments

This work was made possible by the incredible scientists I am surrounded by daily. I extend my deepest gratitude to Dr. Anna Penn for her invaluable guidance and mentorship throughout my thesis journey. Her insights and unparalleled expertise in the field of neuroplacentology illuminated new pathways for exploration, challenging me to think critically and innovatively. It was her consistently pushing me to strive for excellence that has profoundly influenced the trajectory of my research, shaping its scope and impact. I am equally thankful to Dr. Claire Marie Vacher, who has been there since the conceptualization of this project, for her invaluable day-to-day assistance and tireless dedication to troubleshooting. Her constant availability and willingness to provide support and act as a sounding board have been indispensable during challenging times. Her perspective led to some of the most interesting experiments; for this and her friendship I am particularly thankful. I would also like to thank my committee, Dr. James Goldman, Dr. Steve Kernie, and Dr. Elizabeth Bradshaw for being my advocates as I transitioned to Columbia, providing personal experimental expertise, and always keeping my project on track.

I must also extend my heartfelt appreciation to my past and present lab mates, Helene Lacaille, Dana Bakalar, Jiaqi O'Reilly, Jenah Gabby, William Yakah and Serena Nencini for their friendship, camaraderie and help throughout the course of this journey which have made all the difference.

I am endlessly thankful to my parents and sister, Robert, Stephanie and Lena Salzbank who have endured countless hours of biology talk and always believed I could do it, even when I didn't. To my Bubbie who always told me to marry a doctor, I decided to just become one myself. Even though you didn't get to see me graduate, I know you would be proud. To my husband and rock, Elliot Brandwein who was with me from the beginning of this journey, moved to New York with

me and always picked me up when I was down. You make everything better. To the baby in my belly, I love you endlessly already. Thank you for the kicks of support when at the bench. I hope by the time you are born I will make you proud.

# Chapter 1: Introduction

## 1.1 Neuroplacentology, the Cerebellum, and Microglial Regulation of Myelination

Discussing placental function in the context of brain development may initially appear unconventional. However, research has established numerous connections between these two vital aspects of fetal development. Neuroplacentology is a burgeoning field, highlighting the pivotal role of the placenta in facilitating optimal brain development [1]. Approximately 10% of pregnancies are marked by disruptions in placental support with diverse origins [2, 3]. These disruptions leave a considerable portion of infants vulnerable to aberrant brain development. Gross structural abnormalities like maternal vascular malperfusion correlates with compromised motor skills, visual perception, and language development [4]. Gestational diabetes is associated with perturbed levels of brain-derived growth factors and altered language development [5]. Moreover, maternal infections, notably chorioamnionitis, contribute to preterm birth and white matter injury [6], while chronic inflammation, as observed in preeclampsia, is linked to heightened severity of developmental disabilities and autism spectrum disorder [7]. Intriguingly, a sex bias is evident in neurodevelopmental disorders following placental disruptions, with males exhibiting a higher incidence and severity compared to females [8]. This observation serves as the foundation for my overarching hypothesis that the loss of placental support during pregnancy results in sex-specific differences not only in behavioral presentation but also at the cellular and transcriptomic levels.

In the following chapters, I utilize the *akr1c14<sup>cyp19a</sup>KO* (pIKO) mouse model, which features placenta-specific allopregnanolone (ALLO) knockdown, to investigate the sex specific impact of placental hormones on cerebellar development [9]. The cerebellum, susceptible to insults during pregnancy due to its protracted developmental timeline, serves as the focal point of investigation. The cerebellum is among the earliest brain regions to initiate development and

remains one of the final regions to reach maturation [10]. Notably, while many cells, including Purkinje cells (the primary inhibitory cells of the cerebellum) and granule cells (the principal excitatory cells), are born embryonically, a substantial portion of their differentiation, migration, and myelination occurs postnatally in mice, predominantly within the first one to two weeks following birth [11]. It is crucial to note that, in the context of this study, the developmental stage of the mouse brain at birth aligns approximately with that of a human brain entering the third trimester of gestation.

Microglia, the resident immune cells of the brain, emerge as a cell type of interest, given the association between pregnancy complications and inflammation [12]. Microglia surveil their microenvironment for disturbances and play a pivotal role in regulating the development of surrounding cell types including oligodendrocyte populations and myelination [13-16]. During normal development, microglia release growth factors like IGF1 and fractalkine to promote oligodendrocyte maturation [17]. However, following inflammation the production of these factors may be altered affecting maturation. Additionally, microglia prune excess oligodendrocytes and myelin via phagocytosis [18]. To set the stage for my own investigations, in this chapter I will review the necessary background information surrounding my central questions, including placenta anatomy and function, the production of neuroactive steroids such as ALLO and its impact of the developing fetal brain. Additionally, sex differences in neurodevelopment and inflammation will be reviewed along with developmental phenotypes specific to the cerebellum.

## **1.2 Placenta-Brain Axis**

Serving as a crucial link between maternal and fetal circulation, the placenta plays a vital role in fostering fetal development by acting as a barrier, facilitating gas and nutrient exchange, removing waste, and supplying essential hormones that coordinate the intricacies of fetal growth. Despite its critical role, more than 10% of pregnancies experience impaired placental function, a factor associated with perinatal brain injury and abnormal neurodevelopment [2, 3]. Deviations in placental support may result from chronic inflammation or maternal infection, or the abrupt premature loss of placental support in preterm birth [19]. While medical advancements have reduced infant mortality following pregnancy complications, the risk of developing neurodevelopmental disorders remains significant. Given that a substantial portion of brain development occurs embryonically, there is a growing need for increased investigation into the regulation of the uterine environment as a contributor to neurodevelopmental disorders.

### **1.2a Placenta Anatomy and Function**

The functional and anatomical aspects of the placenta in humans and mice exhibit notable similarities, yet they also display significant distinctions. Both species feature discoid-shaped placentas with fetal chorions immersed in maternal blood[20-22]. In both human and mouse placentas, there are three primary compartments: the outer layer composed of maternal decidua, followed by the intervillous space in humans or the junctional zone in mice. On the fetal side, the placental villi in humans play a comparable role to the murine labyrinth, serving as the primary site for the exchange of gases, nutrients, and hormones between the maternal and fetal circulations [20, 23].

## **1.2b Placenta Function and Brain Development**

Throughout the years, numerous links have been established between placental function and brain development [24]. Some of the well explored facets of this relationship studied include variations in the gross anatomy and vasculature of the placenta [4, 25], the intricacies of placental function and nutrient delivery [26, 27], and the pivotal role the placenta plays in shielding the fetus from detrimental factors present in maternal circulation [7, 28, 29]. Many of these links were first identified using epidemiological observations. In terms of gross anatomy, one study identified that factors such as villous maturation and maternal vascular malperfusion were significant predictors of lower scores in motor development, visual perception, and language children during the first 40 months of life [4]. Even in studies where no apparent brain lesions or neurologic abnormalities were observed at birth, placental fetal vascular malperfusion was associated with abnormal infant neurodevelopment at 2 years of age [25]. The identification of associations between placental structural abnormalities and fetal brain development has spurred additional research into various other aspects of placental functions and their potential impact on neurodevelopmental outcomes.

One well-explored facet of placenta-brain axis is the significant impact of nutrition on fetal programming. Disruptions in maternal nutrition can have lasting consequences, including high maternal weight resulting in increased susceptibility to anxiety, depression and communicative disorders [26]. Gestational diabetes and maternal blood glucose levels have been linked to altered neuronal activity during attentional tasks in early life [27], as well as lower levels of brain derived neurotrophic factor (BDNF) and altered language development [5]. Forms of placental dysfunction such as preeclampsia have also been linked to neurodevelopmental disorders such as autism spectrum disorder (ASD)[28]. One population study called the Childhood Autism Risk from Genetics and the Environment assessed children between 24 to 60 months to determine whether

preeclampsia and placental insufficiency was associated with ASD and developmental disability. They found that children with ASD were twice as likely to have been born to mothers who had preeclampsia. Moreover, placental insufficiency was cited to account for the increase in developmental disability risk of pregnancies with severe preeclampsia [7].

Placental inflammation is extensively studied as a mediator of neurodevelopmental outcomes [3, 7, 28, 29]. However, since not all instances of prenatal infections result in neurodevelopmental disorders, the hypothesis has evolved towards a "priming" effect, suggesting that these early exposures may predispose the developing brain to subsequent insults that may arise throughout the course of development [30]. Neuroinflammation emerges as a defining characteristic of perinatal brain injury (PBI), encompassing conditions related to neonatal encephalopathy, perinatal stroke, prematurity, or maternal immune activation (MIA) [6, 31, 32]. The placenta plays a crucial role in regulating the intrauterine immunological state throughout pregnancy, ensuring a delicate balance between an active immune response against potential intrauterine infections and immunosuppression. There are three main mechanisms by which inflammation during pregnancy may lead to neurodevelopmental disorders. Either maternal immune factors cross through the placenta to directly impact the fetal brain, maternal immune factors impact placental function, thereby causing downstream effects in the fetal brain, or factors directly produced by the placenta interact with the fetal brain.

Both acute and chronic inflammatory insults can result in the production of inflammatory agents such as cytokines and chemokines, that rise and circulate in maternal blood. One study focuses on the indirect mechanism by which MIA can impact fetal development. Maternal treatment with a viral mimic, synthetic double-stranded RNA polyinosinic:polycytidylic acid (poly(I:C)), induces an increase in maternally derived IL-6 in the placenta specifically activating

the JAK/STAT3 pathway in spongiotrophoblasts. Offspring were behaviorally tested and exhibited autism spectrum disorder (ASD) and schizophrenia-like behaviors such as decreased pre-pulse inhibition, latent inhibition, and increased anxiety [33]. These studies raise the question as to whether maternal cytokines cross the placenta. Radiolabeled IL-2 administered to pregnant dams crossed the placenta and entered fetal tissues inducing accelerated T cell development and altered neurobehavior such as grooming and motor learning [34]. However, these results are not consistent between cytokines as maternally administered radiolabeled TNF $\alpha$  is mostly found sequestered within the placenta with negligible transfer to the fetus [35]. Studies in humans have shown similar inconsistencies. In *ex vivo* isolated cotyledon human placental perfusion model with cytokines introduced into either maternal or fetal circulations, minimal transfer of TNF $\alpha$  and IL-1 $\alpha$  between maternal and fetal compartments, but a bidirectional flow of IL-6 were demonstrated [36]. These studies suggest the possibility of some maternal immune factors crossing through the placenta to directly impact the fetal brain. In summary, the diverse evidence presented highlights the pivotal role of the placenta in influencing neurodevelopmental outcomes, underscoring its significance as a dynamic interface between maternal factors and fetal brain development.

### **1.2c Biosynthesis of Neurosteroids**

The placenta's significance extends beyond its conventional role as a conduit for nutrient and growth factor exchange; often overlooked is its role in hormone production, capable of synthesizing its own factors, adding another layer to its influence on fetal brain development. As an endocrine organ, the placenta is often called the "third brain," as it assumes the role of producing crucial factors that a mature brain would normally generate independently, but the fetal brain is too immature to produce on its own [37]. The brain is a unique steroidogenic organ capable of endogenously synthesizing steroids with a diverse array of functions. This was confirmed first in

the 1980's with Baulieu's study demonstrating that even after the removal of both gonads and adrenals from laboratory animals, steroids such as dehydroepiandrosterone (DHEA) remained abundant in circulation [38]. In years since, there has been further investigation into the genetic encoding of steroidogenic enzymes in a wide range of cell types in the central nervous system in a region-specific and developmentally appropriate way. These steroids produced by the brain have come to be known as neurosteroids. Neuroactive steroids, may be produced by other organs but are capable of impacting neural activity [39].

Neurosteroids are endogenous regulators of neuronal excitability and are distinct from classic steroids in that they do not act on nuclear receptors but rather by binding to non-genomic targets such as ion gated neurotransmitter receptors [40, 41]. They can be classified into three major groups including pregnane (allopregnanolone, pregnanolone, THDOC, tetrahydro-deoxycorticosterone), androstane (androstaniaol, etiocholanone) and sulfated (PS and DHEAS)[42]. Studies have shown these compounds can modulate everything from GABA receptors, NMDA receptors, acetylcholine receptors and voltage activated Ca<sup>++</sup> channels [41-43]. With such a wide range of targets, neurosteroids can exert extensive control and regulation of development, neuronal excitability and behavior. The following section aims to summarize the biosynthetic pathway of neurosteroid production, the major cell types where these factors are produced, and how the brain can utilize external sources of neurosteroids.

The classic biosynthetic pathway for synthesizing steroids begins with the conversion of cholesterol, a crucial precursor molecule, into various steroid hormones through a series of enzymatic reactions. Neurosteroids are no exception, with cholesterol either made *de novo* or converted from low-density lipoproteins (LDL) after its uptake to the lysosomes [40, 44, 45]. Free cholesterol is then shuttled across the mitochondrial membrane primarily by steroidogenic acute

regulatory protein (StAR). Two classes of enzymes, cytochrome P450 or non-P450 complete further biosynthesis of neurosteroids. P450 enzymes are encoded by single genes but can be used to achieve multiple enzymatic reactions such as the first committed step of steroidogenesis with P450<sub>scc</sub> (CYP11A1) transforming cholesterol into pregnenolone through a sequence of three chemical reactions. CYP11A1 along with other CYP enzymes such as CYP17A1, CYP19A1, and CYP21A2 catalyze hydroxylation and cleavage of steroids [46]. Multiple genes, each with a specific enzymatic function, encode the non-P450 enzymes such as 3 $\beta$  hydroxysteroid dehydrogenase (3 $\beta$ HSD), 17 $\beta$  hydroxysteroid dehydrogenase (17 $\beta$ HSD), and 3 $\alpha$  hydroxysteroid dehydrogenase (3 $\alpha$ HSD). These enzymes mainly play a role in the oxidation and reduction of steroid hormones[46].

The profile of neurosteroids synthesized is intricately regulated by the specific combination of synthesizing enzymes expressed in diverse cell types. Within the brain, both neurons and glia contribute to neurosteroid production through the expression of P450<sub>scc</sub>, facilitating the conversion of cholesterol into pregnenolone and subsequently progesterone[47-50]. Further enzymatic actions, including those of 5 $\alpha$ -reductase (5 $\alpha$ -R) and 3 $\alpha$ -hydroxysteroid dehydrogenase (3 $\alpha$ -HSD), enable the reduction of progesterone into its metabolites, dihydroprogesterone (DHP) and tetrahydroprogesterone (THP) [51]. Notably, the expression of 5 $\alpha$ -R and 3 $\alpha$ -HSD is widespread throughout the brain, encompassing regions such as the cerebral cortex, hippocampus, striatum, and cerebellum[52]. Conversely, although P450<sub>scc</sub> mRNA is expressed across the brain, other enzymes such as P450<sub>c11b</sub> and P450<sub>c11AS</sub> are expressed in the adrenals only, making them the primary producers of glucocorticoid and mineralocorticoid production [53]. Neurosteroid production is not only dictated by cell type but also by developmental stage. For instance, oligodendrocyte progenitors exhibit elevated THP levels, which diminish with differentiation,

while DHP concentrations increase with maturation [54]. This intricate interplay of enzymes underscores the nuanced regulation of neurosteroid synthesis across various cell types, brain regions, and developmental stages.

The intricacies of neurosteroid biosynthesis in the brain surpass *de novo* production, given the lipophilic nature of steroids, enabling them to effortlessly traverse the blood-brain barrier. Consequently, steroids produced exogenously can be extracted from circulation and further transformed by the brain into additional neurosteroid derivatives [42]. Hormones originating from ovarian, testicular, and adrenal production, such as progesterone, 11-deoxycorticosterone (DOC), or testosterone, can be drawn from circulation and converted into neuroactive steroids like  $3\alpha,5\alpha$ -tetrahydroprogesterone (allopregnanolone) and  $3\alpha,5\alpha$ -tetrahydroDOC (THDOC). Numerous cells expressing  $5\alpha$ -reductase ( $5\alpha$ -R) and  $3\alpha$ -hydroxysteroid dehydrogenase ( $3\alpha$ -HSD) contribute to this conversion process [40]. This may be a beneficial process for certain hormones to help govern target tissues affected by these steroids by promoting local synthesis over systemic production. This is particularly relevant with the local synthesis of estrogens in the male rodent brain preventing the substantial feminizing effects that would ensue from heightened peripheral production [55]. Both estrogens and androgens are essential for modulating male circuitry and behavior in various vertebrates despite the low levels detectable in the male bloodstream. Testosterone and other androgens can be pulled from the bloodstream and converted into estrogen steroids by aromatase expressing cells to regulate specific neural processes and behaviors [55, 56]. Thus, it is important to consider the contribution of peripheral steroidogenic tissues to the production of neurosteroids as well.

## 1.2d Placenta and Neuroactive Steroids

In its role as an endocrine organ, the placenta is a major peripheral source of neuroactive steroids that have the capacity to pass through the fetal blood brain barrier and regulate the developing fetal brain. Additionally, many maternally produced steroid hormones have the capacity to pass through the placenta and enter fetal circulation [57]. The junctional zone composed of glycogen cells, spongiotrophoblast cells and trophoblast giant cells forms the major endocrine producing compartment of the mouse placenta. In the human placenta this is achieved by the syncytiotrophoblasts of the intervillous space [21, 58]. The two major classes of hormones produced by the placenta with neurological impact are both steroid and peptide hormones. Of particular interest to the current discussion are the production of neuroactive steroids such as estrogens and progestins which derive from precursors from both maternal and fetal circulation [57]. Unlike the brain, the placenta notably lacks StAR, so an alternative mechanism involving STARD3 and HSP60 has more recently been proposed for transportation of cholesterol into the placenta [59, 60].

The placenta, like other steroidogenic organs, expresses P450<sub>scc</sub> (Cyp11a1), a crucial enzyme responsible for the rate-limiting step of hydroxylating cholesterol into pregnenolone [61]. What distinguishes the placenta from other endocrine glands are unique isoforms, including 3 $\beta$ -hydroxysteroid dehydrogenase (3 $\beta$ -HSD), capable of converting pregnenolone to progesterone [62]. Leveraging progesterone, the placenta produces various active progesterone metabolites, facilitated by enzymes like 5 $\alpha$ -Reductase (yielding 5 $\alpha$ -dihydroprogesterone) [63] and 5 $\beta$ -Reductase (resulting in 5 $\beta$ -dihydroprogesterone) [64]. Moreover, the placenta employs 3 $\alpha$ -hydroxysteroid dehydrogenase (3 $\alpha$ -HSD) or 3 $\beta$ -HSD to synthesize allopregnanolone (ALLO; 3 $\alpha$ ,5 $\alpha$ -THP), pregnanolone (3 $\alpha$ ,5 $\beta$ -THP), epiallopregnanolone (3 $\beta$ ,5 $\alpha$ -THP), or epipregnanolone

(3 $\beta$ ,5 $\beta$ -THP) [45]. Among progesterone derivatives, several neuroactive metabolites are synthesized by the placenta, exhibiting similar properties in modulating GABA type A receptors (GABA<sub>A</sub>Rs) [43]. Allopregnanolone (ALLO), the most potent of these steroids, has been extensively characterized and studied [43]. Significantly, ALLO does not bind to progesterone receptors, [65] emphasizing that its primary mechanism of action involves the direct modulation of GABA<sub>A</sub> receptors and the downstream consequences thereof.

## **1.2 Allopregnanolone**

ALLO is a potent allosteric modulator of the GABA<sub>A</sub> receptor (GABA<sub>A</sub>R) with several key facets regulating their intricate relationship. Extensive research has been devoted to unraveling the mechanisms by which ALLO imparts its influence on GABA<sub>A</sub>R, offering insights into the intricate molecular interactions [66]. Moreover, the following section will focus on the dynamic changes occurring in the pentameric structure of the GABA<sub>A</sub>R, leading to significant shifts in channel kinetics under the influence of ALLO. Finally, an exploration of the developmental changes of GABA<sub>A</sub>Rs will be reviewed, unraveling the intricate changes that unfold across different stages of development. These topics will summarize the pivotal aspects to understanding the complex relationship between ALLO and the GABA<sub>A</sub>R and thereby its control over these neural processes.

### **1.2e ALLO and GABA<sub>A</sub>R Signaling**

The molecular structure of the GABA<sub>A</sub>R regulates its activity as well as its interaction with allosteric modulators. GABA<sub>A</sub>Rs are pentameric ligand gated receptors that, upon binding of GABA, undergo a conformational change, allowing for the diffusion of chloride [66]. The pentameric structure can consist of any of eight different classes of subunits, each permutation conferring unique properties and channel kinetics [67, 68]. The type of subunit composition plays

a pivotal role in determining whether the receptor mediates phasic or tonic inhibition. Phasic inhibition is typically mediated by subunits with a low affinity for GABA, leading to a more rapidly desensitizing conductance. In contrast, tonic inhibition is generally facilitated by subunits with a high affinity for GABA, resulting in a more sustained GABAergic conductance.  $2\alpha2\beta\delta$  type composition characteristic of extra-synaptic GABA<sub>A</sub>Rs mediate tonic inhibition because of the strong affinity of the delta subunit for GABA's structure. Post-synaptic GABA<sub>A</sub>Rs mediate phasic inhibition with their lower affinity for GABA from their  $2\alpha2\beta\gamma$  subunits [69]. This is yet another way the subunit composition highly impacts receptor kinetics and neuronal activity.

Certain subunits exhibit varying expression patterns across developmental stages and are frequently more pronounced in specific brain regions. The  $\alpha6$  subunit is expressed only in the cerebellum while the  $\rho$  subunit is predominantly seen in the retina [70]. Laser microdissection and PCR to assess postnatal changes in GABA<sub>A</sub>R subunit expression of layer 3 pyramidal cells in monkey prefrontal cortex revealed that some subunits like  $\alpha1$  increase across development while  $\alpha2$  decreases [71]. Additionally the composition of the GABA<sub>A</sub>R subunits can rapidly change in response to physiological stimuli or pharmacological treatments. For example, chronic stress exposure has been shown to increase the expression of the  $\beta$  subunits in the hippocampus [72] while a mouse model of temporal lobe epilepsy resulted in a decrease in the  $\delta$  subunit [73]. Pharmacological treatments, including the administration of ALLO can also result in altered expression of GABA<sub>A</sub>R subunit composition. In studying the development of acute tolerance to ALLO, *in situ* hybridization showed a decrease in the  $\alpha4$  subunit in the thalamus following extended ALLO exposure [74]. Bilateral intra-hippocampal ALLO administration resulted in an increase in the  $\gamma2$  subunit expression and antidepressant-like effect [75]. These studies together

highlight the dynamic expression of the GABA<sub>A</sub>R subunits across development, brain region and experimental conditions and their impact on GABAergic circuit function.

ALLO exerts its function on the GABA<sub>A</sub>R by binding to an allosteric site, extending the decay time, allowing the channel to remain open longer, and fundamentally changing the electrophysiological characteristics of normal GABAergic transmission. Notably, this site is distinct from the classic benzodiazepine and barbiturate allosteric site [41, 43]. Cryo-electron microscopy to better understand GABA<sub>A</sub>Rs modulation and binding interactions with ALLO revealed this allosteric site can be narrowed down to the  $\beta$ 2- $\alpha$ 1 subunit interfaces, near the base of the four transmembrane  $\alpha$ -helices comprising the channel [76]. With the ability to activate both post-synaptic and extra-synaptic GABA<sub>A</sub>R, ALLO has the ability to enhance both the tonic and phasic inhibition of GABA [77]. There is substantial evidence indicating that ALLO exhibits a preference for receptors containing the delta subunit, implying its role in enhancing tonic currents [77]. A study utilizing mice lacking the  $\delta$  subunit demonstrated a notable reduction in the sensitivity to neuroactive steroids. Electrophysiological recordings from hippocampal slices revealed a significantly accelerated decay time of miniature inhibitory postsynaptic currents in the absence of the  $\delta$  subunit [78]. Through these mechanisms and its allosteric binding site, ALLO exhibits the ability to diversely alter the electrophysiological characteristics of GABAergic transmission.

While GABAergic synapses are traditionally recognized as the primary inhibitory components of the nervous system, numerous studies propose that during early development, GABA functions to maintain excitatory neurotransmission. As a ligand gated Cl<sup>-</sup> channel, GABA<sub>A</sub>Rs are significantly influenced by developmental changes in intracellular chloride concentration ([Cl<sup>-</sup>]<sub>i</sub>) In intracellular recordings of rabbit hippocampal CA1 pyramidal neurons, a

progressive negative shift in GABA's reversal potential during neuronal maturation [79] is attributed to the high  $[Cl^-]_i$  characteristic of immature neurons. Thus when GABA<sub>A</sub>Rs are activated, Cl<sup>-</sup> passively effluxes and the neuron is depolarized. GABA<sub>A</sub>R activation in the early rodent hippocampus, hypothalamus, neocortex and cerebellum also produced depolarizing currents [80].  $[Cl^-]_i$  is regulated by the dynamic expression of two crucial ion channels, NKCC1 and KCC2, which functionally oppose each other. During early development, NKCC1 expression facilitates Cl<sup>-</sup> influx causing an increase in  $[Cl^-]_i$ . As the brain matures, KCC2 expression rises promoting Cl<sup>-</sup> extrusion, and reducing  $[Cl^-]_i$  [81]. The low  $[Cl^-]_i$  results in passive influx upon GABA<sub>A</sub>R activation and hyperpolarization. In situ hybridization showed NKCC1 was expressed in neurons in the cortical plate where expression levels peaked by the third postnatal week. Alternatively, KCC2's time course of expression began around birth and increased dramatically after the first postnatal week [82]. In situ hybridization showed NKCC1 expression in cortical plate neurons peaked by the third postnatal week while KCC2 expression began around birth and increased dramatically after the first postnatal week [82]. Functionally this suggests that low  $[Cl^-]$  results in inhibitory GABA mediated synaptic transmission while high  $[Cl^-]$  results in GABA mediated excitatory transmission. The functional implications of ALLO during development are highly dependent on the GABA excitatory-inhibitory switch and the role GABAergic circuitry plays in the fetal brain.

### **1.2f ALLO and Myelination**

A growing body of evidence underscores the pivotal role of ALLO as a regulator in diverse neurodevelopmental processes, influencing cell proliferation and survival, and oligodendrocyte (OL) lineage progression [65, 83]. During the prenatal period in mice, reduced placental ALLO

leads to increased proliferation of OL precursor cells (OPCs) in both sexes due to diminished GABAA-R signaling [9, 84]. Indeed, GABA regulates oligodendrocyte differentiation in organotypic cerebral cortex slices from early postnatal mice [84]. In early postnatal mice, ALLO induces the proliferation of early OPCs, aligning with peak ALLO production during critical windows of OPC proliferation in late gestation [65, 85, 86]. However, ALLO not only plays a role in promoting oligodendrocyte (OL) proliferation and differentiation during development but also serves as a regulator of OL lineage in disease models. In patients with multiple sclerosis (MS), the suppression of neurosteroid biosynthetic machinery leads to lower levels of ALLO. This study reports that treating OLs with ALLO enhances the expression of maturation markers, indicating that reduced ALLO levels may contribute to the impaired OPC differentiation observed in MS [87]. Furthermore, the administration of ALLO significantly increased Olig2-positive cells in the corpus callosum of 3xTgAD mice. This effect was accompanied by elevated expression of insulin-like growth factor 1 (IGF-1) and its receptor, suggesting a potential role for these factors in ALLO's promotion of oligodendrocyte proliferation [88].

In the adult brain, ALLO enhances GABAergic inhibition, resulting in sedative, anxiolytic, anesthetic, and anticonvulsant effects [89, 90]. As OLs mature, ALLO plays a crucial role in promoting myelination by increasing the production of myelin basic protein (MBP) [91]. In a guinea pig model of prenatal stress, myelin deficits were alleviated by boosting neurosteroidogenic capacity within the first week of life [92]. Additionally, the administration of Ganaxolone, an analog of ALLO, led to increased myelination in the hippocampus and adjacent subcortical white matter in prematurely born guinea pigs [93]. Experimental studies, such as those involving 3xTgAD mice, demonstrate that ALLO administration increases the presence of 2', 3'-cyclic nucleotide 3'-phosphodiesterase (CNPase), a marker for mature, myelinating oligodendrocytes

[94]. In a neurodegenerative disease model of Niemann-Pick C disease, even a single postnatal injection of ALLO is sufficient to promote myelination [95]. The impact of ALLO on myelination is not only restricted to the central nervous system. In the peripheral nervous system, glycoprotein zero, and peripheral myelin protein 22 (PMP22) was increased in adult male rat sciatic nerve and Schwann cell culture by ALLO treatment. Both proteins play an important role in myelin maintenance [96, 97]. These collective findings underscore the pivotal role of ALLO in oligodendrocyte maturation, emphasizing its significant implications for the myelination process.

In our own previous work, [9] we have extensively investigated the role of placental ALLO on OL lineage progression and myelination. In our study involving a placental-specific knock-out of ALLO production, we observed sex-divergent OL lineage progression in the postnatal cerebellum, characterized by increased maturation in males and decreased maturation in females. By 15 days postnatal, placental knock-out males showed an acceleration in maturation from PDGFR $\alpha$ + OPCs to mature CC1+ OLs. The females showed a reduction in CC1+/Olig2+ ratio. This phenomenon is continued at P30 with males showing a significant increase in the density of OL lineage cells (Olig2+) and mature OLs (CC1+). Placental ALLO loss also significantly affected cerebellar myelination, resulting in elevated levels of myelin basic protein (MBP), myelin-associated glycoprotein (MAG), and myelin oligodendrocyte glycoprotein (MOG) in males, accompanied by thicker myelin. Conversely, females exhibited thinner myelin after placental ALLO loss. Strikingly, these defects were associated with male-specific autism-like behaviors, including reduced sociability and stereotyped behaviors. Treatment with ALLO or muscimol, a GABA<sub>A</sub>R agonist, in pregnant dams effectively rescued both cellular and behavioral defects, underscoring the role of GABA<sub>A</sub>R signaling in ALLO's influence on myelin [9].

## 1.2g ALLO and Inflammation

Traditionally, ALLO's extensively studied mode of action primarily revolves around its function as an allosteric modulator of the GABA-A receptor. Nevertheless, ALLO has maintained a long-standing association with neuroprotection and its anti-inflammatory properties. What has recently gained prominence is the exploration of alternative mechanisms underlying ALLO's activity, which may offer insights into its anti-inflammatory effects. In its role as a steroid, ALLO may also provide neuroprotection by acting as a non-glucocorticoid anti-inflammatory agent. Following traumatic brain injury, ALLO treatment reduces proinflammatory cytokines allowing for a more functional recovery [98]. In a model of middle cerebral artery occlusion in rats, ALLO was shown to successfully reduce infarct volume following cerebral ischemia [99]. Moreover, ALLO treatment not only improves neuropathology but also improves neurobehavioral outcomes as well. ALLO treatment promoted spatial learning ability in parallel with reduced neuronal loss after prefrontal cortex contusions [100]. Treatment with ALLO has also been beneficial in animal models of multiple sclerosis where it reduced inflammation together with neurobehavioral deficits [87].

Given that various conditions such as ischemia, traumatic brain injury, and multiple sclerosis involve proinflammatory signaling through Toll-Like Receptors (TLR), recent research has centered on exploring these receptors as a potential mechanism underlying the anti-inflammatory effects of ALLO. Using monocytes/macrophages (RAW264.7), one study demonstrated that ALLO significantly inhibited LPS-induced TLR4 signaling by blocking TLR4/MD-2 protein interactions. *In vivo* in the ventral tegmental area (VTA) of rats, ALLO reduced TLR4 binding to GABA<sub>A</sub>R  $\alpha$ 2 subunits and MyD88 [101]. Follow up experiments on other TLRs revealed that ALLO acts on the binding of MyD88 specifically to inhibit the

production of downstream pro-inflammatory mediators but not TRIF dependent TLRs. This includes TLR2,4 and 7 to reduce mediators such as TNF $\alpha$ , MCP-1 and IP-10 [102]. Interestingly, in human donor macrophages, ALLO's inhibition of TLR4 activation is observed in both male and female donors but its inhibition of TLR7 signals is specific to female donors. Together, these findings suggest a clear mechanism for ALLO's anti-inflammatory properties, highlighting its role in modulating immune responses [103].

## **1.2h ALLO and Microglia**

Despite a clear association between ALLO and inflammation and recognizing microglia as the principal immune-competent cells of the brain, there are still very few studies investigating the direct impact of ALLO on microglia. Existing research primarily focuses on the expression of GABA-A receptors on microglia and the modulation of inflammatory mediators. For instance, the microglial BV2 cell line showed a decrease in nitric oxide (NO) production following LPS stimulation after treatment with progesterone or ALLO [104]. Similarly, another study shows the normal production of inflammatory mediators following LPS stimulation of microglia was reduced when treated with muscimol, GABA-AR agonist [105]. More recently, ALLO treatment of murine microglial BV-2 cells and primary microglia, has been shown to reduce microglial motility and promote elongation of processes. Additionally, ALLO modulates the phagocytic activity of reactive microglia and inhibits the inappropriate phagocytosis of oligodendrocytes [106]. Interestingly, the administration of bicuculline, a competitive antagonist of the GABA-AR was able to block the elongation of process elongation but had no effect on phagocytosis [106]. This suggests that additional mechanisms for ALLO's modulation of microglia remain to be investigated.

### **1.3 Neurodevelopment and Sex Differences**

Numerous neurodevelopmental and neurodegenerative disorders exhibit a sex bias in both incidence and severity, underscoring inherent distinctions in critical neurodevelopmental processes between males and females [8]. These processes encompass neural cell genesis, death, migration, axon guidance, synaptogenesis, and myelination. While various neurodevelopmental disorders, including autism spectrum disorders, attention deficit hyperactivity disorder, and schizophrenia, display a predominant male bias, the precise factors rendering males more susceptible remain elusive. Some propose that sex hormones may underlie these differences, as evidenced by a study linking elevated fetal testosterone levels to diminished functional connectivity within social brain default mode networks, specifically in males [107]. Furthermore, the androgen, dihydrotestosterone (DHT) was found to disrupt the expression of genes associated with syndromic causes of autism and intellectual disability, particularly those influencing the excitation-inhibition (E/I) balance [107]. Similarly, an examination of female sex hormones in amniotic fluid from the Danish Historic Birth Cohort identified oestradiol, oestrone, and progesterone as having significant effects on autism likelihood [108]. These studies suggest that innate factors contributing to brain sexualization may mechanistically influence neurodevelopmental trajectory towards autistic features, offering insights into the observed sex bias.

Given that the placenta intricately regulates the development of specific brain structures through the release of neuroactive factors that target specific circuits and cells, exploring the role of the placenta could be a promising avenue when investigating sex differences in neurodevelopmental disorders. To probe the potential link between sex differences in placental

function and postnatal autistic traits, a study examined angiogenesis-related markers and placental growth factors in maternal plasma alongside the assessment of autistic traits in children. The findings revealed a higher rate of Placental Growth Factor (PIGF) increase associated not only with male sex but also with a greater number of autistic traits in the general population [109]. Another study with the same goal investigated both rare genetic variants linked to ASD and neurodevelopmental disorders and more common genetic variants. The analysis revealed a notable enrichment of autism-related genes within the set of genes exhibiting differential expression between male and female placentas. Particularly significant was the enrichment of X-linked autism genes observed in male-biased placental genes. Additionally, the study identified a connection between more common genetic variants and the regulation of traits related to steroids [110]. These insights underscore an intrinsic connection between factors mediating physiological sex differences and autism, further emphasizing the crucial role of the placenta in shaping neurodevelopmental outcomes.

### **1.3a Sources of Sex Differences**

There are several sources of sex differences throughout development including chromosomal, genetic, epigenetic, and hormonal. More extensively studied, perhaps due to experimental feasibility is the effect of hormones on sexual differentiation. Sexual differentiation in the brain involves a critical period for masculinization, requiring exposure to androgens within a specific developmental window. These organized circuits are later activated during adulthood by the sex-specific hormonal environment upon reintroduction of hormones [111, 112]. Before the brain is developed the testes are established and commence hormone production, facilitating the maturation of the male reproductive tract. By the second trimester in humans and the third week

of pregnancy in rodents, the male fetus is already generating androgen hormones at levels close to those seen in adults [113]. During the perinatal stage in rodents, the initial rise in testosterone is converted to estrogen (aromatization) in the brain [114], influencing developmental processes like neurogenesis [115], synaptogenesis [116], and dendritic growth [117]. Following this early surge, androgen levels gradually decline to align with female levels. This early-life organization lays the foundation for subsequent differences to manifest during puberty at the reintroduction of gonadal hormones [113].

Since many cells throughout the brain express receptors for sex hormones, later surges in post-puberty gonadal hormones can have lasting effects on cell function. One region that is particularly receptive to neurosteroids such as estradiol and progesterone during early development is the cerebellum. Though in healthy neonates and adults, the cerebellum is not known for sexual dimorphism with relatively similar levels of hormone and receptor levels, substantial differences emerge in the sex-based risk of neuropsychological diseases linked to cerebellar pathology [118]. Many of these pathologies are linked to white matter defects as the result of inflammation [119]. Cerebellar Purkinje cells express estrogen receptor-  $\beta$  (ER- $\beta$ ) which appears to play a role in the formation of cerebellar neuronal circuits by facilitating neuronal growth and synaptic contact. Administering estradiol to neonatal WT or cytochrome P450 aromatase knock-out mice resulted in enhanced dendritic growth, spinogenesis, and synaptogenesis in Purkinje cells via brain-derived neurotrophic factor (BDNF) signaling [120]. In the corpus callosum, sex differences in the density of oligodendrocytes and myelin are observable within the initial 10 postnatal days in the mouse brain. The significance of postnatal androgens in masculinizing myelin, with lasting effects into adulthood, was demonstrated by treating male pups with an androgen receptor antagonist and female pups with 5 $\alpha$ -dihydrotestosterone (5 $\alpha$ -DHT) [121]. Estradiol and two selective estrogen

receptor modulators increased the expression of estrogen receptor-  $\alpha$  ER- $\alpha$  in microglia and decreased LPS induced microglial activation in both male and ovariectomized female rats. This suggests a possible role for ER- $\alpha$  in sex specific responses of microglia to inflammatory insult [122]. These examples highlight how the expression of gonadal hormone receptors allows sex hormones to exert lasting effects on cell function.

However, more complex to unravel are the most basic cause of sex differences, male (XY) and female (XX) sex chromosomes that exist within every cell of the body. The challenge becomes identifying changes due to these sex chromosomes before the influence of hormone changes. For example, one study isolated embryonic cells from male and female mice prior to sexual differentiation and found differential responses to exogenous stressors such as ethanol, camptothecin or influenza A virus in vitro [123]. Placental gene expression differences in early and term placenta are correlated to sex differences in adult tissues particularly in the brain [124]. To further complicate matters, X-chromosome inactivation equalizes gene dosage X-linked genes in females, silencing one X chromosome and plays a vital role in placental and brain transcriptomic differences. In males, who receive only maternally derived X-linked genes, there's less flexibility. However, in females, the ability to inactivate either maternally or paternally derived X genes provides more opportunities for genetic protection. This allows the dominance of the X copy from the parent with more beneficial genes for survival in the tissue, offering an additional layer of genetic advantage [125]. The use of RNA sequencing to analyze sex differences in first-trimester human placentas revealed 58 genes with differential expression, particularly those known to escape X inactivation. Gene ontology analysis indicated variations in molecular signaling that could impact pregnancy outcomes, including cell growth and metabolism, immune regulation activity in the placenta, and ceramide signaling crucial for maintaining placental barrier integrity. Notably,

excess ceramides have been linked to conditions like hypertension and preeclampsia [126]. Some genes can escape X chromosome inactivation such as O-linked N-acetylglucosamine transferase (OGT) and are thereby expressed more highly in XX female placentas. This leads to epigenetic effects such as increased histone methylation. Interestingly, placental specific deletion of OGT had neurodevelopmental impact, recapitulating a model of early prenatal stress accompanied by hypothalamic programming changes [127-129]. In summary, the interplay of sex chromosomes and hormonal influences underscores the complexity of sex differences that extends from early embryonic development to adult tissue function.

### **1.3b Microglia and Sex Differences**

Playing a role in healthy neurodevelopment, many neuroendocrine signaling molecules contribute to the intricate processes of brain development. The impact of inflammatory insults during the perinatal period varies based on both timing and context, as inflammation can either prime the brain for injury or induce protective effects. [6] Although the effects of inflammatory insult on critical stages of cortical development and myelination are well-established [130-132], the development of the brain's resident immune population, including microglia, macrophages, and astrocytes, may also play a critical role in mediating injury during this time.

Many neurodevelopmental disorders are associated with inflammatory conditions and microglial dysfunction [30, 32]. In this context, microglia emerge as significant candidates, given their role as resident brain immune cells and their crucial involvement in brain sexualization. Microglia undergo characteristic step-wise and sex-linked development [133]. In various brain regions, male microglia exhibit a more amoeboid appearance [134-136], while females tend to attain an adult phenotype more rapidly [137]. Studies also suggest sex-linked differences in immune activation and phagocytic capacity [138, 139]. Through their response to immune

activation and proficiency for phagocytosis, microglia play crucial roles in scavenging damaged neurons, developmentally pruning unnecessary synapses, myelination, and fighting infectious agents [13-16]. Due to their sex-linked phenotype, microglia may respond differently to neuroinflammation during gestation. However, many of these sex differences emerge after the postnatal androgen surge that elicits the brain's sexual differentiation. Moreover, treating females with masculinizing sex hormones during this critical period rapidly promotes a more male microglial phenotype [138]. Understanding the role of microglial sex-linked characteristics, such as their capacity to prune synapses and respond to inflammatory injury, is crucial for comprehending how they contribute to sex-linked outcomes of prenatal inflammation and neurodevelopmental disorders.

### **1.3c Microglia and Myelination**

The intricate interplay between microglia and myelin is a multifaceted phenomenon that significantly influences the development and maintenance of the nervous system. Microglia, the resident immune cells of the central nervous system, actively contribute to myelination through the secretion of trophic factors that enhance the survival and differentiation of oligodendrocytes (OL). Beyond trophic support, microglia actively participate in phagocytosis, both during early developmental stages and in response to damaged myelin in disease models [140, 141]. The following sections delve into these intricate aspects of microglial involvement in myelination and phagocytosis, shedding light on their diverse roles in shaping the structure and function of the nervous system.

Microglia contribute to myelination by secreting factors that promote the survival and differentiation of OL. Early investigations into microglial influence on myelination often employed a straightforward methodology, introducing microglial conditioned media to OL cultures. This experimental approach aimed to observe the impact on OL behavior and to identify specific factors within the media responsible for driving these effects. For example, microglia-conditioned media containing increased levels of IGF-1, E-selectin (CD62E), fractalkine (CX3CL1), neuropilin-2 (NRP-2), IL-2, IL-5, and vascular endothelial growth factor (VEGF) were added to myelinating co-cultures and accelerated OL differentiation as seen by increased numbers of mature CC1+, MBP+ OLs [17]. Other similar studies have shown that such conditioned medium increased OPC survival and differentiation by upregulating the PDGFR $\alpha$ -signaling pathway accompanied by NF- $\kappa$ B activation [142]. In an attempt to categorize some of these trophic factors the Barres laboratory identified three main groups including insulin and insulin-like growth factors (IGFs), neurotrophins, and gp130/IL-6 family cytokines (ciliary-neurotrophic factor (CNTF), leukemia inhibitory factor (LIF) and interleukin 6 (IL-6)). While each of these factors promotes OL survival in the short term, in combination their effects on survival are additive [143]. *In vivo* investigations in the postnatal rodent subventricular zone (SVZ) have corroborated these observations, demonstrating that pharmacologically suppressing microglial-secreted pro-inflammatory cytokines like IL-1 $\beta$ , IL-6, TNF- $\alpha$ , and IFN- $\gamma$  inhibits oligodendrogenesis. Moreover, complementary *in vitro* assays revealed that activated microglia significantly increase the population of O4-positive cells while concurrently reducing PDGFR $\alpha$ -positive cells, indicating that activated microglia enhance oligodendrocyte differentiation [144]. As these findings become more complex, single-cell profiling has revealed microglia heterogeneity, with distinct populations in varying locations exhibiting differential support for oligodendrocytes [145]. A unique subset of

microglia found in myelinating tracts expresses CD11c and demonstrates the expression of oligodendrocyte-supportive genes, including *Spp1* and *Igf1*. The targeted deletion of *Igf1* specifically from CD11c<sup>+</sup> microglia results in a significant impairment in primary myelination [146]. The collective findings from these studies underscore the heterogeneity of microglial populations, particularly in white matter-rich regions. These specialized microglia exhibit a unique capacity to release trophic factors, traditionally recognized as inflammatory cytokines, thereby playing a crucial role in promoting the survival and differentiation of oligodendrocyte precursor cells (OPCs).

Beyond the release of signaling molecules, microglia can directly affect OL populations through phagocytosis. The developmental pruning of OPCs by microglia may be a response to overproduction, which could be a mechanism to provide reinforcements against potential early injury [147]. As mentioned above, many single cell profiling studies have identified unique subsets of microglia that exist in white matter tracts. Studies have also shown that functionally, these microglia in early postnatal white matter have higher phagocytic activity and often contain fragments of mature OL colocalized with apoptotic marker cleaved caspase 3 (CC3) and myelin basic protein (MBP) [148]. While microglia are traditionally associated with the phagocytosis of cellular debris, their developmental role primarily involves the phagocytosis of living oligodendrocytes rather than those with apoptotic markers. A groundbreaking study by A. D. Nemes-Baran et al., utilizing OPC fate-mapping in the corpus callosum, demonstrated that microglia engulf live NG2<sup>+</sup> OPCs, peaking at P7 with only about 10% exhibiting apoptotic markers. Furthermore, the study revealed the necessity of fractalkine signaling in controlling this phagocytosis, as the knockout of the fractalkine receptor in microglia resulted in reduced engulfment of OPCs and impaired myelination [18]. In summary, microglia play a multifaceted

role in the modulation of oligodendrocyte populations, displaying heightened phagocytic activity in early postnatal white matter and engaging in developmental pruning of OPCs.

Microglial involvement in myelination extends to the phagocytosis of myelin itself. Studies in the zebrafish eloquently illustrate that microglia actively engage in phagocytosis of myelin sheaths during early developmental stages. Timelapse imaging showed microglia occupy myelinated tracts in the developing spinal cord and exhibit intracellular calcium transients, indicative of phagocytic activity followed by the disappearance of myelin. When microglia were depleted, this led to increased myelination with ectopic ensheathment of neuronal cell bodies [16]. Microglia are also required for the regulation of myelin growth and maintenance. A transgenic mouse model, *Fire*<sup>ΔΔ</sup>, which involves the deletion of the Fms intronic regulatory element (Fire) super-enhancer of the *Csf1r* gene, effectively eliminates microglia during development. *Fire*<sup>ΔΔ</sup> mice exhibit abnormal myelin structure indicative of hypermyelination with enlarged areas of uncompacted myelin. This aberration in myelination is associated with impaired cognitive flexibility in early adulthood [149]. Upon reaching old age, these mice display subsequent demyelination, suggesting a protective role of microglia in preventing demyelination. Pharmacological depletion of microglia using the CSF1R inhibitor PLX5622 produces a similar thickening of myelin followed by patchy demyelination [149]. Notably, the stimulation of lipid metabolism via the TGFβ1–TGFβR1 axis rescues the effects observed in *Fire*<sup>ΔΔ</sup> mice, emphasizing the potential primary mechanism by which microglia maintain myelin health in this model [149]. An important mechanism for regulating the developmental pruning of myelin by microglia is the expression of signal regulatory protein-α (SIRPα) on phagocytes. The natural ligand for SIRPα is CD47, expressed on myelin membranes acts as a “self” signal binding to SIRPα and blocking myelin phagocytosis [150]. The phagocytosis of CD47<sup>+/+</sup> myelin can be triggered

when the binding between myelin CD47 and SIRP $\alpha$  on phagocytes is obstructed by monoclonal antibodies (mAbs) against CD47 and SIRP $\alpha$  [150]. These studies underscore the intricate and multifaceted role of microglia in myelin phagocytosis during early developmental stages. Furthermore, their pivotal involvement extends to the nuanced regulation of myelin growth and maintenance, employing complex mechanisms such as lipid trafficking and "self" signaling, as exemplified by the crucial CD47-SIRP $\alpha$  binding interaction.

Many studies investigating microglial phagocytosis of myelin come from disease models investigating the clearance of degraded and injured myelin fragments. In many of these studies myelin has been shown to interact with microglial phagocytosis signaling receptors such as CX3CR1, Trem2, and MerTK [151-154]. In a cuprizone model of demyelination, the knockout of CX3CR1 drastically reduces microglial phagocytosis of myelin debris preventing remyelination [151]. In a different study utilizing the same model, *Trem2*<sup>-/-</sup> microglia did not amplify expected phagocytic transcripts and resulted in impaired myelin debris clearance [152]. Monocyte derived macrophages of patients with multiple sclerosis (MS) showed decreased expression of the phagocytic tyrosine kinase receptor, MerTK [153]. Moreover, specific MerTK inhibitors reduced myelin phagocytosis and the resultant cytokine responses for both in monocyte derived macrophages and microglia [154]. However, phagocytosis targeting machinery may not be the only important functionality at play. An additional role microglia may play in these disease models are their specialized lysosomes capable of degrading myelin fragments. In a model of frontotemporal dementia, progranulin loss induces microgliosis in white matter, where lysosomal impairment leads to an accumulation of myelin debris [155]. Progranulin deficiency has been shown to enhance immunoreactivity for lysosomal markers such as Lamp1 and cathepsin D [156]. Interestingly, cathepsin D is a lysosomal protease that can digest MBP *in vitro* [157], which may

play a vital role in microglial lysosomes' ability to digest myelin debris. In conclusion, the intricate interplay between microglia and myelin extends to the phagocytosis of damaged myelin, a critical process highlighted in disease models of MS and frontotemporal dementia.

## **1.4 Cerebellum and Prenatal Insult**

Given its involvement in various neurocognitive functions, aberrant cerebellar development is associated with a range of neurodevelopmental disorders including intellectual disability, autism spectrum disorder, and attention-deficit/hyperactivity disorder [11]. Furthermore, many of these disorders exhibit pathophysiologies linked to pregnancy complications and preterm birth [158]. The vulnerability of the cerebellum to intrauterine insults stems from several factors. Notably, it is among the earliest brain regions to initiate development, with the anlage formation commencing during the early embryonic segmental phase of hindbrain development around E8.5 [158-160]. Additionally, the cerebellum stands out as one of the final brain regions to complete development, with neurogenesis of its various cell types spanning most of gestation and the maturation of neurons, as well as myelination, extending into the early postnatal period. Full cerebellar development in the mouse extends between 30 to 35 days. In humans, this extends from 30 days post-conception to the second postnatal year [10]. The prolonged duration of cerebellar development exposes it to an extended period of vulnerability, making it susceptible to insults before attaining the stability of maturity.

### **1.4a Cerebellar Development**

Adult cerebellar morphology and fundamental circuitry have been extensively documented for over a century [161, 162], primarily emphasizing its role in integrating sensory information to guide movement and maintain balance. Only in recent years have researchers begun to recognize

its involvement in higher cognition, social behavior, and executive function [163, 164]. This newfound understanding has sparked a resurgence of interest in the comprehensive study of the cerebellum in a diverse range of neurodevelopmental disorders.

Upon reaching maturity, the cerebellum exhibits a distinct organization comprising three primary cell layers. Progressing from the outermost to the innermost layers are the molecular layer, the Purkinje cell layer, and the granule cell layer. Internally, the white matter envelops the deep cerebellar nuclei [158, 159]. Within these layers are three major classes of cell types including glutamatergic, GABAergic, and glial cells. Among the glutamatergic, or excitatory, cell types are granule cells, unipolar brush cells, and deep cerebellar nuclear neurons. Conversely, Purkinje cells, interneurons, and a subset of deep cerebellar nuclear neurons fall under the category of GABAergic, or inhibitory, cells [158, 159].

The formation of the highly organized layered structure of the cerebellum involves the intricate coordination of various developmental processes. Originating from rhombomere 1 during embryonic development in an *fgf8* dependent manner [165, 166], the cerebellum undergoes the formation of two germinal zones. The cerebellar rhombic lip gives rise to cerebellar glutamatergic neurons, via the expression of atonal bHLH transcription factor 1 (*Atoh1*) [167, 168], and the cerebellar ventricular zone, generates all cerebellar GABAergic neurons defined by pancreas associated transcription factor 1a (*Ptf1a*). [169, 170]

Before attaining its mature 3-layered structure, the embryonic cerebellum manifests as 5 layers: the external granule cell layer (EGL), the molecular layer (ML), the Purkinje cell layer (PCL), the internal granule cell layer (IGL), and the white matter. In the mouse brain, granule cells, the major glutamatergic cells of the cerebellum are born around E10.5-E12.5, and populate the outermost surface, forming the external granule layer (EGL) by E18.5 [167, 168]. EGL cells

undergo rapid proliferation from E13.5 until the third week of postnatal life, when post-mitotic granule cells begin to slowly migrate inward along the Bergmann glia through the Purkinje cell layer to the Internal Granule Layer (IGL), ultimately settling there in adulthood [171]. Purkinje cells, the major GABAergic cells of the cerebellum form the sole output of the cerebellar cortex and are born in the ventricular zone between ~E10-E13. Purkinje cells then migrate to form multi-cell thick clusters with molecularly distinct characteristics by ~E18. Finally, postnatally, Purkinje cells begin to disperse to form their characteristic single cell layer [172].

The white matter in the cerebellum undergoes dynamic changes throughout development, serving as a region where various cell types temporarily or permanently reside during the developmental process. The prospective white matter contains a transient germinal compartment during development that produces postnatally born GABAergic inhibitory interneurons including basket and stellate cells [173]. They use the white matter as a place for transient proliferation before exiting in the first two weeks of life. Cerebellar oligodendrocytes undergo three distinct waves of development, originating from both within the cerebellum and extracerebellar regions. At E11.5, oligodendrocyte precursor cells (OPCs) emerge from the metencephalic ventral rhombomere 1 regions and gradually migrate to the cerebellum by E16.5. A significant proliferative burst occurs at E18.5, with contributions from the cerebellar ventricular zone. Finally, a third and final wave of proliferation takes place at the day of birth (P0) [86, 174]. Within the first couple weeks of life these oligodendrocytes begin to differentiate into mature oligodendrocytes and only reach full myelination by the third week.

## 1.4b Cerebellar Sex Differences

To establish a connection between susceptibility of the cerebellum to inflammatory challenges during development and the variations in cerebellar pathology between sexes, it is essential to explore potential mechanistic mediators. One potential explanation for sex differences in the cerebellum involves the expression of estrogen receptors (ERs), which reach their peak during the second postnatal week in Purkinje cells, together with aromatase, the synthetic enzyme for estradiol [175-177]. Prostaglandins are key regulators of inflammation but are also implicated in neural development [178]. Interestingly, studies have shown that prostaglandins stimulate estradiol synthesis in the immature rodent cerebellum via the enhanced activity of aromatase. Administering cyclooxygenase (COX) inhibitors to block PGE2 production, increased the total length of Purkinje cell dendrites and the number of dendritic spines. Moreover, novel sex differences in electrophysiological properties of Purkinje cells such as input resistance and membrane capacitance were abolished by estradiol treatment [178]. This critical period of prostaglandins inducing sex differences in the developing cerebellum has also exhibited sensitivity to inflammatory insult, influencing Purkinje cell dendritic growth with lasting impact in males, only [179]. As a mediator of sex differences that are sensitive to inflammation, PGE2 has also shown to impact cerebellar microglia function. During the critical period, endogenous estrogens and prostaglandins upregulate the phagocytic activity of microglia, which was assessed via pharmacological inhibition of aromatase [180]. Hence, microglia and PGE2 emerge as potentially critical missing components in the sex-biased susceptibility to cerebellar pathology following inflammatory insults.

## 1.4c Cerebellar Microglia

Microglia, the resident immune cells of the brain, play a pivotal role in neurodevelopment and homeostasis. In mice, they emerge from a primitive erythromyeloid progenitor (EMP) population residing in the yolk sac at approximately embryonic day 8 (E8), making their way to the brain by E9.5, before the closure of the blood-brain barrier [181, 182]. Here, microglia exhibit slow proliferation until birth, followed by a rapid surge in numbers during the first two postnatal weeks. Subsequently, microglia either undergo apoptosis or migrate to their final designated brain regions by P30 [183]. Recent investigations have confirmed the remarkable structural and functional diversity of microglia throughout various brain regions and how these characteristics are tailored to the unique needs of their surrounding environments [148, 184]. The following section reviews the unique characteristics of cerebellar microglia and how they contribute to overall cerebellar development.

Cerebellar microglia are functionally and structurally distinct from classically studied cortical microglia. These microglia are less ramified and do not show the classically "tiled" structure throughout the cerebellar tissue [184-186]. Though they are sparser in density, they also exhibit somatic motility. This unique surveillance dynamic lends itself to a faster and more widespread injury response [186]. Moreover, in their ability to respond to insults, studies have shown cerebellar microglia also exhibit a more "primed" immune status than microglia in the rest of the brain. The cerebellar microglia transcriptomic profile exhibits higher enrichment in immune related genes such as pathogen recognition genes, (*Clec7a*, *Cd209a*, *Fcnb*) and interferon pathway genes (*Stat1*, *Stat4*, *Irf7*) [145]. Moreover, these microglia show increased phagocytic capacity at baseline with increased CD86+ lysosome content [187].

The functionally unique cerebellar microglia probably arise because of environmental cues. All microglia are born in the yolk sac in mice and make their way to the brain between E8.5 and E9.5. After the blood brain barrier closes, microglia locally proliferate and distribute within the central nervous system (CNS). BY E15.5 microglia begin to use local cues to specialize to their regional microenvironment [188]. Cerebellar microglia emerge from the white matter postnatally starting at ~P5-P7 [189], which is substantially later than seen in the cortex and hippocampus. It is for this reason that cerebellar microglia may maintain more transcriptional patterns and functional similarities to white matter microglia across the brain. For example, although microglial maintenance relies on the expression of colony stimulating factor-1 receptor (CSF1-R) which binds both colony stimulating factor 1 (CSF-1) and interleukin-34 (IL-34) as ligands [190], CSF-1 plays a more central role in the regulation of cerebellar microglial populations as seen in white matter microglia. Studies that delete CSF-1 result in a reduction in cerebellar microglia and very little impact in the cortex [191]. Moreover, neonatal microglial cells from the cerebellum treated with IL-34 induces a cortical microglial identity while cortical microglia given CSF-1 begin to resemble those of the cerebellum [191]. Together, this suggests that the contextual expression of IL-34 and CSF-1 play an important role in the maintenance of region-specific microglial profiles.

## **Conclusions**

The literature review of background information sets the stage for my thesis questions. The review on sex differences in neurodevelopment will assist in understanding the disparities in inflammatory profiles between male and female pIKO mice and elucidating their origins. Furthermore, the background on ALLO and its impact on different cell types will provide context for investigating how these divergent inflammatory profiles impact the function of microglia, and subsequently, the implications for oligodendrocyte (OL) populations. Finally, I will use the

existing literature to explore strategies for modulating microglial function in ways that improve myelination and the resulting mouse behavior. (Fig. 1)

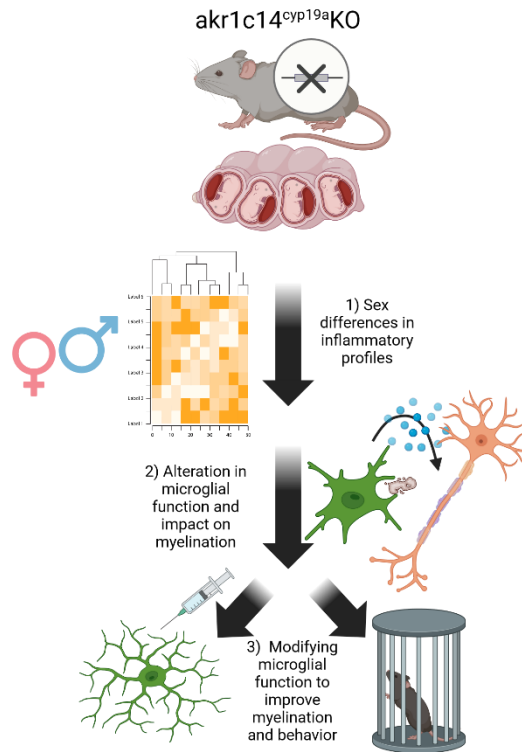


**Figure 1. Loss of placental support during pregnancy results in sex differences in behavioral presentation and at the cellular and transcriptomic levels.** The current study focuses on three main questions including; how inflammatory profiles differ by sex, how altered microglial function during this inflammation impacts myelination, and if we can modify microglial function to improve myelination and behavior.

## Chapter 2: Materials and Methods

Many of the following sub-sections from these materials and methods have been previously described and published in Vacher, CM., Lacaille, H., O'Reilly, J.J. *et al.* Placental endocrine function shapes cerebellar development and social behavior. *Nat Neurosci* **24**, 1392–1401 (2021). <https://doi.org/10.1038/s41593-021-00896-4>. Reproduced with permission from Springer Nature.

### 2.1 Mice

All the procedures on experimental animals were performed in accordance with the protocol approved by the Institutional Animal Care and Use Committee at Children's National Medical Center (protocol no. 30534 (PI: Penn)) and at Columbia University Medical Center (protocol nos. AC-AABE 6553 (PI: Penn) and AC-AABF 5550 (PI: Yang)). Mice were housed on a 12-h light/dark cycle and had ad libitum access to food and water. The *akr1c4*-floxed mouse was constructed with inGenious Targeting Laboratories as previously described. [9] The *Cyp19-Cre* mouse line (#5912 line), which expresses Cre exclusively in trophoblast cells, was obtained from Dr. Gustavo Leone, Ohio State University. The *akr1c14<sup>Cyp19a</sup>KO* (pIKO) mouse was generated by crossing homozygous *Cyp19-Cre* females with homozygous *akr1c14*-floxed males. The resulting females were then positive for Cre with two floxed alleles and were used as the dams of experimental mice together with homozygous *akr1c14<sup>fl/fl</sup>* males. This yielded mixed litters of pIKO mice and their littermate controls. Model validation was previously described [9].

### 2.2 Human Samples

Human cerebellar vermes were obtained as previously described [9] from the National Institutes of Health (NIH) NeuroBioBank (request ID no. 709). Donors consisted of 6-week-old term infants (average age) and corrected age-matched preterm infants, excluding those with major congenital

anomalies or known genetic diagnoses and those with meningitis or stroke as cause of death. Frozen tissues were preserved at  $-80^{\circ}\text{C}$ .

### **2.3 Drug Injections**

For drug injections from Chapter 3, all procedures were completed as previously described in Vacher et. al 2021 [9]. Pregnant dams received one intraperitoneal injection of allopregnanolone (Tocris Bioscience, no. 3653) diluted in sesame oil (vehicle; Sigma-Aldrich, no. S3547) at E15.5 at a dose of  $10\text{ mg kg}^{-1}$  of body weight. Muscimol (Tocris, no. 0289) was diluted in saline solution and injected intraperitoneally in pregnant mice at E15.5 ( $1\text{ mg kg}^{-1}$ ). Allopregnanolone and muscimol injections were done in the morning, during sleep time, to limit the effect of the drug-induced sedation on dams' activity. Doses were chosen based on prior pharmacological studies in mice, [192, 193] and the timing was an empirical choice based on *akr1c14* gene expression peak at E14.5. BrdU ( $50\text{ mg kg}^{-1}$ ) dissolved in saline solution was injected intraperitoneally in dams at E15.5.

The drug injections from Chapter 4 experiments were completed as follows. For pharmacologically testing SIRP $\alpha$ -CD47 signaling, RRx-001 (MedChemExpress: Cat #925206-65-1) was suspended in 5% DMSO and Sesame Oil. Mice were injected once a day subcutaneously at  $10\text{mg/kg}$  from P7-P14. The PGE2 EP4 agonist, L-902,688 (Cayman Chemicals: Cat #10007712) was ordered in a special formulation of neat solid. It was then re-constituted in 0.9% Sodium Chloride. Pups were injected subcutaneously with either  $1\text{mg/kg}$  of drug or Saline Vehicle from P7 to P12.

### **2.4 Mass Spectrometry**

The methods completed in this subsection were previously described and published in (Vacher et. al 2021) [9].

## 2.4a Steroid extraction

Pregnenolone (PREG), PROG, ALLO, epiallopregnanolone (EPIALLO), ALLOTHDOC and 3 $\alpha$ 5 $\alpha$ -tetrahydrotestosterone (3 $\alpha$ 5 $\alpha$ -THT) were identified and quantified simultaneously in individual tissues by gas chromatography–tandem mass spectrometry (GC–MS/MS) as previously described.[194] Placental (65–185 mg) and fetal brain (61–130 mg) tissues of male and female wild-type and pLKO mice at E17.5 were weighed and stored at –20 °C until GC–MS/MS analysis. Briefly, steroids were first extracted from placentas, and brains with 10 volumes of methanol (MeOH) and the following internal standards were added to the extracts for steroid quantification: 2 ng of epietiocholanolone for PREG, ALLO, EPIALLO, ALLOTHDOC and 3 $\alpha$ 5 $\alpha$ -THT and 2 ng of <sup>13</sup>C<sub>3</sub>-PROG for PROG. Samples were purified and fractionated by solid-phase extraction with the recycling procedure [195]. The extracts were dissolved in 1 ml of MeOH and applied to the C18 cartridge (500 mg, 6 ml, International Sorbent Technology), followed by 5 ml of MeOH/H<sub>2</sub>O (85/15, vol/vol). The flow-through, containing the free steroids, was collected and dried. After a previous re-conditioning of the same cartridge with 5 ml of H<sub>2</sub>O, the dried samples were dissolved in MeOH/H<sub>2</sub>O (2/8, vol/vol) and re-applied. The cartridge was then washed with 5 ml of H<sub>2</sub>O and 5 ml of MeOH/H<sub>2</sub>O (1/1, vol/vol), and unconjugated steroids were eluted with 5 ml of MeOH/H<sub>2</sub>O (9/1, vol/vol). The fraction containing the unconjugated steroids was then filtered and further purified by high-performance liquid chromatography (HPLC). The HPLC system is composed of a WPS-3000SL analytical autosampler and an LPG-3400SD quaternary pump gradient coupled with a SR-3000 fraction collector (Thermo Fisher Scientific). The HPLC separation was achieved with a LiChrosorb Diol column (25 cm, 4.6 mm, 5  $\mu$ m) in a thermostated block at 30 °C. The column was equilibrated in a solvent system of 90% heptane and 10% of a mixture composed of heptane/isopropanol (85/15, vol/vol). Elution was performed at a flow rate of 1 ml min<sup>-1</sup>, first 90%

heptane and 10% of heptane/isopropanol (85/15, vol/vol) for 15 min, and then with a linear gradient to 100% acetone in 2 min. The column was washed with acetone for 15 min. Steroids were collected in the time range of 15–29 min and were derivatized with 25  $\mu$ l of HFBA and 25  $\mu$ l of anhydrous acetone for 1 h at 20 °C. Samples were dried under a stream of nitrogen and resuspended in heptane.

#### **2.4b GC–MS/MS analysis**

GC–MS/MS analysis of the biological extracts was performed using an AI 1310 autosampler, a Trace 1310 gas chromatograph and a TSQ 8000 mass spectrometer (Thermo Fisher Scientific). Injection was performed in the splitless mode at 250 °C (1 min of splitless time), and the temperature of the gas chromatograph oven was initially maintained at 80 °C for 1 min and ramped between 80 °C and 200 °C at 20 °C  $\text{min}^{-1}$  and then ramped to 300 °C at 5 °C  $\text{min}^{-1}$  and finally ramped to 350 °C at 30 °C  $\text{min}^{-1}$ . The helium carrier gas flow was maintained constant at 1  $\text{ml min}^{-1}$  during the analysis. The transfer line and ionization chamber temperatures were 300 °C and 200 °C, respectively. Electron impact ionization was used for mass spectrometry with ionization energy of 70 eV, and GC–MS/MS analysis was performed in multiple reaction monitoring mode with argon as the collision gas. GC–MS/MS signals were evaluated using a computer workstation by means of the software Excalibur, release 3.0 (Thermo Fisher Scientific). Identification of steroids was supported by their retention time and two or three transitions. Quantification was performed according to the more abundant transition with a previously established calibration curve. The range of the limit of detection was roughly 0.5–20 pg according to the steroid structure. The GC–MS/MS analytical procedure was fully validated in terms of accuracy, reproducibility and linearity in mouse brain [194].

## 2.5 RNA-sequencing

### 2.5a 3' mRNA sequencing

The methods completed in this subsection were previously described and published in ref [9]. Tissue collection and RNA extraction: Cerebellum, bilateral cerebral cortices and bilateral hippocampi from C and pKO mice (males and females) at P30 (three animals per group) were dissected and flash-frozen. Tissue homogenization and total RNA extraction were performed using the *mirVana* Isolation Kit (Thermo Fisher Scientific, no. AM1560) according to the manufacturer's instructions. The cDNA libraries were prepared using the QuantSeq 3' mRNA-Seq Library Prep Kit FWD for Illumina (Lexogen) as per the manufacturer's instructions. Briefly, total RNA was reverse transcribed using oligo (dT) primers. The second cDNA strand was synthesized by random priming, in a manner that DNA polymerase is efficiently stopped when reaching the next hybridized random primer; therefore, only the fragment closed to the 3' end was captured for indexed adapter ligation and PCR amplification. The processed libraries were assessed for its size distribution and concentration using BioAnalyzer High Sensitivity DNA Kit (Agilent Technologies, no. 5067-4626). Pooled libraries were diluted to 2 nM in EB buffer (Qiagen, no. 19086) and then denatured using the Illumina protocol. The libraries were pooled and diluted to 3 nM using 10 mM Tris-HCl, pH 8.5, and then denatured using the Illumina protocol. The denatured libraries were diluted to 10 pM by pre-chilled hybridization buffer and loaded onto a TruSeq v2 Rapid flow cell on an Illumina HiSeq 2500 and run for 50 cycles using a single-read recipe according to the manufacturer's instructions. De-multiplexed sequencing reads were generated using Illumina bcl2fastq (release version 2.18.0.12) allowing no mismatches in the index read. After the quality and polyA trimming by BBDuk[196] and alignment by HISAT2 (version 2.1.0)[197], read counts were calculated using HTSeq [198] by supplementing Ensembl gene

annotation (GRCm38.78). DE analysis and MA plots were done using TCC R package (version 1.12.1, <https://bioconductor.riken.jp/packages/3.3/bioc/manuals/TCC/man/TCC.pdf>) [199]. After getting DEGs, hierarchical clustering of DEGs as a heat map was performed using Partek Genomics Suite (version 6.6, <http://www.partek.com/partek-genomics-suite/>) (Partek). No outlier was identified in our biological replicates, as indicated by principal component analysis and scatter matrices. DEGs met the following guidelines:  $P < 0.05$ ; fragments per kilobase of transcript per million mapped reads values  $> 1$ ; and fold change  $> 1.5$ . The limits of these cutoffs were validated by RT-PCR on samples from other mouse cohorts. IPA was used to identify the top biological functions and disease processes that were differentially regulated. This software is based on the Ingenuity Pathway Knowledge Base for genetic interaction, which derives from the scientific literature, each network connection being supported by previous publications [200]. To determine and visualize the degree of gene overlaps in datasets, Venn analysis was performed using Venny 2.1 (<http://bioinfogp.cnb.csic.es/tools/venny/>).

## **2.5b Time-Course RNA-sequencing**

RNA sequencing was conducted by New York Genome Center using Illumina TruSeq Stranded mRNA Library prep (Illumina, catalog number 20020595) for mRNA library preparation in accordance with manufacturer recommendations, and using IDT for Illumina TruSeq DNA UD Indices (Illumina, catalog number 20022370) for adapters. A total of 500ng of RNA underwent purification and mRNA fragmentation. The purified mRNA underwent both first and second strand cDNA synthesis. Subsequently, the cDNA was adenylated, ligated to Illumina sequencing adapters, and subjected to PCR amplification (8 cycles). Quantification of the cDNA libraries was performed using the Fragment Analyzer 5300 kit FA-NGS-HS (Agilent, catalog number DNF-

474-1000) and Spectramax M2 kit Picogreen (Life Technologies, catalog number P7589). The libraries were then sequenced on an Illumina NovaSeq sequencer, employing 2 x 100 bp cycles. rRNA abundance was measured by mapping with Bowtie2 and quality control was performed using Picard (v1.83) and RSeQC (v2.6.1). The reads were then aligned with STAR (version 2.5.2a), and genes annotated in Gencode vM16 and quantified with featureCounts (v1.4.3-p1).

For the analysis Quantro was then used to test for global differences in distributions [201]. The result shows that there were statistically significant differences in the distribution of expression between samples, so the use of smooth quantile (qsmooth) normalization was required [202]. Differential expression was assessed using Limma-Voom with duplicate correlation [203-205]. The Limma package allows for increased flexibility in model specification with multiple categorical (i.e. genotype, sex and region) and continuous (age) variables [203]. Duplicate correlation allows for model to be adjusted for samples from different regions that belong to the same mouse [205]. The Voom transformation estimates the mean variance relationship of the log-counts to generate a weight for each observation [204]. The counts with duplicate correlation and Voom transformation were then fit to a linear model and Empirical Bayes statistics were used to generate DEG lists with log fold-change and p-values. DEG lists from each group comparison were then entered into IPA (Qiagen) for pathway analysis. Cutoffs for DEGs were set to Log<sub>2</sub>Fold Change of +/- 20% (down regulated -0.514537 and up regulated 0.378512) and a P-value of <0.05.

## **2.6 RT-PCR/ Biomark**

For whole CB experiments, tissues were homogenized in TRIzol Reagent (Thermo Fisher Scientific) and total RNA was extracted with the RNeasy Mini Kit (Qiagen, no. 74104) according to manufacturer instructions. To extract RNA from sorted microglia, cells were directly sorted into

TRIzol Reagent and subsequently mixed with 400ul of phenol:chloroform, pH 4.5 (Invitrogen, no. AM9722) for phase-separation. After a 15 minute centrifugation at 20,000 g, the top aqueous phase was transferred and mixed with 450ul of isopropanol and 2ul of GlycoBlue for coprecipitation. (Thermo Fisher no. AM9515). After a 10 minute incubation, samples are centrifuged at 12,000g for 1 hour. RNA was then washed twice with 75% ethanol and the pellet was resuspended with 15ul of water. For all RT-PCR experiments, 1 µg or 300ug of RNA for whole CB or microglia samples, respectively, was used to make cDNA with the iScript cDNA Synthesis Kit (Bio-Rad, no. 1708891). In whole CB samples RT-PCR experiments were performed on cDNA samples using PowerUp SYBR Green Master Mix (Thermo Fisher Scientific, no. 1725271) with specific primers at 100 nM using the CFX96 Touch Real-Time PCR Detection System (Bio-Rad). For sorted microglia high-throughput RT-qPCR was performed using the Biomark™ HD System (Standard Biotools), which supports the 96.96 Dynamic Array™ IFC. The microglial cDNA was pre-amplified using the Fluidigm Preamp Master Mix (Fluidigm PN 100-5580 or PN 100-5581) according to Fluidigm Preamplification of cDNA for Gene Expression Quick Reference (100-5875). All samples were diluted 5-fold. Samples and primers were then loaded according to the protocol described in Gene Expression with the 96.96 IFC Using Delta Gene Assays Quick Reference (100-9792) using SsoFast EvaGreen Supermix with low ROX (BioRad, 172-5211) and 20X DNA Binding Dye (Fluidigm, 100-7609) for samples and 2X Assay Loading Reagent (Fluidigm100-7611) for primers. All primer pairs were designed and validated in-house for efficiency and specificity. The cDNA-generated signals for target genes were internally corrected with phosphoglycerate kinase 1 (*pgkl*) in mouse postnatal brains, tyrosine 3-monooxygenase/tryptophan 5-monooxygenase activation protein zeta (*ywhaz*) in mouse

placentas and Ferritin Heavy Chain 1 (*fth1*) and beta actin (*actb*) for sorted microglia. The regulation fold changes were determined with the  $2^{-\Delta\Delta Cq}$  method [206].

## 2.7 Histology

Animals were anesthetized using isoflurane (Isothesia, Henry Schein Animal Health) and transcardially perfused with 1× PBS followed by 4% PFA. Brains were post-fixed for 24 h in 4% PFA and cryoprotected in 20% sucrose in PBS. Serial 40- $\mu$ m-thick sagittal cerebellar sections were then collected using a freezing microtome. The following described histological staining from chapter 3 were previously described and published in ref [9]. Placentas were collected at E17.5 after deep anesthesia of the dams, drop-fixed in 4% PFA and cryoprotected in 30% sucrose. Frozen 20- $\mu$ m cross-sections were obtained with a cryostat. Immunohistochemistry on brain or placenta sections was performed using the following antibodies: rabbit anti-MBP (Abcam, no. ab40390, 1:500), mouse anti-APC clone CC1 (EMD Millipore, no. MABC20, 1:500), rabbit anti-Olig2 (Abcam, no. ab9610, 1:500), rat anti-mouse PDGFR $\alpha$  (CD140a; BD Biosciences, 17-1401-81, 1:500) and chicken anti-GFP (Abcam, no. ab13970, 1:500). Sections were incubated with primary antibodies overnight at 4 °C containing 0.3% Triton and 10% normal donkey serum. Sections were then incubated with secondary antibodies (1:500) together with DAPI (Invitrogen, no. D1306, 1:1,000) for 2 h at room temperature. Secondary antibodies were used as follows: donkey anti-mouse Alexa-488 (Invitrogen, A-21202), donkey anti-rabbit Alexa-488 (Invitrogen, A-21206), donkey anti-mouse Alexa-555 (Invitrogen, A-31570), donkey anti-rabbit Alexa-555 (Invitrogen, A-31572), donkey anti-mouse Alexa-647 (Invitrogen, A-31571) and donkey anti-rabbit Alexa-647 (Invitrogen, A-31573). Finally, floating sections were mounted and cover-slipped using ProLong Gold Antifade Mountant (Thermo Fisher Scientific, P36930) before imaging.

For the staining in chapter 4, 40- $\mu$ m-thick sagittal cerebellar sections incubated with goat anti-IBA1 (Novus Biologicals 1:500) overnight at 4 °C containing 0.3% Triton and 10% normal donkey serum. Sections were then incubated with secondary antibody, donkey anti-goat Alexa-647 (1:500) together with DAPI (Invitrogen, no. D1306, 1:1,000) for 2 h at room temperature. Floating sections were then mounted and cover-slipped using ProLong Gold Antifade Mountant (Thermo Fisher Scientific, P36930) before imaging.

## **2.8 Fluorescence imaging and cell counting**

The following described imaging methods from chapter 3 were previously described and published in ref [9]. Placenta cross-sections and whole brain or cerebellum lateral parasagittal sections were imaged using a virtual slide microscope using cellSens version 2.3 (VS 120, Olympus Life Science) under a  $\times 20$  objective. High-magnification images were taken under a confocal microscope with LAS X Life Science Microscope software version 2.7 (TCS SP8, Leica Microsystems). z-stack images were acquired with a step size of 1.55  $\mu$ m and viewed using NIH ImageJ 1.53c (<http://imagej.nih.gov/ij>). The different cerebellar layers were delineated manually using the freehand selection tool in ImageJ. The density of Olig2-, CC1-, PDGFR $\alpha$ - and BrdU-positive cells was estimated using Stereo Investigator (MBF Bioscience). After delineating the cerebellar WM using the freehand selection tool on corresponding DAPI images, immunopositive cells were manually counted under the  $\times 40$  objective (Zeiss Axio Imager M2) using the optical fractional as a probe in grids randomly distributed on and covering 30% of the cerebellar WM. Cell densities were then calculated by using the individual WM area values and the mean measured section thickness. The linear density of Purkinje cells (Purkinje cells per millimeter) was determined in the lobule VI–VII by drawing a freehand line through the center of the cell bodies.

For the imaging and cell counting from chapter 4, lateral cerebellar parasagittal sections were imaged using a Nikon Ti Eclipse inverted microscope with A1 scanning confocal unit under a  $\times 20$  objective. Z-stack images were acquired with a step size of  $2.0\ \mu\text{m}$  and viewed using NIH ImageJ 1.53c (<http://imagej.nih.gov/ij>). The different cerebellar layers were delineated manually using the freehand selection tool in ImageJ and measured for area. Cropped sections of IBA1-stained CB were uploaded to Imaris 9.90 (Oxford Instruments) and processed through the machine learning-based spots creation wizard workflow. The resulting Spots object allows for automatic modeling of point-like structures, with an editor available for manual correction of detection errors. The algorithm for spot detection was trained with a nucleus size of  $8\ \mu\text{m}$ . Using an autogenerated grid overlaid on the image, microglial nuclei were identified within seven randomly selected grid boxes, and any errors were corrected. The trained algorithm was subsequently applied to images, and relevant statistics were obtained.

## **2.9 Electron Microscopy**

All methods pertaining to electron microscopy and its analysis has been previously described and published in ref [9].

### **2.9a Sample preparation**

P30 mice were anesthetized with a 10:1 mixture of ketamine/xylazine in saline vehicle such that each mouse receives  $100\ \text{mg}\ \text{kg}^{-1}$  of ketamine and  $10\ \text{mg}\ \text{kg}^{-1}$  of xylazine, respectively. Under deep anaesthesia, mice were perfused with 20 ml of 0.12 M cacodylate buffer followed by 30 ml of fixative made of 2.5% glutaraldehyde and 1% PFA (electron microscopy grade, EMS nos. 16221 and 15713) in cacodylate buffer (pH 7.4). Brains were removed and post-fixed for 1 h in the same fixative. Next, 300- $\mu\text{m}$ -thick sagittal slices were made using a vibratome (VT 1000S, Leica Biosystems). Slices were post-fixed with 1% osmium tetroxide in 0.12 M cacodylate buffer

for 2 h at room temperature and ‘en block’ stained with 1% uranyl acetate in 0.1 M acetate buffer overnight at room temperature. After several washes in acetate buffer, slices were dehydrated by passing them through increasing concentrations of ethyl alcohol (up to 100%). Slices were then progressively infiltrated in epoxy resin and placed for 48 h at 60 °C for resin polymerization. Then, 100-nm-thick sagittal ultrasections were performed using an ultramicrotome (Ultracut UC7, Leica Biosystems) through the whole cerebellum (+ brainstem) or the whole anterior brain (for corpus callosum analyses).

### **2.9b Image acquisition**

Large ultrathin sections absorbed on silicon were observed with a FEI Helios NanoLab 660 FIBSEM field emission scanning electron microscope (FEI, Thermo Fisher Scientific) using high-resolution immersion mode and equipped with a solid-state concentric ring (insertable) back-scattering electron detector. Image acquisition was done using MAPS Software version 3.7 (Thermo Fisher Scientific). Low-magnification images ( $\times 600$ ) were first taken to delineate our regions of interest (vermal inter-lobule 6–7 of the cerebellum). Then, high magnifications of two-dimensional image registration ( $\times 20,000$ – $50,000$ ) were taken using 4 kV/0.2 nAmp landing electron beam.

### **2.9c Myelin thickness measurement**

The outer diameter (including myelin sheath) and inner diameter of at least 400 randomly selected myelinated axons were measured on one ultrathin section per animal (three animals per group). The g-ratio (equal to the ratio of the inner-to-outer diameter of a myelinated axon) of each axon was calculated. Scatter plots of the axon caliber and g-ratios were then analyzed. The slopes and elevations of the linear regressions from C and pIKO mice were compared.

## 2.10 Proteins

### 2.10a Western Blots

All methods pertaining to electron microscopy and its analysis has been previously described and published in ref [9].

Whole mouse cerebellums and human vermal samples were homogenized in 250  $\mu$ l of radioimmunoprecipitation assay lysis buffer consisting of (in mM) 50 Tris-HCl, pH 7.4, 150 NaCl, 2 EDTA, 50 NaF, 1  $\text{Na}_3\text{VO}_4$ , 1% Triton X-100, 0.1% SDS, 0.5% Na-deoxycholate and a Protease/Phosphatase Inhibitor Cocktail (Santa Cruz Biotechnology). After centrifugation at 14,000g for 10 min, protein concentration was determined using Bradford protein assay kit (Bio-Rad). Sample total proteins were resolved by sodium dodecyl sulfate-polyacrylamide gel electrophoresis using 10% Bis-Tris precast gel (Thermo Fisher Scientific) and transferred to polyvinylidene fluoride membranes. Membranes were incubated with blocking buffer consisting of 4% non-fat milk in 1% Tween-20 in Tris-buffered saline (TBS-T) for 1 h, followed by overnight incubation at 4 °C with one of the following primary antibodies diluted in 3% BSA TBST-T: rabbit anti-MBP (Abcam, no. ab40390, 1:500), rabbit anti-MAG (Thermo Fisher Scientific, no. PA5-79620, 1:500), rabbit anti-MOG (Abcam, 1:500), mouse anti-cofilin-1 (Cfl1) (Santa Cruz Biotechnology, no. sc-53934, 1:500), mouse anti-prosaposin (Santa Cruz Biotechnology, no. sc-390184, 1:500), rabbit anti-hnRNP $\kappa$  (R332) (Cell Signaling Technology, no. 4675, 1:500) and rabbit anti-GAPDH (Cell Signaling Technology, no. 5174, 1:2,000). After three washes with TBS-T, membranes were incubated with horseradish peroxide-conjugated secondary antibodies (Jackson ImmunoResearch, 1:2,000), and protein bands were visualized using the chemiluminescent ECL detection system (Bio-Rad) according to the manufacturer's instruction.

Signal intensities of protein bands were quantified using Image J software (<http://rsb.info.nih.gov/ij/>) and normalized with GAPDH as an internal control.

### **2.10b Protein extraction and cytokine assay**

Proteins were extracted from whole cerebellum homogenized in 150ul of extraction buffer containing: 20 mM Tris HCl (pH 7.5), 0.5% Tween 20, 150 mM NaCl, with 1 tablet cOmplete, Mini, EDTA-free protease inhibitor dissolved per 10 ml of buffer solution (Roche 11836170001). Homogenate was then centrifuged at 10,000xg for 10 minutes at 4° C and supernatant frozen at -80° C. Protein concentrations were assessed using Pierce BCA total protein assay and normalized for concentration. For the cytokine multiplex assay, samples were shipped to Eve Technologies (Calgary, Alberta, Canada) for the Mouse Cytokine/Chemokine 44-Plex Discovery Assay® Array (MD44). Cytokine levels were assessed by Luminex 200 instruments running on Bio-Plex Manager™ software (with compatible BioRad calibration kits).

### **2.10c ELISA assays**

The PGE2 competitive enzyme immunoassay ELISA kit (mybiosource.com) was completed according to manufacturer instructions. Briefly, the assay sample and buffer are incubated together with PGE2-HRP conjugate in anti-PGE2 pre-coated plate for one hour at 37 °C. Wells were then washed five times with wash buffer and incubated HRP enzyme substrate for 30 minutes at 37 °C. A stop was added to stop the reaction and color intensity was spectrophotometrically measured at 450nm.

## **2.11 Flow Cytometry**

### **2.11a Cell Suspension**

Cell suspension of microglia for flow cytometry was performed according to an adapted protocol from Bohlen et. al, 2019 [207]. Briefly, mice were perfused with ice cold PBS and CB were extracted and placed into 1mL of sample buffer containing 1xPBS and DNase for homogenization. Samples were then centrifuged at 9,300g for 1 minute and pellets suspended in 0.9 mL MACS buffer (Miltenyi Biotec MACS® BSA Stock Solution, 1x PBS, Fetal Bovine Serum, 0,5 M EDTA, 1M HEPES) with 100ul of myelin removal beads (Miltenyi Biotec, 130-096-433). Samples were incubated for 15 minutes with gentle flicking every 5 minutes to mix the beads. Samples were diluted with 1mL of MACS buffer and centrifuged at 9,300g for 1 minute. Samples were then re-suspended in MACS buffer and applied to LS columns (Miltenyi Biotec, 130-042-401) on the QuadroMACS™ Separator. Columns were washed to elute any remaining cells. Flow-through was collected, centrifuged, and resuspended in PBS pHrodo™ Red (Invitrogen P36600), CD11b Monoclonal Antibody (M1/70), FITC (11-0112-82), PE/Cyanine7 anti-mouse CD206 (BioLegend, 141720) and BV605 Rat Anti-Mouse CD86 (BD Biosciences, 563055) for 30 minutes. Lastly, samples were spun down and pellets were re-suspended in flow buffer containing DAPI (Invitrogen, D1306) and Vybrant™ DyeCycle™ Ruby Stain (Invitrogen, V10309). Microglial sorting was done on the Sony MA900 Multi-application Cell Sorter (Sony Biotechnology). Further microglial population statistics were obtained on the NovoCyte Quanteon (Agilent.)

## 2.11b Image Stream

Cells were suspended as previously described above. Cells were first stained with CD11b Monoclonal Antibody (M1/70), FITC (11-0112-82) for 30 minutes followed by 20 minutes of fixation in 4% paraformaldehyde solution. Paraformaldehyde was decanted and cells were resuspended in permeabilization buffer with 0.3% Triton X-100 with 0.5% BSA 10 minutes. Cells were then stained with intracellular stain including PE-Dazzle 594-LAMP1 (Biolegend, 121624, 1:100), Alexa Fluor 647-MBP (Biolegend, 850910, 1:200) and DAPI for an additional 30 minutes. Cells were re-suspended in 35 ul of 1X PBS for acquisition on the ImageStreamX Mk II imaging cytometer using Channel 1 (Brightfield for Camera 1), Channel 2 (FITC, CD11b), Channel 4 (PE-Dazzle 594-LAMP1), Channel 6 (Side Scatter), Channel 7 (DAPI), Channel 9 (Brightfield for Camera 2), and Channel 11 (Alexa Fluor 647-MBP). The laser powers were set up measuring the Raw Max Pixel feature for each active channel insuring no saturation. Images were acquired at 60x magnification and recorded on a plot of Area against Aspect Ratio for brightfield (Channel 1) to exclude Speed Beads from the file. Compensation was performed using the compensation wizard in INSPIRE, and Anti-Rat Ig, κ/Negative Control (BSA) Compensation Plus (7.5 μm) Particles Set (BD Bioscience Cat# 560499) for the antibody conjugates and a control was prepared using cells for DAPI. Amnis IDEAS software was used to analyze data. Data was analyzed first by selecting focused cells using the Gradient RMS feature of Channel 1(Camera 1 brightfield). Then, single cells were selected in a plot of Area against Aspect Ratio of Channel 1. DAPI+ and CD11b+ objects (microglia) were selected using the Intensity feature of each channel. To assess the presence of myelin inside of microglia, the IDEAS Internalization Wizard was used.

## **2.12 Animal behavior**

All methods pertaining to behavioral testing and its analysis has been previously described and published in ref [9].

### **2.12a Pup ultrasonic vocalizations**

Mouse pups emit USVs when separated from the dam. This innate behavior is essential for eliciting maternal care behaviors that the pups need to survive. Separation-induced vocalizations were tested on postnatal days 4, 6, 8 and 11, with vocalizations declining drastically after P12. USVs were recorded for 3 min, and the number of calls was tracked using Avisoft-SASLab Pro software (Avisoft Bioacoustics).

### **2.12b Spontaneous behavior/ stereotypies**

Assessment of repetitive behavior was done to test autism-like behavior. Mice were allowed to habituate to the testing room before placement in a new, empty cage with bedding materials. A video camera was set with a lateral view to record spontaneous behavior for 15 min. Videos were manually scored for time spent engaging in behaviors, including digging, gnawing, grooming, rearing and jumping.

### **2.12c Marble Burying**

The anxiety and stereotypic and/or obsessive–compulsive-like behavior components of ASD-like behavior can be assessed in mice by their behavioral responses to new ‘diggable’ media [208, 209] in the marble burying test. This test was performed in a clean, large (26 ×16 cm) cage filled with 5 cm of bedding and 12 glass marbles evenly spaced on the bedding surface. The animal was left to explore the cage for 30 min undisturbed. Marbles covered 2/3 or more with bedding were counted as buried.

### **2.12d Socialization test**

The three-chamber test (Crawley's paradigm [210]) was used to assess social behavior as previously described [211]. A three-chamber Plexiglas box was used with small openings in each dividing wall to allow free access to each chamber. The center chamber was kept empty, whereas the flanking chambers were each equipped with an identical wire cup. After a 10-min habituation period to allow for exploration of the three-chamber equipment (session 1), an unfamiliar adult mouse of similar weight and coloration was placed within the wire cup in one of the side chambers and an 'object' within the wire cup in the opposite chamber. The dividers were raised to allow the test subject to move freely throughout all three chambers of the apparatus over a 10-min test session (session 2). The second session was analyzed for social preference given by the social preference index (SPI). SPI was calculated as follows: if time spent with the mouse (social) is  $S$  and the object (non-social) is  $NS$ , then  $SPI = S/(S + NS)$ .

### **2.12e Autism severity score**

We used the same procedure as previously described in ref [212]. The score calculation allows for the combination of individual discrete symptoms of the autistic syndrome, in a continuous manner, so that higher values reflect higher severity of autistic-like behavior. For each mouse, we recorded their spontaneous behaviors (grooming, digging, rearing, jumping and gnawing) and determined their SPI in the three-chamber test. The significant readouts (digging time, gnawing time and SPI) were then z-standardized and averaged to establish the autism composite severity score.

### **Statistics**

All statistics pertaining to chapter 3 and its analysis has been previously described and published in ref [9].

Mouse assignment to groups was not randomized, because it relies on their known genotype (C versus plKO), but mice from at least three different litters were used in each group for all experiments. No litter-associated effect was seen. All data analyses were conducted blinded to group allocation. Statistical analysis was carried out with GraphPad Prism 7 software. Detection of EYFP in Cyp19-cre:R26R-EYFP placenta and brain sections, and *in situ* hybridizations in placenta sections, were performed in at least three animals. Cell and area quantification on cerebellar immunofluorescent-labelled sections was done on six sections per animal, homogeneously distributed throughout the cerebellar vermis. Myelinated axon g-ratios were measured from more than 400 axons on one electron microscopy scan per animal. For western blot analyses, at least two technical replicates were performed. When more than ten samples, and, thus, several membranes, needed to be compared at once, two common samples were resolved in the different electrophoresis gels and used as reference for quantification. The sample sizes are shown in the legends and chosen to meet or exceed sample sizes typically used in the field. Robust regression and outlier removal methodology with Q value equal to 1 was used to determine outliers. Before conducting all analyses, variable distributions were evaluated for normality. If distribution was not normal, non-parametric methods were used. Differential gene expression across development in C and plKO mice was analyzed using one-way ANOVA with Dunnett's multiple comparisons test. Comparisons between two groups were analyzed using parametric test (unpaired *t*-test with Welch's correction) or non-parametric test (Mann–Whitney test). The Holm–Sidak method was used for multiple unpaired *t*-test comparison. Analyses involving data from three or more groups while considering only one independent variable were performed using one-way ANOVA with Tukey's multiple comparisons test. Two-way ANOVA was used to compare

means across two or more dependent variables. Summary data are presented in the text as mean  $\pm$  s.e.m. from  $n$  animals. Differences were considered significant at  $P < 0.05$ .

For statistics in chapter 4 the following procedures were followed. All data analyses were conducted blinded to group allocation. Mouse assignment to groups were not randomized as knowledge of genotype (pIKO versus Control) is required. Mice from several litters were used per group. All sample sizes are presented in legends. Interquartile range (IQR = Q3 – Q1) was used to assess each group for outliers. All analyses were evaluated for normality and if not normal, non-parametric tests were used. Comparison between two groups (control and pIKO) in Biomark high throughput RT-qPCR were analyzed using unpaired Welch's  $t$ -test. Two-way ANOVA was used to compare means across two or more independent variables (i.e. sex and genotype) with Sidak multiple comparisons testing. For comparisons with three factors (i.e. age, sex, and genotype) a three-way ANOVA with Tukey's multiple comparisons testing was used. For comparison of means with one independent variable such as treatment with RRx-001, one-way ANOVA or non-parametric Kruskal-Wallis with Dunn's Multiple Comparisons was used. Summary data are presented in the text as mean  $\pm$  s.e.m. from  $n$  animals. Differences were considered significant at  $P < 0.05$ .

## **Chapter 3: Placental endocrine function shapes cerebellar development and social behavior**

The work from this chapter has been adapted from a previously published paper to emphasize personal contributions and data that supports the sexually dimorphic phenotype of this model. Use is with permission from Springer Nature: Vacher, CM., Lacaille, H., O'Reilly, J.J. *et al.* Placental endocrine function shapes cerebellar development and social behavior. *Nat Neurosci* **24**, 1392–1401 (2021). <https://doi.org/10.1038/s41593-021-00896-4>.

Contributions: performed pilot experiments and some molecular validation of RNA sequencing in Appendix B, histological experiments in Figures 3 and 4 and Appendix E, and behavioral experiments including social preference and stereotypies in Figure 5.

### **Abstract**

The intricate interplay between placental function and sex specific neurodevelopmental disorders is increasingly gaining scientific recognition. This study focuses on the placenta's role in endocrine support of the developing brain by delving into the sex specific influence of allopregnanolone (ALLO), a GABA<sub>A</sub> receptor (GABA<sub>A</sub>R) modulator derived from progesterone. We created a novel conditional mouse model, selectively deleting ALLO's synthetic enzyme (*akr1c14*) in placental trophoblasts. This model allows for a direct examination of the consequences of placental ALLO insufficiency on neurodevelopment at the molecular, cellular, and functional levels. Placental ALLO loss resulted in sex-specific cerebellar white matter abnormalities, accompanied by autistic-like behavior in male offspring, only. Notably, a single late-gestation injection of ALLO or a GABA<sub>A</sub>R agonist, muscimol, mitigates these abnormalities, pointing towards potential therapeutic interventions. Moreover, we demonstrate the translational

relevance of our findings by investigating parallels between our mouse model and similar sex-linked alterations in myelination markers of human preterm infants. This study unveils a new dimension in the relationship between placental hormones and neurodevelopment, highlighting the specific impact of ALLO insufficiency. It also emphasizes the clinical significance of our observations and the importance of understanding how placental hormones, such as ALLO, shape the developing brain and its therapeutic opportunities in preventing neurodevelopmental disorders.

## **Introduction**

The impact of placental function on fetal brain development and neurodevelopmental disorders has been a focal point of extensive research [24]. Moreover, many neurodevelopmental disorders exhibit a sex bias in presentation [8], particularly for males, including autism spectrum disorders, attention deficit hyperactivity disorder, and schizophrenia, though the factors rendering males more susceptible remain elusive. Many studies investigating this association emphasize insults such as altered gas exchange or nutrition but inadvertently overlook the crucial neuroendocrine role of the placenta. Many obstetric insults have the potential to disrupt placental endocrine function, spanning from maternal infection to genetic abnormalities. Exploring the role of the placenta becomes a promising avenue in investigating sex differences in neurodevelopmental disorders, as it intricately regulates the development of specific brain structures at their earliest stages by releasing neuroactive factors that target specific circuits and cells.

ALLO, a GABAergic neurosteroid, emerges as a pivotal placental hormone shaping the fetal brain. Derived from progesterone, ALLO acts as a positive allosteric modulator of GABA<sub>A</sub>R, delaying the opening of the GABA-gated Cl<sup>-</sup> channel [66]. In the adult brain, ALLO enhances

GABAergic inhibition, yielding sedative, anxiolytic, anesthetic, and anticonvulsant effects [213]. Substantial evidence indicates that ALLO, through GABA<sub>A</sub>R signaling, serves as a potent regulator of diverse neurodevelopmental processes, including neurogenesis, cell survival, synapse stabilization, and myelination [214]. In fetal sheep and guinea pigs, brain ALLO levels increase in response to immune challenges, hypoxia, and other acute prenatal stressors. Treatment with finasteride, a 5 $\alpha$ -reductase inhibitor hindering ALLO production, increases the occurrence of excitotoxicity and apoptosis and impairs myelination in males [85]. Studies have also shown that ALLO is neuroprotective functionally and behaviorally, with greater sensitivity in females [215, 216]. The findings imply that ALLO has a sex-dependent neuroprotective role. However, the direct impact of these sex-specific ALLO effects on the sexually dimorphic neurobehavioral phenotypes observed after birth remains unclear.

Our innovative mouse model, specifically engineered to reduce placental ALLO, facilitates a direct investigation into the neurodevelopmental consequences of altered placental endocrine function at molecular, cellular, and functional levels. Employing a comprehensive approach involving microscopy, gene and protein expression analysis, neurobehavioral assessments, and pharmacological interventions, our model demonstrates that insufficient placental ALLO leads to abnormalities in cerebellar myelination, associated with autistic-like behaviors in a sex-linked manner. This investigation illuminates how particular placental hormones influence typical brain development and how the absence or dysfunction of the placenta contributes to neurological impairments in individuals born extremely preterm or after compromised pregnancies. These insights lay the groundwork for developing hormone replacement strategies aimed at maintaining the normal developmental environment and safeguarding the brain from further injuries.

## Results

### Deletion of *Akr1c14* in Cyp19+ cells disrupts the production of placental ALLO

Throughout fetal development, *Akr1c14*, the gene responsible for encoding the ALLO-synthesizing enzyme 3 $\alpha$ -hydroxysteroid dehydrogenase (3 $\alpha$ -HSD), exhibits predominant expression in the placenta, peaking in late gestation (Fig. 2a). To investigate the neurodevelopmental role of placental ALLO, *akr1c14*-floxed mice were generated and crossed with placenta-specific Cyp19a-Cre mice (Fig. 2b) [217]. Crossing Cyp19-Cre with R26R-EYFP reporter mice were used to ensure recombinase activity was restricted to the placenta (Fig. 2c), and not the brain (Fig. 2d) and *Akr1c14*-mRNA can be seen co-localized with Cyp19a-Cre:R26R-EYFP-positive cells (arrows, Fig. 2c). Further confirmation of placenta specific recombination is exhibited with polymerase chain reaction (PCR) with no recombination seen in control animals (Fig. 2e). In order to confirm the genetic recombination resulted in reduced ALLO levels in the pKO mice both transcriptomic and direct steroid measurements were used. In the pKO mice, *akr1c14* transcript was significantly reduced in the placenta but not brain (Fig. 1f,g). ALLO levels were also significantly reduced in the placenta and fetal brain in late gestation with no detectable sex differences (Fig. 2h, Appendix A a-g). Both peak *akr1c14* gene expression and conversion rate between progesterone to ALLO coincides at E14.5, suggesting the most dramatic effect of ALLO loss will be seen at this developmental stage.

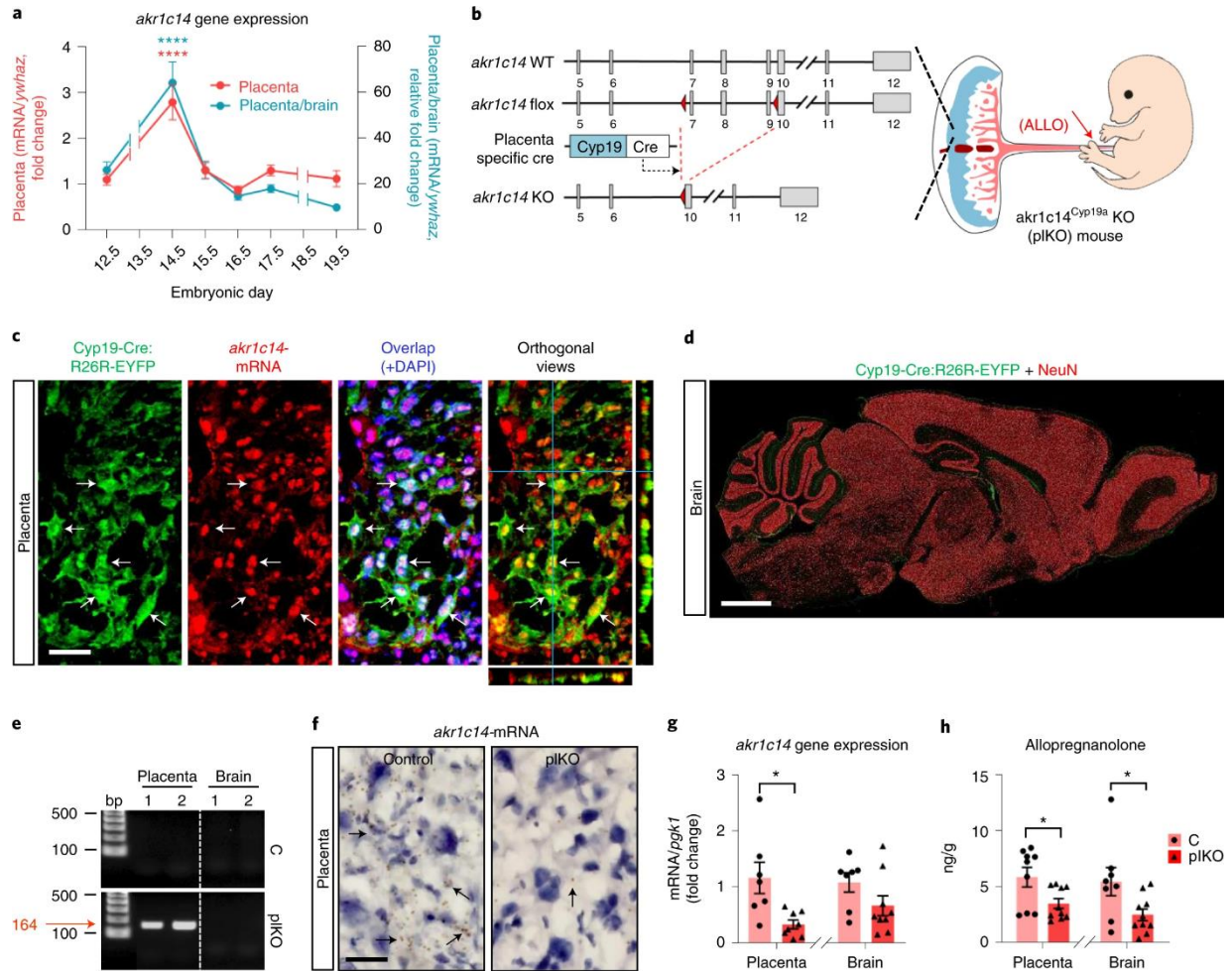


**Figure 1. Conditional deletion of *akr1c14* in *Cyp19a*-expressing trophoblasts results in reduced ALLO levels in the fetal brain.** a, qRT-PCR for *akr1c14* in wild-type (WT) mice. Data presented as mean fold changes  $\pm$  s.e.m. E12.5: n = 12 C and 12 plKO; E14.5: n = 12 C and 12 plKO; E15.5: n = 10 C and 8 plKO; E16.5: n = 7 C and 7 plKO; E17.5: n = 12 C and 12 plKO; E19.5: n = 12 C and 11 plKO. One-way ANOVA with Dunnett's multiple comparisons ( $P < 0.0001$  compared to E12.5 value). There was no significant difference between males and females. ywhaz, tyrosine 3-monooxygenase/tryptophan 5-monooxygenase activation protein zeta. b, *akr1c14* genetic locus before and after recombination. Exons 7–9 are conditionally targeted. *Cyp19a* promoter drives expression of Cre in the placenta only. LoxP sites are indicated by red triangles and exons 5–12 by gray boxes. c, In situ hybridization for *akr1c14* in placenta from *Cyp19a*-Cre:R26R-EYFP mice at E17.5. Arrows show co-localizations. Scale bar, 50  $\mu$ m. d, Sagittal section of a *Cyp19a*-Cre:R26R-EYFP mouse brain immunostained against YFP (green) and NeuN (red). No *Cyp19a* promoter activity was evidenced in the brain at P30. Scale bar, 1 mm. e, A 164-bp-long PCR product ascertains the presence of the recombined LoxP site in the placenta of plKO mice. f, In situ hybridization for *akr1c14* in the placenta at E17.5. *akr1c14*-mRNA levels are drastically decreased in the spongiotrophoblasts (arrows) of plKO compared to C mice. Scale bar, 30  $\mu$ m. g, qRT-PCR for *akr1c14* normalized to *pgk1* at E17.5. Data are presented as mean  $\pm$  s.e.m. Two-tailed unpaired t-test with Welch's correction ( $*P < 0.05$ ). Placenta: n = 7 C and 8 plKO ( $P = 0.0247$ ); Brain: n = 8 C and 9 plKO ( $P = 0.122$ ). *Pgk1*, phosphoglycerate kinase 1. h, Mass spectrometry ALLO assays at E17.5. Data are presented as mean  $\pm$  s.e.m. Two-tailed unpaired t-test with Welch's correction ( $*P < 0.05$ ). Placenta: n = 9 C and 10 plKO ( $P = 0.0315$ ); Brain: n = 8 C and 10 plKO ( $P = 0.0329$ ).

To investigate sex-specific, predominant altered pathways in the postnatal brain following placental ALLO loss, male and female postnatal day 30 (P30) mice were collected for bulk RNA sequencing (RNA-seq) in the cerebral cortex, hippocampus and cerebellum. Threshold criteria used to identify significant differentially expressed genes (DEGs) were validated by RT-PCR and western blots. (Appendix B) The number of differentially expressed genes (DEGs) was 3–5 times higher in the male pLKO cerebellum compared to any other region. (Appendix C. a-d) The DEGs from the male and female cerebellum were run through Ingenuity Pathway Analysis (IPA, Qiagen) and identified white matter (WM)-associated pathways in the top categories in both sexes (Appendix C. e,f). The comparison of these cerebellar DEGs were compared to publicly available oligodendrocyte (OL) and myelin transcriptomes [218, 219] revealed striking sexual dimorphism with quantitatively more gene overlap with males (204) than females (68). (Appendix C. g) The effect was also qualitatively different between the sexes with upregulation of OL-/myelin-related DEGs in pLKO males but down-regulated in pLKO females (Appendix C. h,i).

### **OPC proliferation and differentiation rate diverges in pLKO males and females**

The effect of placental endocrine disruption on cerebellar myelination is unexpected as this process primarily occurs postnatally [86, 220, 221]. However, the thickness of the myelin sheath is significantly influenced by the density of OL, which are mainly produced before birth as oligodendrocyte progenitor cells (OPCs) [86] when ALLO levels are at their peak. ALLO is a potent positive allosteric modulator of GABA<sub>A</sub>R [66]. GABA<sub>A</sub>R signaling is associated with blockade of OPC proliferation [84, 222]. To understand the immediate consequences of ALLO loss, we needed to examine its acute effects on oligodendrocyte populations. BrdU labelling at E15.5 and co-labelled with Olig2 at P30 revealed increased OPC proliferation in both male and female pLKO embryonically (Fig. 3a-c). Additionally, within the OL lineage, an acceleration of

the maturation from PDGFR $\alpha$ <sup>+</sup> OPCs to mature CC1<sup>+</sup> OLs was observed in the plKO mice at P15 (Fig. 3d-i). Interestingly, a sexual divergence begins to emerge in OL lineage by P15 with an acceleration of the maturation of PDGFR $\alpha$ <sup>+</sup> OPCs to mature CC1<sup>+</sup> OLs in the plKO in male plKO mice (Fig. 3d,h). In female plKO the OL maturation (given by the CC1<sup>+</sup>/Olig2<sup>+</sup> cell number ratio) was reduced (Fig.3j,k). By P30 this divergence remained with significantly increased numbers of mature, CC1<sup>+</sup> OL in male plKO compared to controls (Fig.3f). These results indicate short-term, sex-independent embryonic OPC and long-term, sex-dependent OL maturation modifications of cerebellar OL lineage in mice lacking placental ALLO.

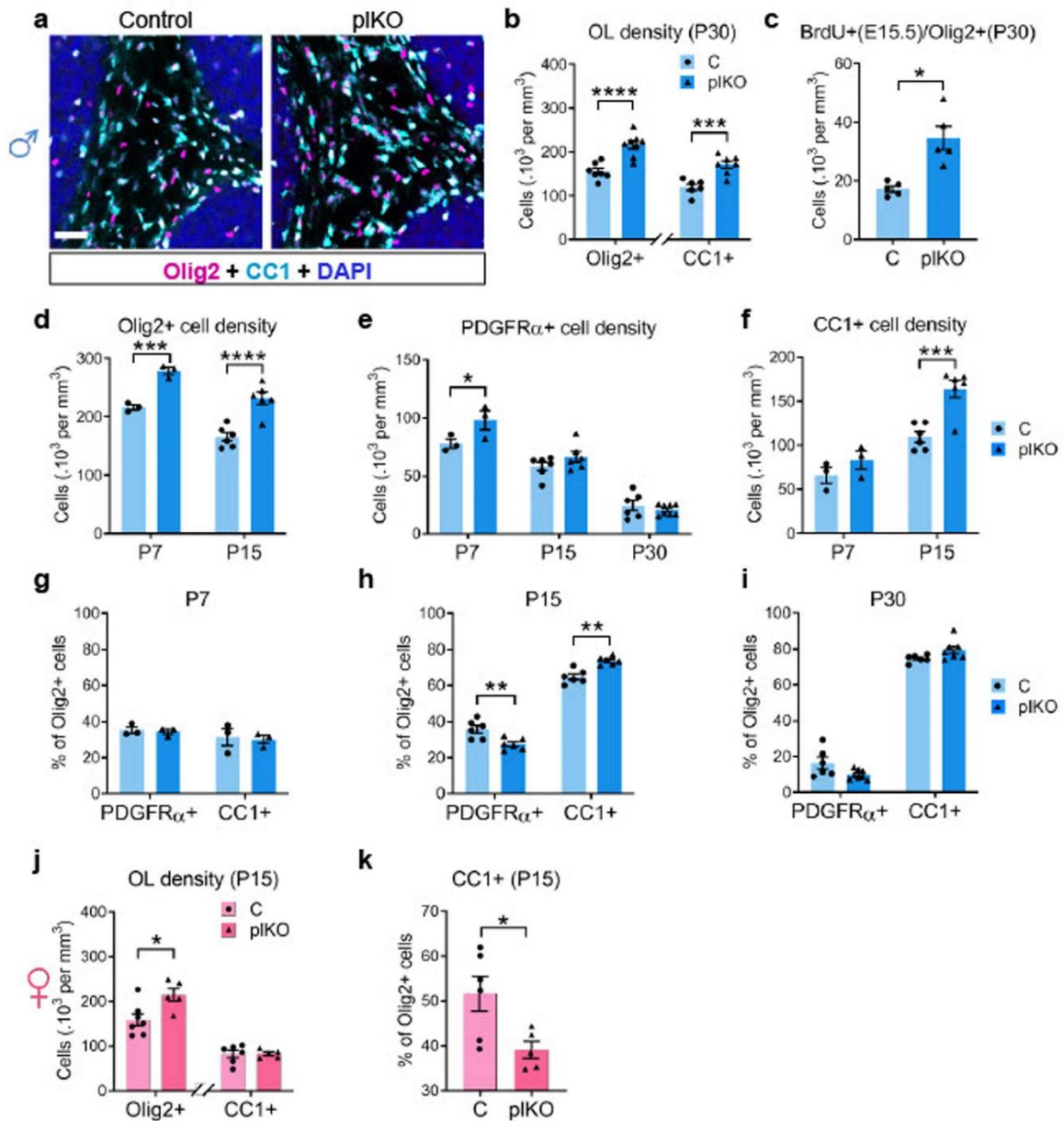


**Figure 3. Oligodendrocyte lineage progression during the postnatal period.** a, Immunofluorescent staining of Olig2 and CC1 in inter-lobule VI-VII WM at P30. Scale bar, 60  $\mu$ m. b, Quantification of Olig2+ and CC1+ cell density in the male P30 WM. Data presented as means  $\pm$  SEM. Two-way ANOVA with Sidak's multiple comparisons test (\*\* $p < 0.005$ , \*\*\*\* $p < 0.0001$ ). Olig2:  $n = 7$  C and 8 pIKO ( $p < 0.0001$ ); CC1:  $n = 6$  C and 7 pIKO ( $p = 0.0005$ ). c, Quantification of BrdU+ /Olig2+ cell density in the male cerebellar WM at P30. BrdU (50 mg/kg) was injected to dams at E15.5. Data presented as means  $\pm$  SEM. Two-tailed unpaired Student's t test with Welch's correction (\* $p < 0.05$ ).  $n = 5$  C and 5 pIKO ( $p = 0.0107$ ). d, Quantification of Olig2+ cell density in the male cerebellar WM at P7 and P15. Data is presented as means  $\pm$  SEM. Two-way ANOVA with

Sidak's multiple comparisons test (\*\*p < 0.005, \*\*\*p < 0.00010). P7: n = 3 mice/group (p = 0.0026); P15: n = 6 mice/group (p < 0.0001). The density of Olig2+ cells in the cerebellar WM is significantly increased in plKO males as compared with C littermates. e, OPC (PDGFR $\alpha$  + cell) density at P7, P15 and P30. Data is presented as means  $\pm$  SEM. Two-way ANOVA with Sidak's multiple comparisons test (\*p < 0.05). P7: n = 3 mice/group (p = 0.0435); P15: n = 6 mice/group (p = 0.3644); P30: n = 6 C and 8 plKO (p = 0.8558). The density of OPCs in the cerebellar WM is transiently higher in plKO males as compared with C littermates at P7. f, Quantification of mature OL (CC1 + cell) density within the male cerebellar WM at P7 and P15. Data is presented as means  $\pm$  SEM. Two-way ANOVA with Sidak's multiple comparisons test (\*\*p < 0.005). P7: n = 3 mice/group (p = 0.4951); P15: n = 6 mice/group (p < 0.0004). The density of mature OLs in the cerebellar WM is significantly increased in plKO males as compared with C littermates at P15. g-i, Ratios of OPCs (PDGFR $\alpha$  + cells) or mature OLs (CC1 + cells) within the total oligodendrocyte lineage (Olig2 + cells) in the male cerebellar WM across postnatal period. Data is presented as means  $\pm$  SEM. Two-way ANOVA with Sidak's multiple comparisons test (\*\*p < 0.005). P7: n = 3 mice/group [p = 0.9741 (PDGFR $\alpha$ ), p = 0.9393 (CC1)]; P15: n = 6 mice/group [p = 0.002 (PDGFR $\alpha$ ), p = 0.001 (CC1)]; P30: n = 7 C and 8 plKO [p = 0.052 (PDGFR $\alpha$ ), p = 0.17 (CC1)]. At P15, a transient acceleration of the OL maturation is observed in the male plKO. j, Quantification of total OL lineage (Olig2 +) and mature OL (CC1 +) cell densities in the female cerebellar WM at P15. Data is presented as means  $\pm$  SEM. Two-way ANOVA with Sidak's multiple comparisons test (\*p < 0.01). Olig2+: n = 7 C and 5 plKO (p = 0.0058); CC1+: n = 6 C and 5 plKO (p = 0.9984). The density of total OL is increased in the cerebellar WM of plKO females compared to C littermates. k, Ratio of mature OLs (CC1 + cells) within the total OL lineage (Olig2 + cells) in the female cerebellar WM at P15. Data is presented as means  $\pm$  SEM. Two-tailed unpaired Student's t test with Welch's correction (\*p < 0.05). n = 6 C and 5 plKO (p = 0.0225). A significantly reduction of OL maturation is observed in the female plKO as compared with littermate C.

## **Placental ALLO loss alters postnatal cerebellar myelination**

Since the sex divergence in OL lineage begins postnatally, we next investigated the effect of placental ALLO loss on myelin development. Examination of cerebellar myelin proteins at P30 unveiled substantial sex-related variations: in pIKO males, there were significant increases in myelin basic protein (MBP), myelin-associated glycoprotein (MAG), and myelin oligodendrocyte glycoprotein (MOG) levels (Fig. 4a,b). Conversely, pIKO females exhibited a reduction in cerebellar MBP content (Fig. 4c,d), a contrast further affirmed by immunohistochemistry (Fig. 4e–h) and RT–PCR (Appendix B. i). To investigate myelin thickness, scanning electron microscopy within lobule VI–VII of the cerebellum revealed thicker myelin as measured by g-ratio, and fewer unmyelinated axons in male pIKO (Fig.3j,k,l,o,s,p). This increased myelin thickness did not coincide with significant alterations in axonal inner calibers (Fig. 4t). In females the opposite effect was seen with considerably thinner myelin sheath and higher number of unmyelinated axons (Fig. 4m,n,q,r,u), although axonal inner diameters remained unchanged (Fig. 4v). These observations underscore the pronounced sex-specific disparities in cerebellar myelin composition and structure.

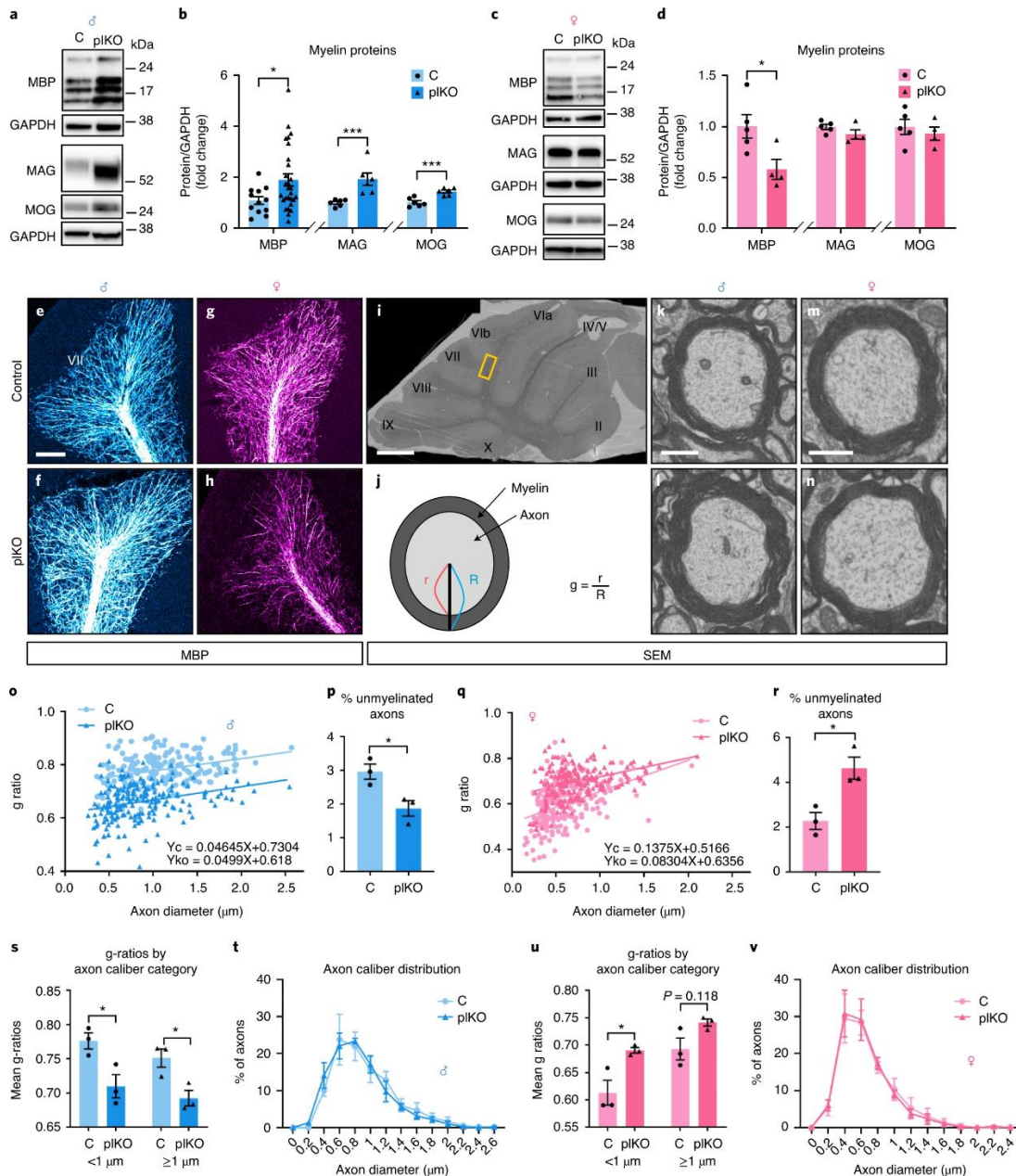


**Figure 4. Placental ALLO insufficiency results in sex-linked cerebellar WM abnormalities at P30.** a,b, Western blot analysis of myelin-related proteins in the male cerebellum. Data are presented as mean fold changes  $\pm$  s.e.m. Multiple unpaired *t*-tests with Holm–Sidak multiple comparison test (\**P* < 0.05; \*\*\**P* < 0.005). MBP: *n* = 12 C and 28 pIKO (*P* = 0.038); MAG: *n* = 6 C and 6 pIKO (*P* = 0.004); MOG: *n* = 6 C and 6pIKO (*P* < 0.0001). c,d, Western blot analysis of myelin-related proteins in the female cerebellum. Data are presented as mean fold changes  $\pm$  s.e.m. Multiple unpaired *t*-tests with Holm–Sidak multiple comparison test (\**P* < 0.05). MBP: *n* = 5 C and 4 pIKO (*P* = 0.031); MAG: *n* = 5 C and 4 pIKO (*P* = 0.18); MOG: *n* = 5 C and 4 pIKO (*P* = 0.54). GAPDH, glyceraldehyde 3-phosphate dehydrogenase. e–h, Immunofluorescent staining of MBP in cerebellar lobule VII in males (e and f) and females (g and h). Scale bar, 150  $\mu$ m. i, Scanning

electron microscopy acquisition of a whole cerebellum ultrathin section showing the different cerebellar lobules (I–X) in a control mouse ( $\times 650$  low magnification). The region of interest (inter-lobule VI–VII) for high-magnification acquisitions and g-ratio quantifications is indicated by the yellow rectangle. Scale bar, 300  $\mu\text{m}$ . j, Schematic representation of an axon and its myelin sheath illustrating g-ratio. r, axon inner diameter; R, axon outer diameter. k–n, Representative scanning electron microscopy acquisitions ( $\times 20,000$ ) of myelinated axons in inter-lobule VI–VII WM in males (k and l) and females (m and n). Scale bar, 300 nm. o, Scatter plot of g-ratios of  $>400$  individual axons in males; data are from one representative control and one representative pIKO mouse. Fitted lines are linear regressions. p, Percent of unmyelinated axons. Data are presented as mean  $\pm$  s.e.m. Two-tailed unpaired Student's *t*-test with Welch's correction ( $*P < 0.05$ ).  $n = 3$  C and 3 pIKO ( $P = 0.0275$ ). q, Scatter plot of g-ratios of  $>400$  individual axons in females; data are from one representative control and one representative pIKO mouse. Fitted lines are linear regressions. r, Percent of unmyelinated axons. Data are presented as mean  $\pm$  s.e.m. Two-tailed unpaired Student's *t*-test with Welch's correction ( $*P < 0.05$ ).  $n = 3$  C and 3 pIKO ( $P = 0.0194$ ). s, g-ratios by axon caliber category in males. Data are presented as mean  $\pm$  s.e.m. Two-way ANOVA with Sidak's multiple comparisons test ( $*P < 0.05$ ).  $n = 3$  C and 3 pIKO ( $<1 \mu\text{m}$ :  $P = 0.0299$ ;  $>1 \mu\text{m}$ :  $P = 0.0165$ ). t, Axon caliber distribution in males ( $n = 3$  C and 3 pIKO). u, g-ratios by axon caliber category in females. Data are presented as mean  $\pm$  s.e.m. Two-way ANOVA with Sidak's multiple comparisons test ( $*P < 0.05$ ).  $n = 3$  C and 3 pIKO ( $<1 \mu\text{m}$ :  $P = 0.0162$ ;  $>1 \mu\text{m}$ :  $P = 0.1185$ ). v, Axon caliber distribution in females ( $n = 3$  C and 3 pIKO).

## **Placental ALLO insufficiency leads to autism spectrum disorder-like behaviors in males**

Although the cerebellum is classically associated with coordination and motor learning, recent acknowledgement of its role in cognitive processing and emotional control has come to the forefront. [163, 164] This is becoming apparent with the increased association between cerebellar impairments, specifically cerebellar WM abnormalities and ASD symptoms [223-226]. Since our mice exhibit these deficits, we next tested whether placental ALLO loss results in autistic-like traits in our mice. To assess behavioral sex-linked differences between C and pLKO mice in early postnatal development, ultrasonic vocalizations (USVs) emitted by the pups when separated from the dam were evaluated as a measure of early communicative behavior. This revealed pLKO males produced fewer USVs than their littermate controls when separated from the dam (Fig. 5a). By contrast, no significant change was evidenced in the pLKO females (Fig.4b). This data is consistent with previously described deficits in isolation calling response described in other models of ASD [227]. To determine whether sex-specific ASD traits extended into adulthood of mice with placental ALLO loss we completed the three-chamber social behavior test which revealed significant deficits in social interaction in pLKO males but not females (Fig. 5c). Spontaneously behaving mice were then assessed for stereotyped motor behavior which revealed male specific defects, particularly with gnawing (Fig.5 d,e). In addition, male pLKO mice spent less time digging spontaneously or during a marble burying test. Difficulties in social interactions and motor stereotypies are two ASD hallmarks, especially in males [211]. In addition, both increased and decreased digging and marble burying were noted as secondary ASD-like features related to emotional state and anxiety in several genetic ASD mouse models [228, 229].

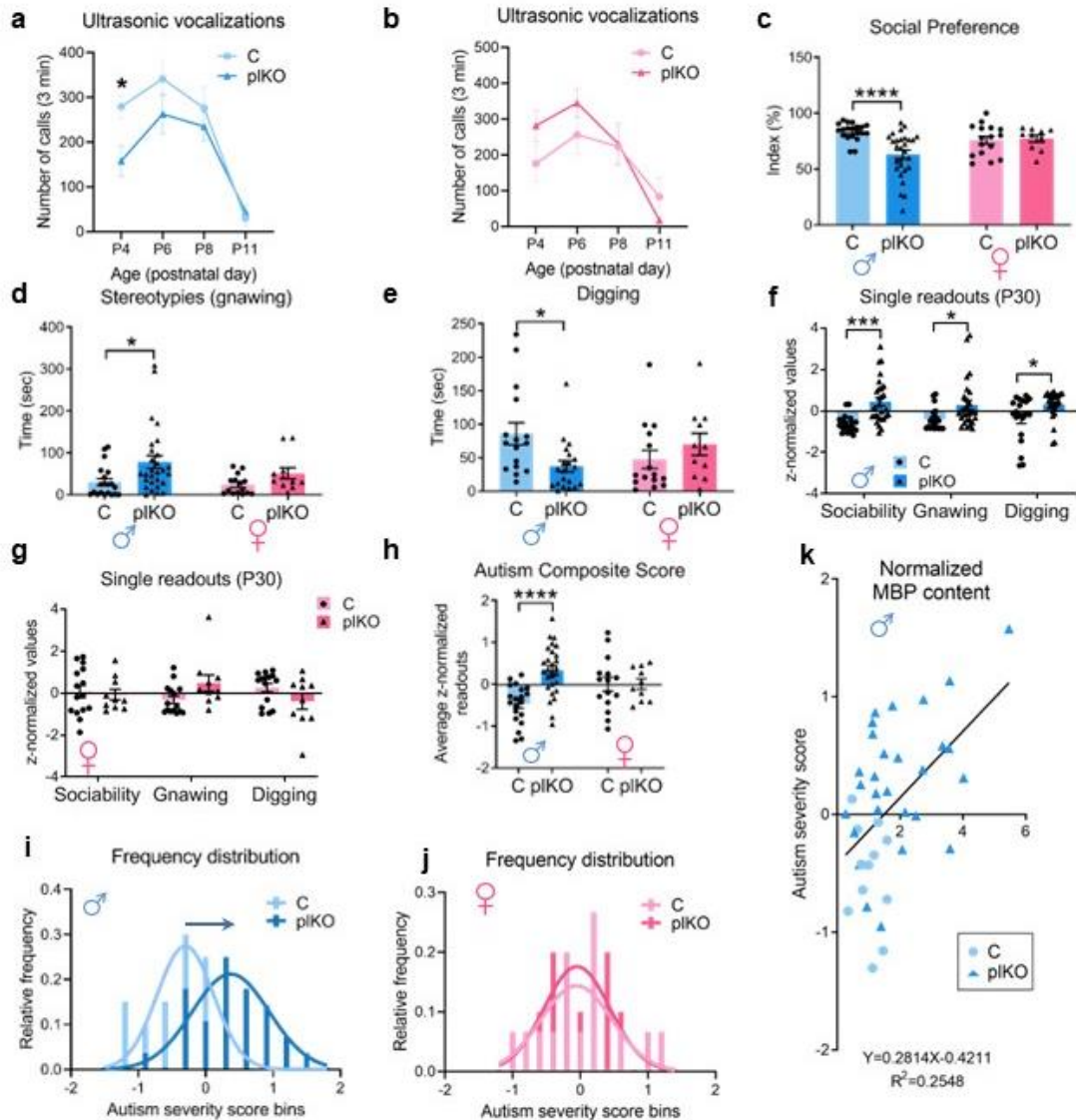


**Figure 5. Male plKO mice exhibit ASD-like behavior.** **a,b** USVs at P4, P6, P8 and P11. **Individual pups, males a,** and females **b,** were separated from the dam and littermates, and their calls were recorded for 3 min. Data are presented as mean  $\pm$  s.e.m. Two-way repeated measures ANOVA followed by Sidak's multiple comparisons test ( $*P < 0.05$ ). Males:  $n = 13$  C and 15 plKO (P4:  $P = 0.0378$ ; P6:  $P = 0.5714$ ; P8:  $P = 0.9299$ ; P11:  $P = 0.9609$ ); Females:  $n = 7$  C and 7 plKO (P4:  $P = 0.4587$ ; P6:  $P = 0.6051$ ; P8:  $P > 0.9999$ ; P11:  $P = 0.7135$ ). **c,** Three-chamber sociability test at P30. Data are presented as mean  $\pm$  s.e.m. Two-way ANOVA with Sidak's multiple comparison test ( $****P < 0.0001$ ). Males:  $n = 20$  C and 28 plKO ( $P = 0.0001$ ); Females:  $n = 16$  C and 10 plKO ( $P > 0.9999$ ). **d,** Spontaneous gnawing time over 15 min at P30. Data are presented as mean  $\pm$  s.e.m. Two-way ANOVA with Sidak's multiple comparison test ( $*P < 0.01$ ). Males:  $n = 20$  C and 28 plKO ( $P = 0.0094$ ); Females:  $n = 15$  C and 11 plKO ( $P = 0.3982$ ). **e,** Spontaneous digging time over 15 min at P30. Data are presented as mean  $\pm$  s.e.m. Two-way ANOVA with Sidak's multiple comparison test ( $*P < 0.05$ ). Males:  $n = 20$  C and 28 plKO ( $P = 0.0148$ ); Females:  $n = 15$  C and 11 plKO

( $P = 0.4781$ ). f, z-standardized single significant behavior readouts that are integrated into the autism composite score in males at P30. Data are presented as mean  $\pm$  s.e.m. Two-way ANOVA with Sidak's multiple comparisons test ( $*P < 0.05$ ;  $***P < 0.0005$ ).  $n = 20$  C and 28 pIKO. Sociability:  $P = 0.0002$ ; Gnawing:  $P = 0.0239$ ; Digging:  $P = 0.0301$ . g, z-standardized single significant behavior readouts that are integrated into the autism composite score in females at P30. Data are presented as mean  $\pm$  s.e.m. Two-way ANOVA with Sidak's multiple comparisons test.  $n = 15$  C and 10 pIKO. Sociability:  $P = 0.9802$ ; Gnawing:  $P = 0.1419$ ; Digging:  $P = 0.2979$ . h, ASD composite severity score at P30. Data are presented as mean  $\pm$  s.e.m. Two-way ANOVA with Sidak's multiple comparison test ( $****P < 0.0001$ ). Males:  $n = 20$  C and 28 pIKO ( $P < 0.0001$ ); Females:  $n = 16$  C and 10 pIKO ( $P > 0.9997$ ). i,j, Relative frequency distribution of autism composite score bins at P30. Males:  $n = 20$  C and 28 pIKO; Females:  $n = 16$  C and 10 pIKO. k, Positive correlation between cerebellum MBP levels determined by western blot (normalized with GAPDH) and autism severity score in males at P30 ( $n = 12$  C and 28 pIKO). Linear regression. Deviation from zero:  $P = 0.0009$ . GAPDH, glyceraldehyde 3-phosphate dehydrogenase.

## **ASD-like symptom severity correlates with cerebellar MBP level**

In order to summarize our behavioral findings, we computed an autism severity composite score utilizing previously established scoring systems [212]. Behavioral measures were standardized using z-scores, with higher values indicating greater symptom severity. Notably, individual behavioral scores were significantly elevated in pIKO males compared to control (C) males, but not in females (refer to Fig. 5f,g). Consequently, the combined z-scores resulted in an increased autism severity score among males (see Fig. 5h). Analysis of the relative frequency distribution of individual autism severity scores revealed Gaussian distribution curves diverged in pIKO males, shifting towards the right along the x-axis (see Fig. 5i,j). It is noteworthy that certain pIKO mice displayed scores akin to those of control mice, indicating a spectrum of behavioral alterations in male pIKO specimens. This variability may arise from inherent differences in placental progesterone and ALLO levels, variable deletion of *akr1c14*, the heterogeneous genetic background of the mice, or subtle variations in hormone exposure attributable to the *in-utero* position of the fetus.

Since transient WM hyperplasia, myelin thickening and/or over-expression of OL lineage and myelin markers such as *olig2*, *mbp* and *mag* have been documented in the cerebellum of patients with ASD [225, 226] and several genetic ASD-like mouse models [230, 231] we were interested in investigating this link in our model. We used the autism severity scores to assess the correlation between these symptoms and cerebellar MBP levels and found a significant positive correlation in pIKO males (Fig.5k). The abnormal maturation speed of the OL lineage in pIKO mice suggests dynamic, rather than uniform, changes of WM development, similar to the pattern seen across the lifespan of patients with ASD [225]. Overall, our placental mouse model

recapitulates several characteristics of human studies, including the male greater vulnerability to perinatal brain injuries and ASD [226, 232].

### **Myelin genes show similar sex divergence in preterm infants and plKO mice**

To evaluate the translational value of our findings, we asked whether human preterm birth, a condition characterized by premature loss of placenta and a risk factor for ASD [233], showed similar sex differences in cerebellar myelination as seen in our plKO mice. We examined 24 postmortem cerebellar vermises from term (>37 weeks of gestation) and preterm (<34 weeks of gestation) infants who died at a mean corrected age of 6 weeks. (Fig. 6a-c and Appendix D) MBP expression in preterm males and females showed compelling similarities with our plKO mice (Fig. 6d–h,k). Similarly, the migration downshift of MAG on western blots of preterm male cerebella suggests a similar accelerated maturation of myelin (Figs. 4a, 6d). The higher levels of *pdgfra*- and *cspg4*-mRNA in the cerebellum of preterm males also suggest increased OPC proliferation (Fig. 6i,j,l) as temporarily seen in the plKO males (Fig. 3e). This striking similarity between mice with placental ALLO loss and infants born preterm suggests that altered ALLO exposure might contribute to abnormal preterm brain development.

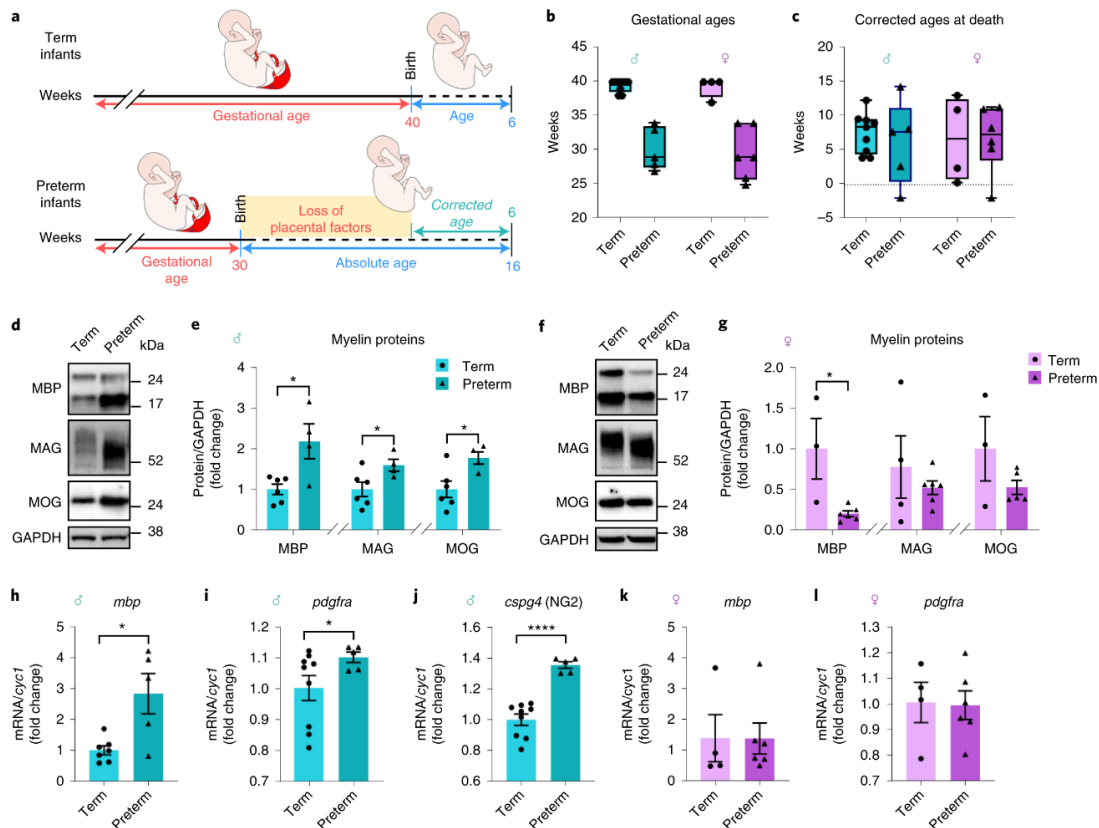


**Figure 6 Myelin proteins are dysregulated in a sex-linked manner in the cerebellar vermis of preterm infants** a, Schematic of the age terminology during the perinatal period used for the human study. b, Distribution of donors' gestational age at birth. c, Distribution of donors' corrected age at death. Graphs in b and c show box and whisker plots (including minima, maxima and median values) with single values. d,e, Western blot analysis of myelin-related proteins in the cerebellar vermis of term and preterm male infants at an average corrected age of 6 weeks. Data are presented as mean fold changes  $\pm$  s.e.m. ( $n = 6$  T and 4 PT). Multiple unpaired  $t$ -tests with Holm–Sidak multiple comparison test (\* $P < 0.05$ ). MBP:  $P = 0.014$ ; MAG:  $P = 0.044$ ; MOG:  $P = 0.024$ . f,g, Western blot analysis of myelin-related proteins in the cerebellar vermis of term and preterm female infants at an average corrected age of 6 weeks. Data are presented as mean fold changes  $\pm$  s.e.m. Multiple unpaired  $t$ -tests with Holm–Sidak multiple comparison test (\* $P < 0.05$ ). MBP:  $n = 3$  T and 6 PT ( $P = 0.015$ ); MAG:  $n = 3$  T and 6 PT ( $P = 0.169$ ); MOG:  $n = 3$  T and 5 PT ( $P = 0.179$ ). h–j, qRT–PCR for myelin- and OL-related genes normalized to *cyc1* in male infants. Data are presented as mean fold changes  $\pm$  s.e.m. Two-tailed unpaired Student's  $t$ -test with Welch's correction (\* $P < 0.05$ , \*\*\*\* $P < 0.0001$ ). *mbp*:  $n = 7$  T and 5 PT ( $P = 0.046$ ); *pdgfra*:  $n = 9$  T and 5 PT ( $P = 0.0482$ ); *cspg4*:  $n = 9$  T and 5 PT ( $P < 0.0001$ ). k,l, qRT–PCR for myelin- and OL-related genes normalized to *cyc1* in female infants. Data are presented as mean fold changes  $\pm$  s.e.m. Two-tailed unpaired Student's  $t$ -test with Welch's correction. *mbp*:  $n = 4$  T and 6 PT ( $P = 0.9923$ ); *pdgfra*:  $n = 4$  T and 6 PT ( $P = 0.9122$ ). *Cspg4*, chondroitin sulfate proteoglycan 4 gene; *Cyc1*, cytochrome C1 gene; GAPDH, glyceraldehyde 3-phosphate dehydrogenase; *Pdgfra*, platelet-derived growth factor receptor alpha gene. PT, preterm; T, term.

## **ALLO or GABA<sub>A</sub> agonist rescues cerebellar and behavioral impairments**

To test whether ALLO administration has therapeutic potential for cerebellar white matter and behavioral abnormalities, we treated mice with either ALLO (10 mg kg<sup>-1</sup>) or vehicle (sesame oil) to dams carrying mixed litters at E15.5, the period of maximal difference of ALLO levels in the plKO mice compared to C. This single injection was sufficient to prevent the increased MBP expression in the cerebellum (Fig. 7a), to normalize OL density (Appendix E. a) and reduce autism severity scores (Fig. 7b,c).

To assess the role of GABA<sub>A</sub>R signaling in the ALLO rescue, muscimol (1 mg kg<sup>-1</sup>), a selective GABA<sub>A</sub> agonist, was administered instead of ALLO. Muscimol injection resulted in similar molecular and behavioral rescue in plKO males (Fig. 7a-c), although the contribution of other minor, GABA<sub>A</sub>-independent ALLO actions cannot be completely excluded. [234-236]

Interestingly, some of the control mice given ALLO exhibited decreased social preference and higher autism scores, suggesting too much ALLO may also be detrimental. (Appendix E:b,c) Our findings underscore the potential therapeutic efficacy of administering ALLO during gestation, particularly in cases where ALLO or its precursors are identified to be deficient, as may occur in instances of chronic placental insufficiency. However, they also emphasize the importance of maintaining fetal ALLO exposure within an optimal physiological range.

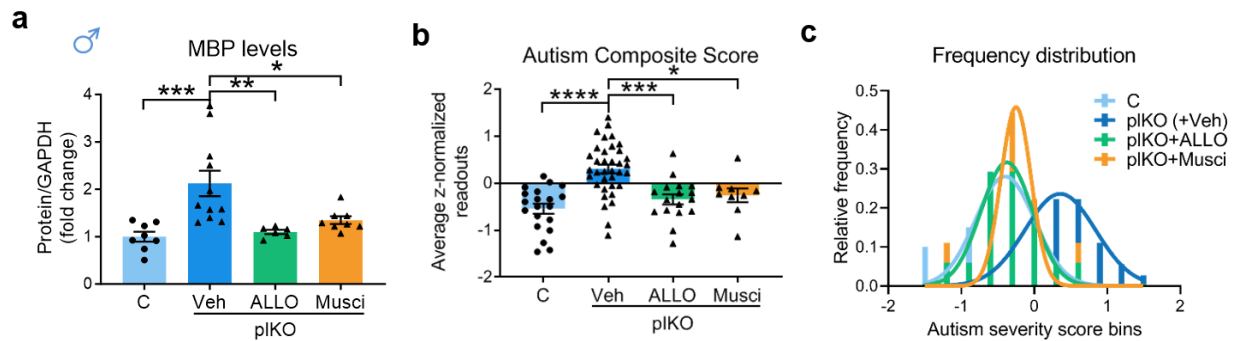


**Figure 7. ALLO or muscimol administration during late gestation rescues MBP expression and abnormal behaviors in pIKO males at P30** a, Western blot determination of MBP contents in the cerebellum at P30. Normalized data to GAPDH contents are presented as mean fold changes  $\pm$  s.e.m. Dams received an intraperitoneal injection of ALLO (10 mg kg<sup>-1</sup>) or muscimol (Musci; 1 mg kg<sup>-1</sup>) at E15.5. One-way ANOVA with Tukey's multiple comparisons test (\* $P < 0.05$ ; \*\* $P < 0.01$ ; \*\*\* $P < 0.005$ ).  $n = 8$  C, 11 pIKO+Veh, 6 pIKO+ALLO and 8 pIKO+muscimol. Comparisons: C versus pIKO+Veh:  $P = 0.009$ ; C versus pIKO+ALLO:  $P = 0.988$ ; C versus pIKO+muscimol:  $P = 0.607$ ; pIKO+Veh versus pIKO+ALLO:  $P = 0.0058$ ; pIKO+Veh versus pIKO+muscimol:  $P = 0.027$ ; pIKO+ALLO versus pIKO+muscimol:  $P = 0.8436$ . b,c, ASD composite score and frequency distribution of autism severity score bins at P30. pIKO and pIKO+Veh mice were combined because there was no significant difference between both groups (named pIKO(+Veh)). One-way ANOVA with Tukey's multiple comparisons test (\*\*\* $P < 0.005$ ; \*\*\*\* $P < 0.0005$ ).  $n = 20$  C, 3 pIKO(+Veh), 17 pIKO+ALLO and 9 pIKO+muscimol. Comparisons: C versus pIKO(+Veh):  $P < 0.0001$ ; C versus pIKO+ALLO:  $P = 0.6226$ ; C versus pIKO+muscimol:  $P = 0.4933$ ; pIKO(+Veh) versus pIKO+ALLO:  $P = 0.0002$ ; pIKO(+Veh) versus pIKO+muscimol:  $P = 0.0187$ ; pIKO+ALLO versus pIKO+muscimol:  $P = 0.9765$ . GAPDH, glyceraldehyde 3-phosphate dehydrogenase.

## Discussion

The present study delineates a pivotal role for placental ALLO in modulating sex-specific fetal brain developmental trajectories during late gestation, with discernible consequences extending into the postnatal period. While numerous neuroactive hormones synthesized by the placenta possess the capacity to influence processes such as neurogenesis, gliogenesis, and circuit formation, our focus centered on ALLO due to its characteristic surge during the latter half of gestation, coinciding with the onset of placental insufficiency and the occurrence of preterm birth. Moreover, ALLO has been implicated in various pregnancy complications linked to preterm birth and ASD, such as preeclampsia, wherein plasma ALLO levels are notably diminished [237]. Such associations serve to bolster the potential connection among ALLO, prematurity, and the risk of ASD.

The consistent observation of structural and functional abnormalities in the cerebellum stands out as a hallmark feature in brains affected by ASD, a finding reiterated across multiple studies [238-240]. This significance is further underscored by the elevated risk of ASD associated with early cerebellar injury or dysfunction, highlighting the pivotal role of the cerebellum in the pathophysiology of ASD [224]. The abnormalities often cited involve dysfunction in cerebellar Purkinje cells, and WM changes. Our initial cerebellar RNAseq analysis highlighted WM-associated pathways as a top category of altered genes with sex-specific features. Our transcriptomic findings were then validated by the apparent sex-specific alterations in OL lineage progression and myelination. Initially, oligodendrocyte density was calculated separately within each lobule to compare densities across the cerebellum with no statistically significant differences (unpublished). Therefore, the presented data represents OL density across the entire para-sagittal CB WM. When assessing myelin thickness, the lateral WM of the lobule VI/VII of the cerebellum

was specifically analyzed for this lobules function in social behavior and higher cognitive functioning [241] connecting these WM defects to the ASD-like behavioral pathologies. While it is well established that male and female brains may undergo distinct developmental trajectories, [111, 242]our findings indicate that despite the ALLO loss being placental in nature, the sex divergence in cerebellar myelination primarily manifests during the postnatal period. Furthermore, these sex-linked anatomical changes in cerebellar white matter are accompanied by sex-linked phenotypes in ASD-like symptoms.

The intricate sexual dimorphism observed subsequent to placental ALLO loss is shaped by numerous factors throughout prenatal and postnatal development. Our findings play a pivotal role in laying the groundwork for the development of hormone replacement strategies aimed at restoring the developmental milieu and ameliorating long-term neurobehavioral impairments. The concurrent rescue of both MBP expression and autism severity scores following ALLO and muscimol administration underscores the potential benefits of hormone replacement therapy for pregnant women. While muscimol exhibited comparable rescue effects to ALLO administration, it is essential to acknowledge that other ALLO actions, independent of GABA<sub>A</sub> receptors, might also contribute to these effects, such as its potential impact on inflammation. Furthermore, the full scope of the sex-specific white matter defects and their underlying mechanisms in this model remain incompletely understood. Analysis of WM in additional brain regions like the prefrontal cortex would enhance our understanding of the sex-specific impact of ALLO loss across the entire brain. Furthermore, while the increase in myelin thickness in pIKO males is transient, the behavioral phenotype is persistent (P60, unpublished data) suggesting other unexplored regions with WM defects may remain. It is imperative to delve deeper into the potential mechanisms driving these differences and to explore why the same prenatal insult can yield significantly

divergent postnatal outcomes based on sex. This insight will significantly enhance the translational impact of our research by enabling us to refine treatment strategies for prenatal insults associated with placental insufficiency, considering the sex-specific nuances.

## **Chapter 4: Microglia Alter Sex-linked Cerebellar Myelination following Placental Allopregnanolone Loss**

Contributions: I conceived of the project and designed the experiments. I analyzed the RNA sequencing data and produced Figures 8, 14a, Appendix F, Appendix H. I performed the RT-qPCR in Figures 12, 13, and Appendix I, the histology and cell counting in Figure 11, the flow cytometry experiments in Figures 11, 12, and 13 and the protein extraction and cytokine/ELISA analysis in Figures 9 and 14b.

### **Abstract**

Placental insufficiency is linked to lifelong neurodevelopmental disorders. The frequency and expression of these disorders are often influenced by the sex of the offspring. To investigate placental hormone insufficiency in the generation of neurodevelopmental disorders, we previously developed a transgenic mouse line, *akr1c14cyp19aKO* (pIKO) in which there is a targeted reduction of placental allopregnanolone (ALLO), a neuroprotective and anti-inflammatory progesterone derivative that enters the fetal brain to modulate GABAergic responses. PIKO mice show sex-divergent alterations of cerebellar oligodendrocyte (OL) maturation leading to enhanced myelination in male and reduced myelination in female cerebellum, alterations in female corticogenesis and sex-specific behavioral deficits at postnatal day (P) 30. Although placental ALLO suppression is equal in males and females, the responses of the brain and placenta are distinct. Longitudinal time-course RNA sequencing demonstrated sex-linked differential expression of microglial and inflammatory genes, particularly in the cerebellum (CB) where significant white matter sex-linked differences occurred. Profiling of microglial cytokines revealed sex-specific inflammatory patterns, particularly those driven by Prostaglandin E2 (PGE2)/E-type

prostanoid receptor 4 (EP4). Microglial phagocytosis of myelin was also altered in a sex-linked manner, consistent with the sexually divergent myelination of pIKO mice. Finally, PGE2/EP4 pharmacological manipulation postnatally rescues the behavioral alterations in male pIKO. The loss of placental ALLO results in sex-linked microglial dysfunction and altered prostaglandin signaling that drives long-term neurodevelopmental impairments.

## **Introduction**

The role of placental endocrine support in normal brain development is often overlooked. Over 10% of pregnancies experience placental dysfunction, which can disrupt the placental endocrine support of fetal development, particularly the developing brain[2]. Limited neuroprotective interventions leave many of these infants at risk of cognitive and motor deficits [3, 24]. Identifying the hormones and mechanisms through which placental endocrine function supports brain development may have implications for the prevention and treatment of neurodevelopmental disorders in compromised pregnancies. Allopregnanolone (ALLO) is one such hormone, produced from progesterone in large quantity by the placenta during the second half of gestation[9, 85]. It is a positive allosteric modulator of the GABA<sub>A</sub> receptors that regulates a variety of neurodevelopmental processes such as neurogenesis and myelination[66, 83, 214]. ALLO also exhibits anti-inflammatory properties by inhibiting toll-like receptors (TLRs), and regulating cytokine expression [101, 102, 106, 243-247]. ALLO, however, has no glucocorticoid activity[248]. It has been proposed that placental ALLO helps maintain the immune balance of the intrauterine environment and protects the fetus against exogenous stressors [85, 249, 250].

We recently created a mouse model to investigate the impact of placental ALLO insufficiency on brain development. In this model named pIKO, the *akr1c14* gene, encoding the ALLO synthesis enzyme 3 $\alpha$ -hydroxysteroid dehydrogenase (3 $\alpha$ -HSD), is specifically ablated in

Cyp19-cre expressing trophoblasts [251], lowering placental ALLO production by 50% [9]. Neurodevelopment in the pKO mice revealed extensive sex differences across brain regions. In the cerebellum (CB), males display an increased oligodendrocyte (OL) maturation rate and thicker myelin, while females show an opposite phenotype. These sex differences in cerebellar myelination were paralleled by sex-specific neurobehavioral impairments in pKO mice, males exhibiting several autistic-like behavioral traits, including reduced sociability and increased stereotyped behaviors[9]. Interestingly, no such behavioral deficits were exhibited in female pKO. However, a female-predominant reduction in pyramidal neuron populations in the primary somatosensory cortex (S1) and accompanying deficits in novel object recognition were found [252].

Since ALLO production by the placenta peaks in late gestation, it is an attractive target for corrective treatment. However, to develop effective interventions, there is an increased need to understand the complex interplay between placental pathology, sex, and neurological disease. Many neurodevelopmental disorders exhibit sex bias in frequency, severity, and phenotypic presentation [8], but the mechanisms by which sex influences brain development are not well understood. The current study aims to decipher the mechanisms driving the sex-linked neurodevelopment trajectories of the pKO brain during the postnatal period.

## **Results**

### **Placental ALLO loss alters inflammatory pathways in the postnatal brain**

We conducted RNA sequencing (RNA-seq) analyses of the primary somatosensory cortex (S1), cerebellum (CB), and hippocampus at postnatal day 0, 7, 15, and 30 (P0, P7, P15, P30) on both male and female pKO and littermate controls (C) to characterize the regional, developmental and sex effects of placental ALLO loss. The Limma-Voom with duplicate correlation method was

used to account for multivariate data and align samples across regions from the same mouse [203-205, 214] (Appendix F a,b). After analyzing the significant differentially expressed genes (DEGs) using Ingenuity Pathway Analysis (IPA, Qiagen), we identified the key dysregulated canonical pathways as *phagosome formation* and *S100 Family signaling*. The CB was particularly affected, as indicated by the gene-set z-scores (Appendix Fc).

In exploring the number of cerebellar DEGs at each time point, we observed the most significant effects within the first postnatal week (Fig. 1a). A new differential expression analysis, factoring in both sex and genotype as variables, allowed us to generate DEGs that consider the interaction between both factors. Upon analyzing these new DEG lists in IPA, the top dysregulated canonical pathways were identified and included *pathogen-induced cytokine storm*, *multiple sclerosis signaling*, *pattern recognition receptors*, *retinoic acid receptor (RAR) activation*, and *interferon signaling* (Fig. 8b). Collectively, these pathways suggest an underlying inflammation. However, a more comprehensive understanding of their nuances and differences could be achieved by examining the specific gene lists and identifying the common target molecules within each pathway. While the *pathogen-induced cytokine storm* pathway primarily contained genes in the interleukin, cytokine, and chemokine families, the *multiple sclerosis signaling* pathway included inflammatory genes known to impact myelination and remyelination (*lif*, *mbp*, and *calpain* gene family) (Fig. 8c,d). Several toll-like receptor (*tlr*) genes were also involved in the majority of the implicated pathways. TLRs are well-established contributors to anti-inflammatory signaling, including in ALLO's anti-inflammatory activity[101, 102]. Together with the variations in the number of inflammation related DEGs across the postnatal period (Fig. 8e), these results highlight the predominant inflammatory profile in the CB, with the most dynamic changes occurring within the first postnatal week.

## **The pIKO cerebellum shows sexually divergent inflammatory profiles across the lifespan**

Given that inflammation-associated genes contribute to the sex-linked alterations of postnatal pIKO neurodevelopment, we next identified the differences in inflammatory profiles between the male and female cerebellum. Mouse 45-Plex Discovery Assay Array #MD45 (Eve Technologies, Calgary, Canada) revealed distinct patterns. Female pIKOs showed a progressive anti-inflammatory response, characterized by escalating levels of anti-inflammatory cytokines such as LIF, IL-9, m-CSF, and Timp1, and a consistent reduction in pro-inflammatory cytokines such as IL-12p70, MCP-1 (Fig. 9a,c; Appendix G a-m). The anti-inflammatory effects in females become more pronounced as they mature. In contrast, males did not show a similar anti-inflammatory pattern (Fig. 9b,c; Appendix G a-m). This complex evolution underscores the dynamic nature of the inflammatory milieu, highlighting a sex-dependent trajectory.

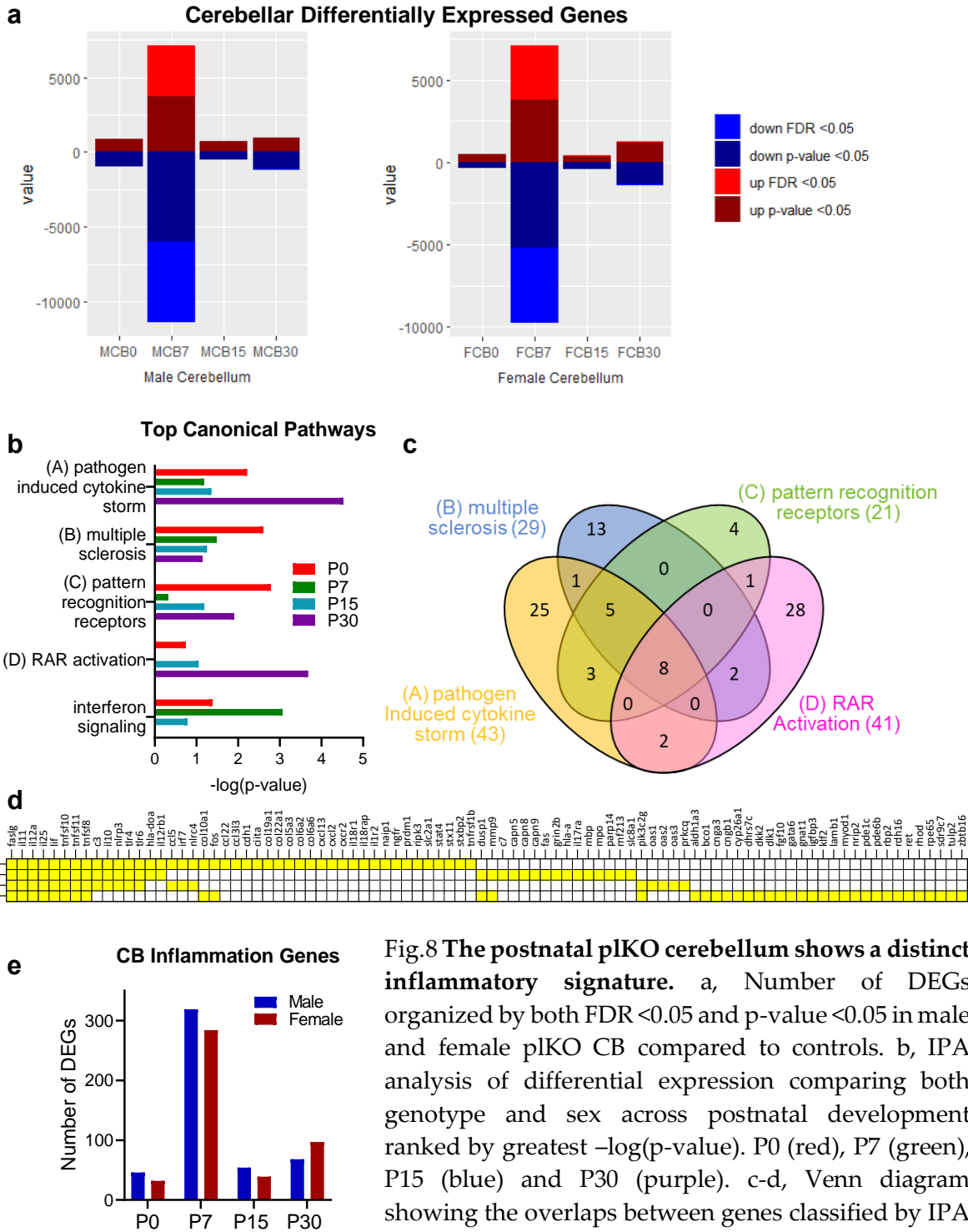


**Fig. 8 The postnatal plKO cerebellum shows a distinct inflammatory signature.** a, Number of DEGs organized by both FDR < 0.05 and p-value < 0.05 in male and female plKO CB compared to controls. b, IPA analysis of differential expression comparing both genotype and sex across postnatal development ranked by greatest  $-\log(p\text{-value})$ . P0 (red), P7 (green), P15 (blue) and P30 (purple). c-d, Venn diagram showing the overlaps between genes classified by IPA within each canonical pathway. e, Number of DEGs (p-value < 0.05) associated with inflammation across postnatal development. **Males in blue, females in red.**

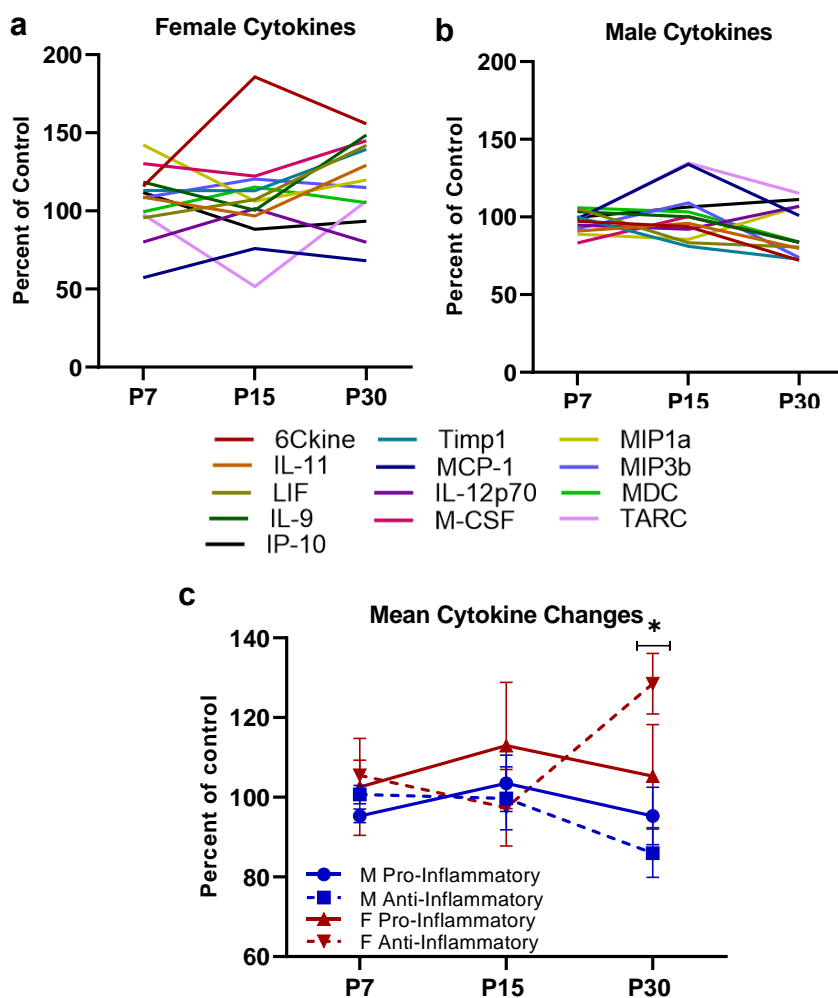
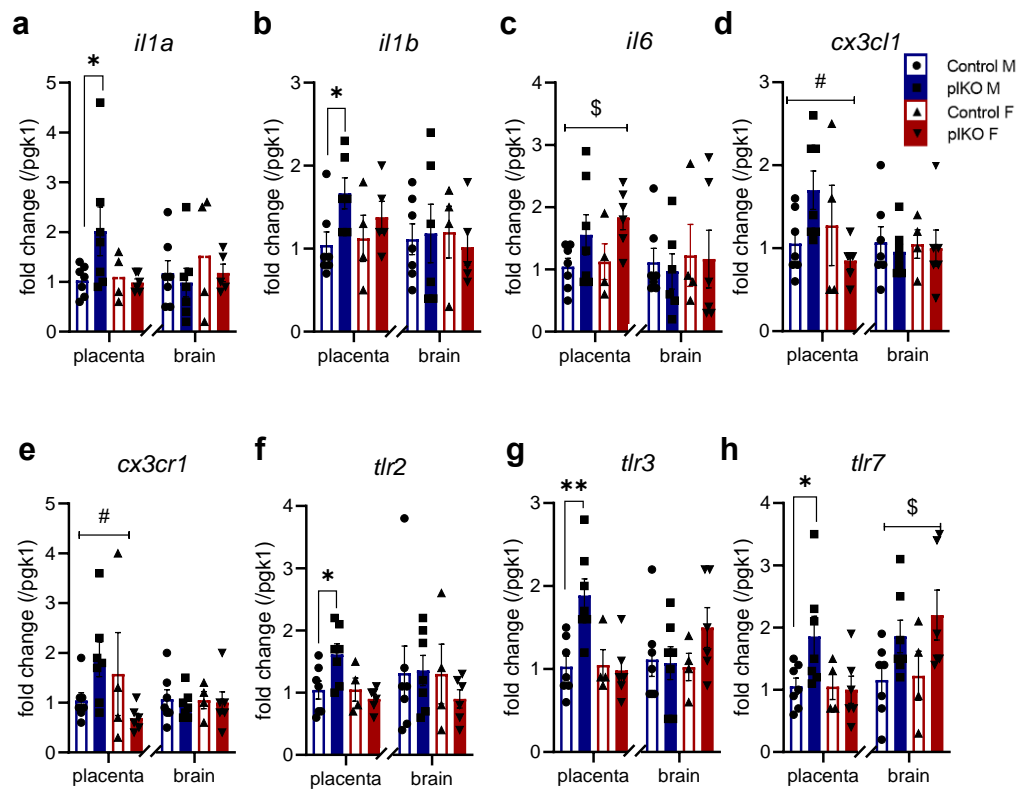


Fig. 9| **The pKO cerebellum shows a progressive anti-inflammatory cytokine signature in females but not in males.** a-b, Cytokine levels in whole cerebellar tissue across postnatal development were assessed by Mouse 45-Plex Discovery Assay Array #MD45 (Eve Technologies, Calgary, Canada). 13 cytokines were chosen based on significant difference at any time point (Extended Data Fig. 2). Cytokine level variation are presented as percent of control age matched values. c, Averaged cytokines classified as pro-inflammatory (MCP-1, MIP1a, MIP3b, IP-10, 6Ckine, and IL-12p70) and anti-inflammatory (TARC, MDC, IL-11, IL-9, Timp1, and LIF) are presented as percent of control age-matched animals compared across development. Data are presented as mean  $\pm$  s.e.m, n=7-8 animals per group. Three-way ANOVA comparing sex, genotype and age followed by Tukey's Post Hoc multiple comparison test. \*p < 0.05 (females)

### **Placental inflammatory response to ALLO loss differs by sex.**

The initial insult to the pIKO brain occurs embryonically and the initial prenatal inflammatory state could be generated by cells in either the fetal brain or the placenta itself. Tissue from embryonic paired brain and placenta was collected to assess the expression of critical inflammatory cytokines at embryonic day (E) 14.5, which corresponds to the most significant loss of *akr1c14* gene expression in the placenta [9](Fig. 10a-c). Gene expression of *il1a*, *il1b*, and *il6* showed a male predominant increase in the pIKO placenta, but not in the brain. (Fig. 10a-h) An acute inflammatory response that was detectable at the transcriptional level particularly in the male placenta but not the male embryonic brain suggests that the alterations in the inflammatory milieu following placental ALLO loss originate in the placenta itself, not the brain. Sex-linked postnatal brain changes likely originate from sex-linked placental inflammatory response due to ALLO loss, despite equal ALLO suppression in both male and female placenta[9].



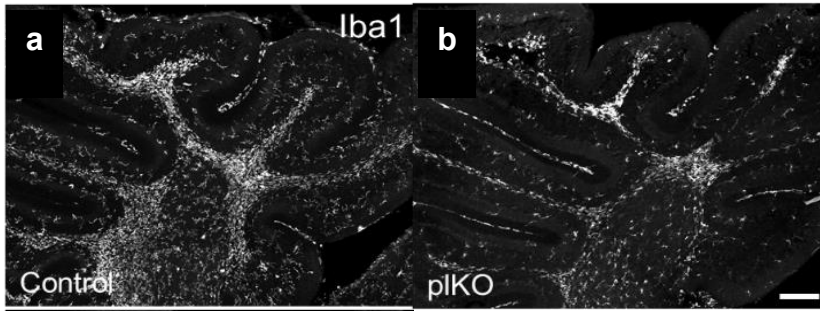
**Fig. 10| Embryonic inflammation is more predominant in male pIKO placentas.** a-h, Inflammation-related gene expression determined by RT-qPCR in paired E14.5 placenta and brain tissues. Data are presented as mean fold change  $\pm$  s.e.m. Two-way ANOVAs were performed comparing sex and genotype with Sidak Post Hoc multiple comparisons tests;  $n=7$  male controls,  $n=7$  male pIKOs,  $n=4$  female controls,  $n=6$  female pIKOs. \* $p < 0.05$ , \*\* $p < 0.01$ , significance between identified groups. # $p < 0.05$ , interaction between sex and genotype, \$ $p < 0.05$ , overall genotype effect (males in blue, females in red).

## **pIKO mice show sex- and age-specific alterations in cerebellar white matter microglia.**

Microglia, the resident immune cells of the brain, play crucial roles in regulating inflammation, influencing brain sexualization, and orchestrating developmental pruning across multiple cell types, including myelin [135]. Developmental heatmaps of microglia-enriched genes showed striking differences across genotype and sex, beginning in the first postnatal week and persisting through adolescence (P30) (Appendix H a-c). Analysis of the microglial distribution throughout the different cerebellar layers revealed a significant effect of sex and genotype in the developing white matter (Fig. 11a,b). Specifically, the density of microglia in the cerebellar white matter was significantly decreased in female pIKO at P7 and in male pIKO mice at P30, compared to their littermate controls (Fig. 11c).

We next determined the inflammatory profiles and phagocytotic capabilities of the cerebellar microglia. Using CD11b+ fluorescence-activated cell sorting (FACS) microglia were isolated from C and pIKO cerebella and assessed for CD86 and CD206 expression to identify any changes in pro-inflammatory and anti-inflammatory microglial populations, respectively (Fig. 11d-h). An increase in CD86+ and a decrease in CD206+ microglial percentages was observed in P7 pIKO females, suggesting an early but transient spike in pro-inflammatory microglia (Fig. 11 j,k). In contrast, the percentages of CD86+ and CD206+ cells were not significantly altered in the developing cerebellum of male pIKOs compared to their littermate controls (Fig. 11 j,k). Since microglia can regulate myelination through phagocytosis, phagocytosis was assessed *ex-vivo* using the pH indicator, pHRodo, conjugated to inactivated, unopsonized E. coli. At P7, there was a significant interaction effect between sex and genotype with a decrease in pIKO male phagocytosis and an increase in pIKO female phagocytosis (Fig. 11l). Both male and female pIKO mice showed

a transient genotype-based increase in pHRodo<sup>High</sup> microglia at P15 (Fig. 111). In sum, placental ALLO loss results in dynamic, sex-specific postnatal changes in the cerebellar white matter microglia, with altered activation and phagocytosis, highlighting the contribution of microglia to the observed myelination anomalies in the pKO cerebellum.



WM Microglia Across Development

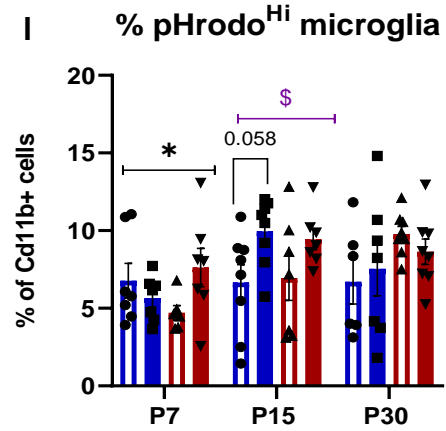
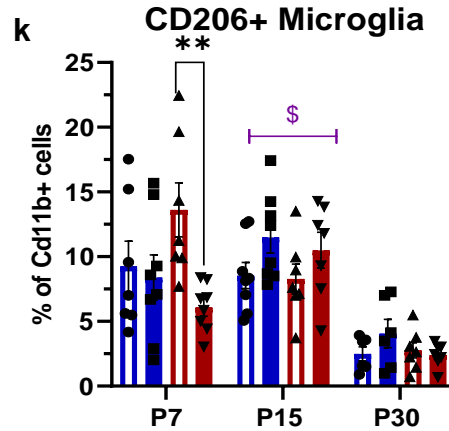
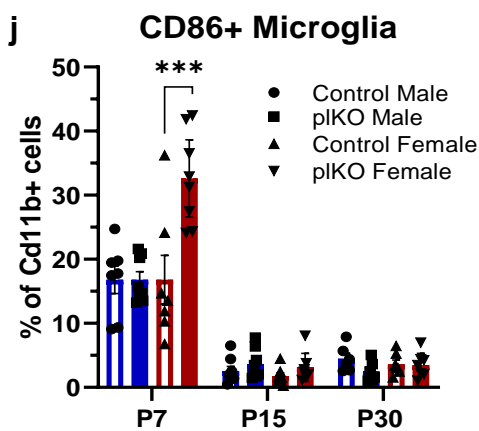
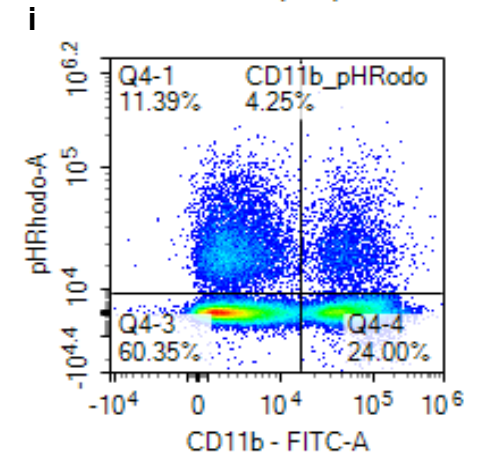
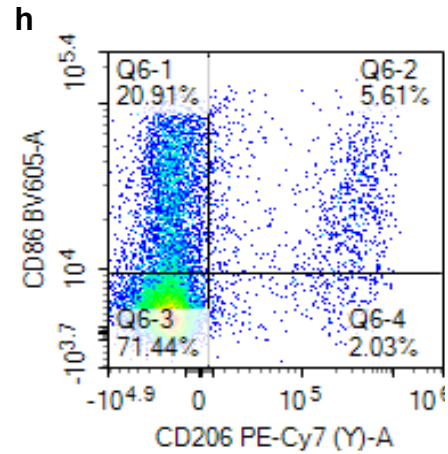
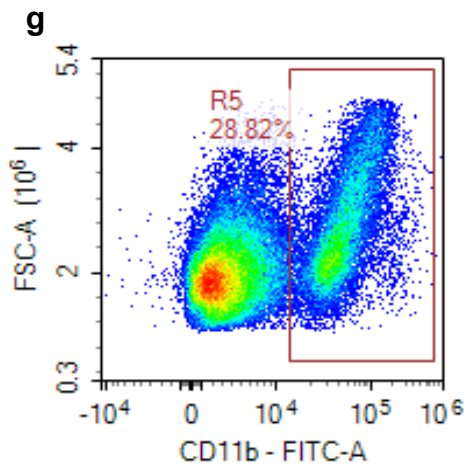
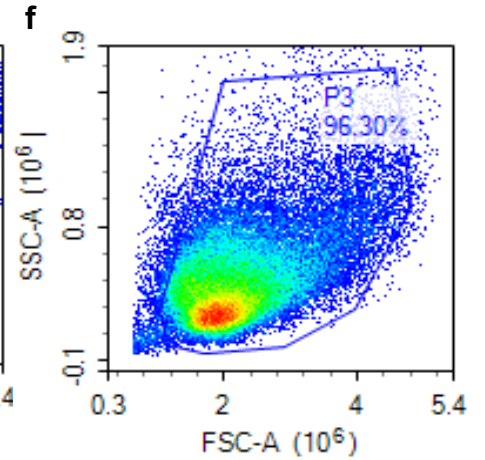
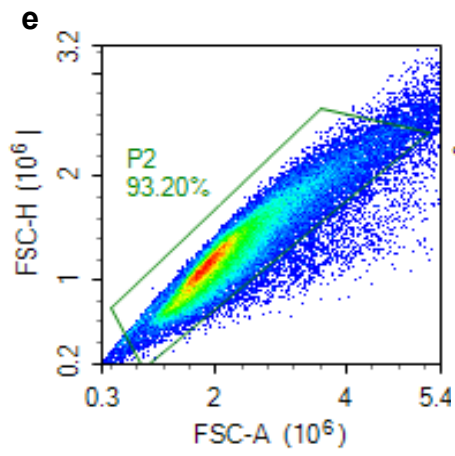
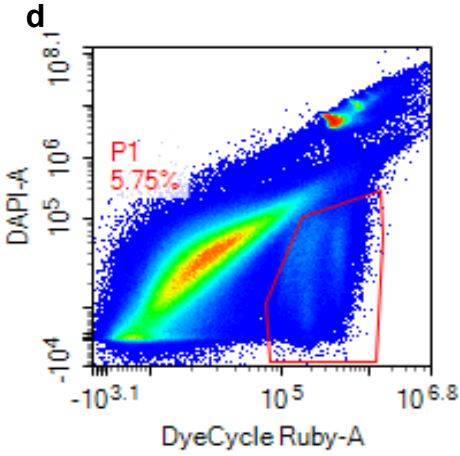
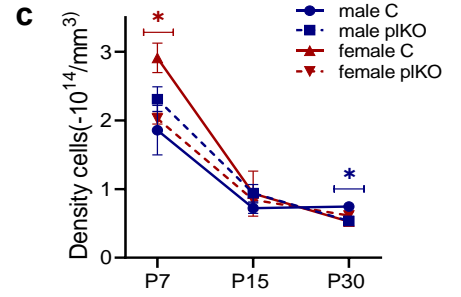


**Fig. 11 | pIKO microglia exhibit sex-linked functional differences in the postnatal cerebellum.** a-b, Representative sagittal sections of control and pIKO P7 female cerebellum immunostained for Iba1. c, Iba1+ cell densities in the cerebellar white matter (WM). Data are presented as mean  $\pm$  s.e.m. Three-way ANOVA comparing sex, age and genotype with Tukey's Post Hoc multiple comparisons tests. \* $p < 0.05$  (males in blue, females in red). d-i, Representative gating strategy of flow cytometry plots for live (DyeCycle Ruby+) CD11b+ microglia, and thresholding for CD206, CD86 and pHRodo. j-l, Percent of CD11b+ microglia expressing CD86, CD206 and pHRodo, respectively. Data are presented as mean  $\pm$  s.e.m. Two-way ANOVAs were completed at each age with Sidak Post Hoc multiple comparisons tests.  $n=5-9$  independent samples per group. \* $p < 0.05$ , \*\* $p < 0.01$ , \*\*\* $p < 0.001$  significance between identified groups. \$ $p < 0.05$ , overall genotype effect (statistics symbols: males in blue, females in red, combined sexes in purple).

## **pIKO mice show sex and genotype linked differences in microglial phagocytosis machinery.**

To characterize the mechanisms underlying altered phagocytosis suggested by the shift in pHrodo-positive microglia, an extensive gene expression analysis on sorted CD11b+ microglia was done, focusing on genes regulating phagocytic targeting, engulfment, and lysosome acidification. Consistent with the FACS data, phagocytosis-associated gene expression was most significantly altered at P15, particularly in males. While many genes involved in phagosome acidification such as *lamp1*, *ctsd* and *cd68* exhibited sustained expression elevation, many of the genes vital to microglial phagocytosis such as *axl*, *merlk*, *tyrobp* and *lgals1/3* show decrease in expression by P30 in male pIKO (Fig. 12a).

We further analyzed the expression of *sirpa*, a key gene that inhibits microglial phagocytosis by preventing necessary cytoskeletal rearrangement in CD11+ cells (Fig. 12b). At P7, *sirpa* gene expression increased in female pIKO microglia compared to their male pIKO littermates (Fig. 12c). Conversely, a significant upregulation of *sirpa* expression was observed in male pIKO microglia compared to female pIKO microglia at P15 (Fig. 12c). This was accompanied by opposite regulation on cofilin-1 (*cfl1*) gene expression in the same pool of sorted microglia (Fig. 12d). Cofilin-1, a cytoskeletal rearrangement protein that promotes phagosome formation, is negatively regulated by SIRP $\alpha$  ([253]; Fig. 12b). Since microglial SIRP $\alpha$  is known to bind to CD47 on myelin and inhibit all other “eat me” signals necessary for phagocytosis [150], these findings suggest a male-dominant mechanism that impedes the proper functioning of the phagocytic machinery in pIKO microglia.

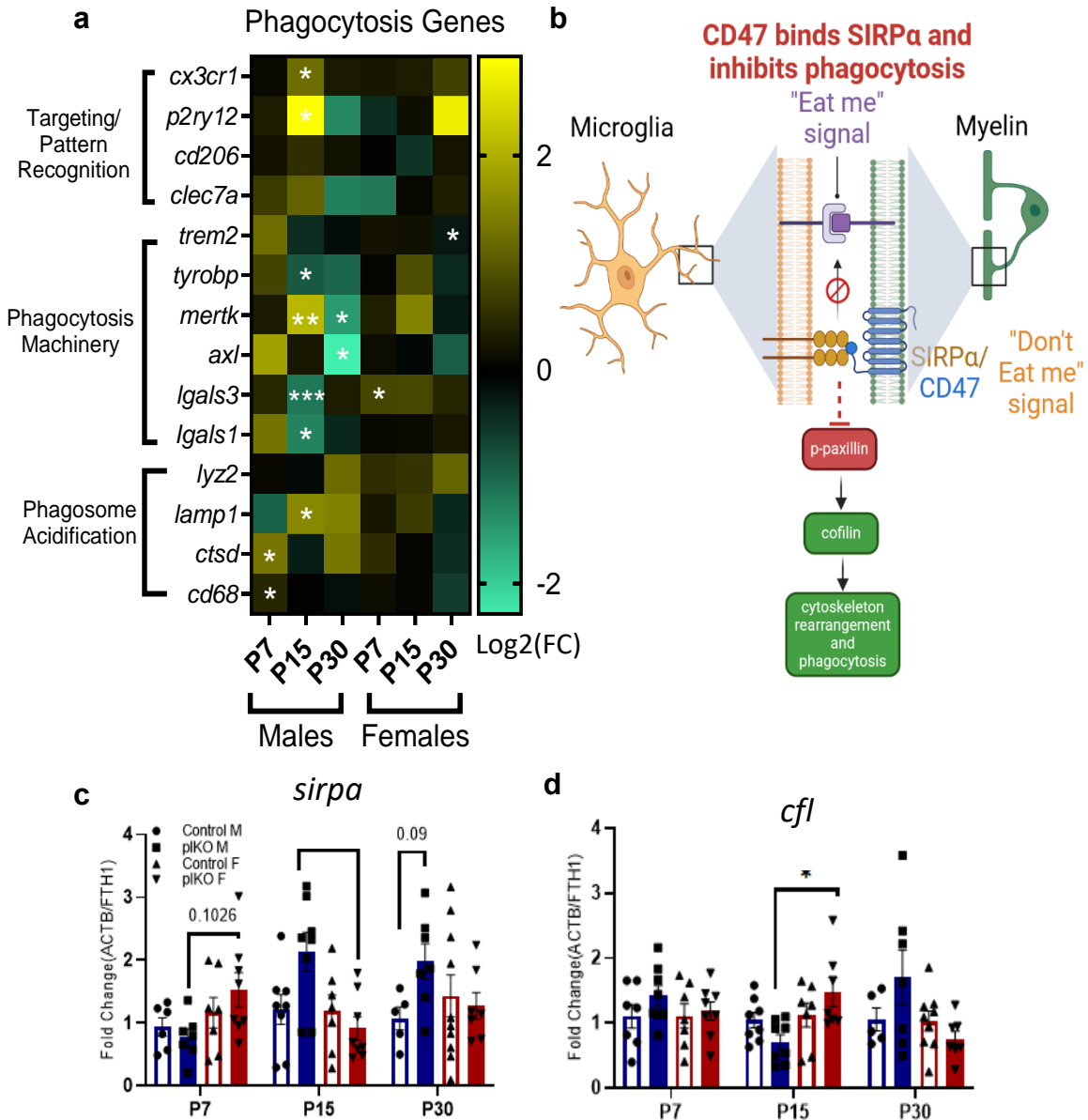


Fig. 12| **plKO males exhibit altered cerebellar phagocytosis machinery.** a, Heatmap representing Log<sub>2</sub> fold changes in phagocytosis-related gene expression determined by high throughput RT-qPCR (Biomark™ HD System) on sorted microglia. Multiple t-tests between genotypes at each age, for each sex without assuming consistent SD ( $\alpha=0.05$ ). Results are presented as log<sub>2</sub>FC; n=5-10 independent samples per group. \*p < 0.05, \*\* p < 0.01, \*\*\* p < 0.001. b, Schematic of SIRP $\alpha$  function in binding CD47 and overriding phagocytic signals. SIRP $\alpha$  on the surface of microglia are proposed to bind to CD47 on myelin and inhibit necessary cytoskeletal rearrangement that promotes phagocytosis. (Gitik, Liraz-Zaltsman et al. 2011). c-d, RT-qPCR for both *sirpa* and *cfl1* expression in microglia. Data are presented as mean  $\pm$  s.e.m. Two-way ANOVAs were completed at each age with Sidak Post Hoc multiple comparisons tests. n=5-10 independent samples/group. \*p < 0.05, \*\* p < 0.01

## Male pIKO microglia engulf fewer myelin components.

We next hypothesized that the phagocytosis of myelin by pIKO microglia was altered in a sex-linked manner, contributing to the cerebellar myelin phenotype of our model. Given that myelin proteins, including myelin basic protein (MBP), and myelin oligodendrocyte glycoprotein (MOG), are translated locally [254], we reasoned that myelin-related mRNA may be detected in sorted microglia that recently phagocytosed myelin. In male pIKO microglia, we observed a significant decrease in *mbp* transcript levels at P15 and P30 (Fig. 13a). Female pIKO microglia showed an increase in *mbp* mRNA within sorted microglia at P7 (Fig. 13b). A similar trend emerged when we expanded the analysis to other myelin markers (*mog*, *plp1*) (Appendix Ia-c). Linear regression analysis demonstrated a significant negative correlation between *sirpa* gene expression and *mbp* mRNA content in microglia (Fig. 13c). While both male and female pIKO cerebellum show increased microglia phagocytosis, the myelin component engulfment which differs in males and females may contribute to the myelination changes previously reported[9].

To validate the decreased myelin internalization by male pIKO microglia, we conducted imaging flow cytometry on male pIKO and control microglia at P15 (Fig. 13d). Internalized MBP staining within CD11b<sup>+</sup> cells showed a trend toward less internalized myelin in pIKO males at P15 compared to littermate controls (Fig. 13e). Colocalization of Lamp1 and MBP revealed that myelin fragments within microglia were primarily in lysosomes, confirming microglial engulfment of myelin for subsequent digestion (Fig. 13f).

To assess the role of SIRP $\alpha$  in inhibiting myelin phagocytosis, we used the small molecule inhibitor of the SIRP $\alpha$ -CD47 axis, RRx-001, to treat pIKO mice[255]. After replicating our pHRodo-based flow cytometry experiment with RRx-001 treatment, pIKO microglia displayed significantly elevated levels of phagocytic cells (Fig. 13g). In addition, RRx-001 treatment

normalized *mbp*-mRNA levels within sorted microglia (Fig. 13h). This further underscores the role SIRP $\alpha$  signaling in managing the microglial engulfment of myelin during development.

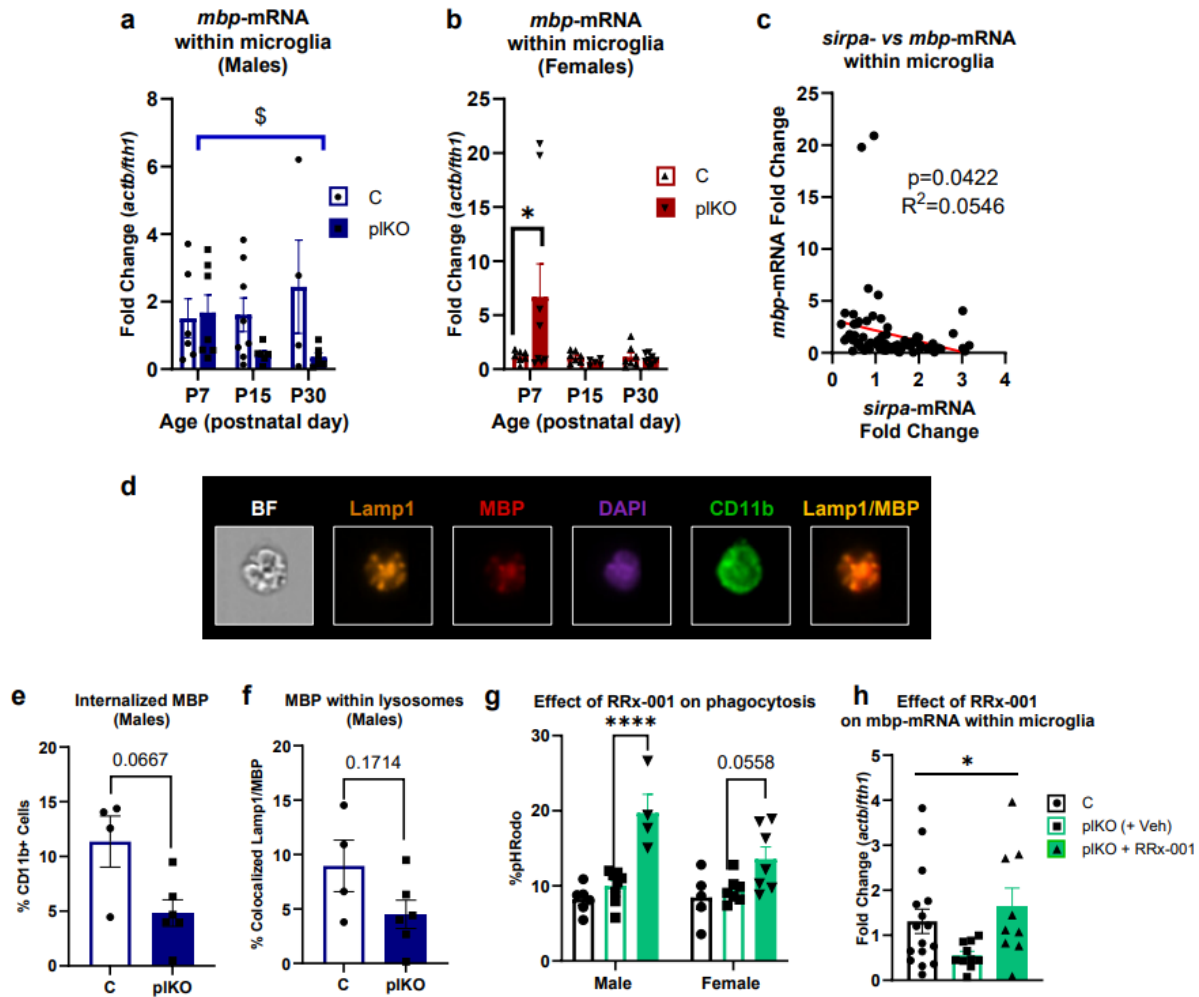


**Fig. 13 | MBP phagocytosis is altered in the pIKO microglia in a sex-linked manner.** a-b, RT-qPCR data of *mbp* found within sorted microglia. Data are presented as mean  $\pm$  s.e.m. Two-way ANOVAs were completed for each sex with Sidak Post Hoc multiple comparisons tests.  $n=5-10$  independent samples per group.  $*p < 0.05$ ,  $\$p < 0.05$  overall genotype effect. c, Pearson R correlation analysis between *sirpa*-mRNA levels and corresponding *mbp* transcripts in microglia.  $n=76$  samples. d, Representative images of cells from imaging flow cytometry. Cells were imaged at 60x magnification. e- f, Quantification of the flow cytometry imaging in P15 males for internalized MBP stain within CD11b+ microglia and for co-localization with lysosomal marker Lamp1. Data are presented as mean  $\pm$  s.e.m. Mann Whitney was completed comparing controls ( $n=4$ ) and pIKO ( $n=6$ ). g, Percent pHrodo positive CD11b microglia following 7 day treatment with RRx-001 (10 mg/kg/day; s.c.). Data are presented as mean  $\pm$  s.e.m. Two-way ANOVA was completed with Sidak Post Hoc multiple comparisons tests.  $n=4-7$  independent samples per group.  $****p < 0.0001$  h, Male and female combined *mbp* mRNA found within sorted CD11b+ microglia following 7 day treatment with RRx-001 (10 mg/kg/day; s.c.). Data are presented as mean  $\pm$  s.e.m. Kruskal-Wallis test was performed  $n=10-16$  independent samples per group.  $*p < 0.05$

## **Cerebellar PGE2 contributes to the sex-linked pIKO ASD-like behaviors.**

Using our time-course RNAseq, we identified the top upstream regulators predicted to drive these sex-linked transcriptional changes by the highest absolute z-scores. The top upstream regulators included *ptger4*, *cx3cl1*, and *trem2*, genes with well-recognized roles in inflammation, particularly concerning microglial pathology [18, 152, 180]. The most consistent upstream regulator candidate was the prostaglandin E2 (PGE2) receptor EP4 (*ptger4*). Prostaglandins are critical in microglial sexualization, particularly in the cerebellum where PGE2 promotes estradiol synthesis [178, 180]. The EP4 receptor, highly expressed in microglia, reduces inflammatory stimuli and promotes microglial phagocytosis [256]. When comparing female pIKO CB to male pIKO CB transcriptomes, IPA projections suggested a more activated *ptger4* pathway in males than females at P0 and P30 (positive z-scores), while the pathway was more activated in female pIKO CB at P7 and P15 (negative z-scores) (Fig. 14a). ELISA assessments showed reduced cerebellar PGE2 levels at P15 in male pIKOs and increased levels in females, compared to their respective littermate controls (Fig. 7b).

To assess the sex-specific impact of dysregulated PGE2 microglia and its role in the pIKO behavioral phenotype, mice were treated with the selective EP4 agonist, L-902,688, from P7 to P14, a critical time in brain sexualization. The previously described autism-like sex-specific behavioral defects in the pIKO mice [9], including sociability and spontaneous stereotypies, were then evaluated by calculating an ASD composite score. Treatment of pIKO mice with L-902,688 normalized pIKO behaviors to that of male controls (Fig. 14c), resulting in complete normalization of ASD composite scores (Fig. 14d,e). L-902,688 treatment did not affect female pIKO behaviors (Appendix J). These findings suggest that deficient EP4 prostaglandin signaling contributes to the ASD-like behavior in male pIKO mice and is amenable to rescue.

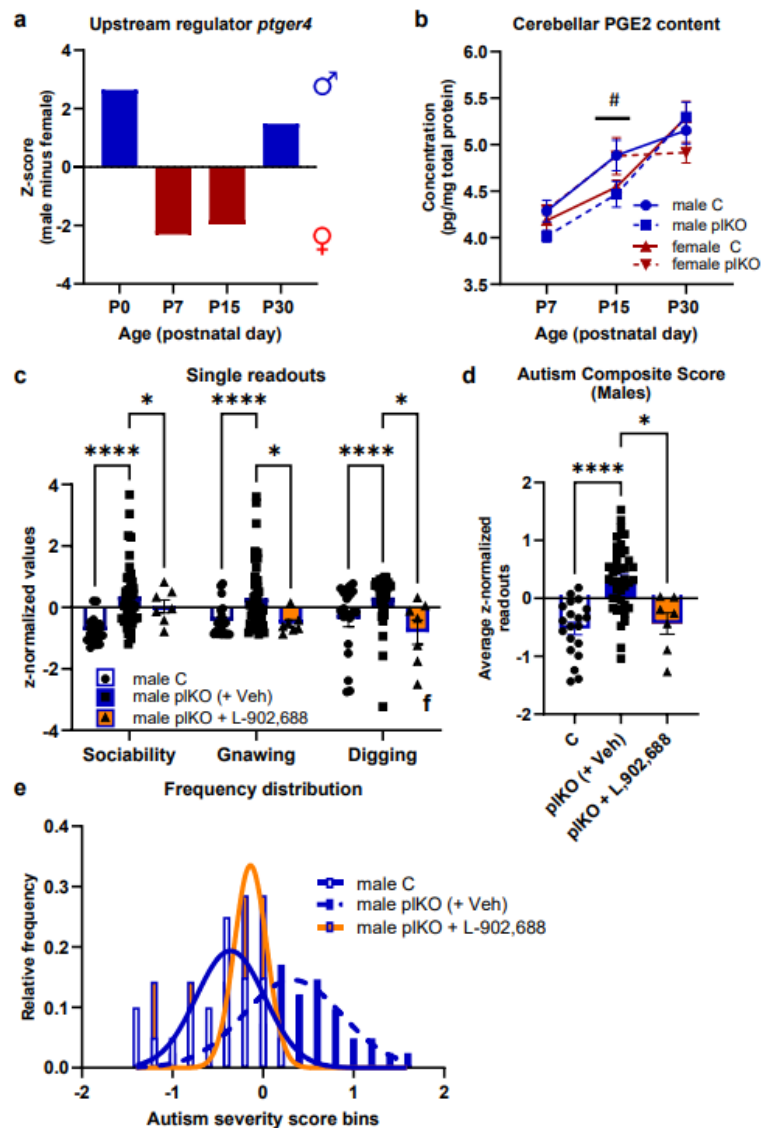


**Fig. 14 | Cerebellar PGE2 contributes to the sex-linked pIKO ASD-like behaviors.** a, Z-score plot for gene families regulated by *ptger4* at P0, P7, P15, and P30 comparing male pIKO (positive z-score) to female pIKO (negative z-score). b, PGE2 levels in the cerebellum at P7, P15 and P30 determined by ELISA. Data are presented as mean  $\pm$  s.e.m concentration (pg/mg of total extracted proteins). Two-way ANOVAs for sex and genotype were completed at each age with Sidak Post Hoc multiple comparisons tests.  $n=7-9$  independent samples/group. # $p < 0.05$ , sex vs. genotype effect. c, z-standardized single significant behavior readouts that are integrated into the autism composite score in males at P30 following 6-day injection series of PGE2 agonist, L-902688 (1 mg/kg/day; s.c.). Data are presented as mean  $\pm$  s.e.m. Two-way ANOVA with Tukey multiple comparison tests. d, ASD composite severity score in males at P30 following 6-day injection series of PGE2 agonist, L-902688 (1 mg/kg/day; s.c.). Data are presented as mean  $\pm$  s.e.m. Two-way

ANOVA with Sidak's multiple comparison tests. e, Relative frequency distribution of autism composite score bins at P30 following 6-day injection series of PGE2 agonist, L-902688 (1 mg/kg/day; s.c.). Data are presented as mean  $\pm$  s.e.m. In group "pIKO (+Veh)", mixed populations from non-injected and saline-injected animals are pooled as they show no significant behavioral differences. Control and pIKO group scores were published in Vacher, et al. 2021. n=7-41 animals per group.

## Discussion

Our longitudinal transcriptomic analysis across postnatal development in brain regions vulnerable to perinatal insults, considering sex and genotype as variables, revealed that inflammatory pathways are key contributors to the sexually dimorphic phenotype of the pIKO brain. This is particularly significant in the cerebellum, where the most pronounced sex-divergent phenotype is seen.

The placenta plays a critical role in regulating the intrauterine immunological state during pregnancy. Placental trophoblasts secrete cytokines and chemokines that maintain a balance between the relative immunosuppression needed for semi-allogeneic fetal development and an active immune response against potential intrauterine infections [1, 257, 258]. Maternal infection, placental inflammation, and elevated levels of pro-inflammatory cytokines are associated with neonatal brain damage and neurodevelopmental disorders[3]. Pregnancy pathologies like preeclampsia and preterm delivery are also associated with alterations in placental immune status[259-262]. High serum levels of IL-6 increase the risk of ASD in children, as well as in rodent models of maternal immune activation[263-265]. Our study suggests that high placental ALLO production is important in maintaining this immunological balance and may normally prevent prenatal inflammation-associated neurodevelopmental disorders, especially for male offspring. Our study provides strong evidence that non-infection related inflammation can be generated by specific placental hormone insufficiency and that this specific placental change can alter the inflammatory milieu of the developing brain through altered microglia function leading to long-term behavioral alteration.

Prior studies have shown that under normal conditions, female rodents and humans have less inflammatory signaling in the developing brain, while inflammation in the male brain

increases during the process of brain masculinization[266]. We hypothesized that decreased placental ALLO exposure would further increase these sex-linked developmental differences in the cerebellum. Indeed, insufficient placental ALLO resulted in increased anti-inflammatory cytokines across postnatal development in females, while male pKO cerebellum remained in an heightened inflammatory state. Many studies have suggested that exposure to placental inflammation brings male brains closer to a threshold of vulnerability that can be easily crossed if inflammation occurs during a sensitive developmental period, translating into higher risk of neurodevelopmental disorders. Our work points to a previously unrecognized mechanism, placental endocrine alteration, that may place male fetuses at increased risk of neurodevelopmental disorders.

Microglia, the main cellular mediators of the changes we describe, not only mediate and regulate neuroinflammation, but they also play a key role in shaping the sexually dimorphic brain [135]. Clusters of microglia are found in the developing WM, where they secrete factors regulating OL lineage cell survival, maturation, and apoptosis [16, 18, 146, 267]. They also regulate myelin production by phagocytosing excess OLs and improperly formed myelin membranes. Our flow cytometry results indicate an elevated phagocytic capacity in the cerebellar microglia of pKO cerebellum, particularly in males. Interestingly, this is accompanied by a reduced internalization of myelin components, such as OL-enriched transcripts and myelin proteins, in male pKOs. Conversely, we observed an increase in OL-associated transcripts in female pKO microglia. This new data links sex-divergent myelination anomalies in the pKO cerebellum[9] and male-specific neurobehavioral impairments with changes in microglial phagocytosis of myelin during postnatal development.

Treating pKO mice with RRx-001, an inhibitor of the SIRP $\alpha$ -CD47 axis, during the postnatal period normalized *mbp*-mRNA levels within sorted microglia, indicates that SIRP $\alpha$

signaling mediates the sex-linked altered engulfment of myelin in our model. SIRP $\alpha$  (Signal Regulatory Protein-alpha) is an immune inhibitory receptor that, when bound to its ligand CD47, overrides the "eat me" signals for phagocytosis. CD47, expressed on myelin, can inhibit myelin uptake when bound to SIRP $\alpha$ . Given the growing interest in the SIRP $\alpha$ -CD47 axis as a target for macrophage phagocytosis of tumors [255, 268], this signaling pathway may also be a promising candidate for promoting normal microglial pruning of hypermyelination.

Our study further identified prostaglandins, specifically the PGE2-EP4 signaling pathway, as mediators of sex-specific inflammatory responses and altered behavioral outcomes following placental ALLO loss. The EP4 receptor is highly expressed in microglia and typically restricts their response to inflammatory stimuli. The rise in circulating PGE2 in pIKO females precedes the increase in anti-inflammatory cytokine profile, consistent with previous reports of cerebellar PGE2 signaling contributing to downstream changes in cytokine secretion and in sexually dimorphic behavior[178]. PGE2 promotes estradiol synthesis in the cerebellum, particularly during the first two postnatal weeks of development when the myelination deficits develop in our mice[113, 269]. Here we show that inhibiting EP4 signaling in male pIKO mice during this developmental window prevents the onset of ASD-like behaviors, implicating impaired EP4 prostaglandin signaling in the expression of male-specific neurobehavioral alterations, and suggesting a new pathway that could be therapeutically targeted to reduce ASD-like pathologies. Our findings underscore the need for further investigation into mechanisms underlying sex differences in neurodevelopmental disorders to better tailor therapeutic interventions following pregnancy complications.

## **Chapter 5: General Discussion**

The placenta plays a vital role as the intermediary between maternal and fetal systems but is often overlooked for its production of neuroactive endocrine factors. Many pregnancy complications result in placental dysfunction leaving fetal brains vulnerable to injury and abnormal neurodevelopment. Despite improvement in clinical practices, the risk of neurodevelopmental disorders remains significant, but curiously display distinct differences in vulnerability depending on sex. Since early brain development is exposed to the uterine environment, a crucial look into how placental function is setting the stage for later sex specific neurodevelopmental trajectories is necessary.

### **Future directions for WM differences in pIKO**

White matter injury, primarily associated with prematurity, is rising as a leading outcome of many pregnancy complications and associated with lasting disabilities and neurodevelopmental disorders such as cerebral palsy, ASD and schizophrenia [270, 271]. Though myelin starts developing late in human pregnancy and postnatally in rodents, [220] oligodendrogenesis and OL maturation begins much earlier leaving them vulnerable to prenatal and perinatal insults [86] (Fig.15a). During the subsequent weeks, a combination of secreted factors and phagocytosis by microglia help to guide the process of myelination, ultimately leading to normal levels by early adulthood [140, 141] (Fig.15a). With this model, we can describe the role placental ALLO plays in regulating OL/myelin development. By as early as two postnatal weeks, male pIKO show precocious maturation of OL lineage cells and subsequent increases in myelin basic protein and myelin thickness at P30[9]. Importantly, this increase in myelin thickness is temporary, as it normalizes by P60 (unpublished data). This is also accompanied by ASD-like behaviors such as decreased sociability and increased repetitive behaviors. The female pIKO show decreased OL

maturation, reduced myelin thickness, and no major cerebellum-associated behavioral deficits [9]. The myelin based histological experiments were focused on the lateral WM of the lobule VI/VII of the cerebellum specifically because this lobule participates in social behavior and higher cognitive functioning[241]. However, many behaviors cannot be limited to the contributions of one region alone. Future experiments on the WM development in other regions such as the prefrontal cortex should be examined to further characterize the whole brain effect of early ALLO loss. Moreover, since the increased myelin thickness seen in male pIKO is temporary, but the behavioral phenotype persists, this may suggest the residual effect of ALLO loss persists longer in other regions that have yet to be investigated.

The *akr1c14<sup>cyp19a</sup>*KO model recapitulated the cerebellar phenotype described in ASD patients, including a transient WM hypertrophy in males [225]. However, there were several questions that were prompted by this finding. Primarily, the loss of ALLO is placental in nature and the sex difference in cerebellar myelination primarily appears postnatally. Bridging this gap was also necessary to better understand how these white matter defects arise. Additionally, although treatment with the GABA<sub>A</sub>R agonist, muscimol rescued the myelination phenotype in the pIKO males [9], it is essential to acknowledge that other GABA<sub>A</sub> receptor independent mechanisms may also contribute to these effects such as toll-like receptor inflammatory signaling. Finally, further investigation into *how* the same prenatal insult resulted in divergent white matter defects in males and females was necessary.

## **Bridging the gap between prenatal insult and postnatal phenotype**

The current data indicates a heightened pro-inflammatory response in the male placenta at a transcriptomic level following ALLO loss (Fig. 15b). Moreover, postnatally, cytokine levels suggest a progressive anti-inflammatory profile in pIKO females (Fig. 15c). This finding provides the basis for many future questions and experiments, such as how the removal of placental ALLO can have lasting inflammatory impact in the postnatal cerebellum. To bridge the gap between embryonic insult and postnatal phenotype we must also investigate the circulating cytokines made by the placenta and determine whether they can be found in the fetal brain. Experiments utilizing *in situ* hybridization in both placenta and fetal brain would help to pinpoint the cytokine-producing cells, and a comprehensive cytokine analysis at embryonic timepoints like what was done in the postnatal cerebellum would also be helpful.

An additional next step would be to explore the impact of embryonic cytokines on early microglial populations in the developing cerebellum to observe their acute effects. During pregnancy, the placenta's high ALLO production may shield the maternal-fetal interface from external stressors like maternal inflammation or infection [85, 272, 273]. Studies have shown ALLO can inhibit inflammatory signals induced by activated MyD88-dependent toll-like receptors (TLRs), such as TLR4 and TLR7, in a sex-linked manner [101, 102, 243, 244]. This inhibition lessens NF $\kappa$ B activity and decreases pro-inflammatory cytokines such as IL-1 and IL-6 [101, 102, 274, 275]. While the exact molecular processes are unclear, recent findings suggest ALLO disrupts the interaction between TLR4 (or 7) and MyD88 and blocks TLR4's interaction with GABA<sub>A</sub>R  $\alpha$ 2 subunit [101], whose expression peaks in tandem with *akr1c14* at E14.5 in the mouse placenta (unpublished data).

While the connection between placental ALLO insufficiency and placental inflammation is clear, it is still an open question as to how this leads to *postnatal* brain inflammation without causing similar *prenatal* brain inflammation. One hypothesis is that placental ALLO loss primes embryonic microglia resulting in lasting functional changes. Studies have shown that chronic TLR7 activation results in lasting desensitization in microglia [276]. Since ALLO inhibits TLR signaling embryonically, removing ALLO effectively mimics persistent activation. It may then result in lasting modifications to microglial function and contribute to later white matter developmental defects. Pre-conditioning with a TLR7 agonist in fetal sheep significantly improved white matter outcomes[277]. Moreover, recent studies have shown that persistent prenatal activation of TLR7 results in sex specific social behavior defects, stereotypies, and ultrasonic vocalizations. This is paired with morphological alterations in microglia and sex specific molecular signatures that persist into adulthood [278]. Future experiments investigating the role of ALLO loss in TLR activation could be achieved through co-immunoprecipitation studies. This would validate whether ALLO loss enhances the binding of MyD88 with TLRs, consequently increasing downstream signaling, and whether any desensitization persists postnatally.

### **Contribution of sex differences to pIKO WM defects**

While it is well established that male and female brains undergo distinct developmental trajectories [111, 242], the exact mechanisms underlying their sex specific vulnerabilities during development is not well understood. Neuroinflammation emerges as a defining characteristic of many disorders with white matter injury following pregnancy complications [279, 280]. For this reason, the identification of inflammation- and microglia-related pathways from our time-course RNA sequencing experiment in the pIKO brain and in the cerebellum was particularly attractive. Interestingly, one of the key regulators of the sex-based genotype effect identified by IPA pathway

analysis in our mice was the prostaglandin EP4 receptor, highly expressed in microglia and generally serves to constrain its response to inflammatory stimuli [256]. This is particularly interesting considering the increased level of circulating PGE2 in pIKO females, just before the rise in anti-inflammatory cytokine profile. Moreover, when treating pIKO mice with PGE2 EP4 agonist, has behavioral ramifications, reducing the ASD composite score in males only. This is consistent with previous experiments manipulating PGE2 signaling in the cerebellum and sexually dimorphic behavior [180]. Direct, intracerebellar injection of COX inhibitors reduced play levels and sensory threshold in males but not females [180]. The specific role of prostaglandins in the sexualization of cerebellar behavior may be mechanistic as PGE2 promotes estradiol synthesis in the cerebellum. Many of these sex differences emerge after the postnatal androgen surge that elicits the brain's sexual differentiation which temporally aligns with the beginning of our white matter defects[113].

Aside from the general sexualization of microglia, it was important to connect these differences with their relationship to white matter development. One of the main sexually dimorphic functions of microglia identified in the literature is their phagocytic capacity across development [138, 139, 281]. However the comparison between males and females varies drastically based on age and brain region. In some regions like the hippocampus, female microglia exhibit more phagocytic activity than males [138]. However, during neonatal development in the amygdala male microglia show increased phagocytosis of newborn cells [281]. In our model, microglia exhibit dynamic sex and genotype specific alterations in phagocytic activity (Fig. 15d). Moreover, phagocytic machinery are altered in pIKO male mice which contributes to their ability to developmentally regulate and prune surrounding OL populations. This may be in part due to the increased expression of the phagocytic inhibitor SIRP $\alpha$  (Signal Regulatory Protein-alpha), in male

microglia. SIRP $\alpha$  belongs to a family of immune inhibitory receptors which becomes activated when bound to its ligand CD47 and overrides traditional "eat me" signals for phagocytosis. Though microglial SIRP $\alpha$  activity has not been thoroughly studied in normal brain development, studies have shown that CD47-SIRP $\alpha$  interaction can regulate both myelin and synaptosome phagocytosis by microglia.[150, 282] With synaptosomes both SIRP $\alpha$  knock out on microglia and CD47 knockout in synaptosomes were sufficient to increase phagocytosis but when combined did not produce an additive effect. Moreover, microglia preferentially phagocytosed synaptosomes lacking CD47 expression suggesting specificity on a cell-by-cell basis [282]. CD47 is also present on the myelin sheath [146]. When blocking the binding of myelin CD47 to microglial SIRP $\alpha$ , myelin phagocytosis is increased [150]. In our model, administration of RRX-001, a drug designed to enhance macrophage phagocytosis by disrupting the SIRP $\alpha$ -CD47 interaction, leads to increased microglial phagocytosis and initial improvement in the levels of myelin component mRNA within microglia. However, additional research is required to determine whether changes in microglia, myelin, or both are causing the altered myelin phagocytosis in the developing pIKO cerebellum.

In both pharmacological experiments utilizing RRX-001 and the PGE2 EP4 agonist L902-688, promising preliminary results suggest necessary future experiments. While RRX-001 increases microglial phagocytosis and the uptake of myelin by microglia, it would be interesting to see whether this is sufficient to normalize the total MBP levels in the male pIKO cerebellum. A similar experiment could be done in the mice treated with L902-688 to see whether the behavioral rescue of ASD-like behaviors is correlated with the rescue of myelin levels.

### **Teasing out the many roles of ALLO in the developing brain**

Finally, one of the most complex questions yet to be investigated is regarding the contribution of ALLO to multiple pathways of action including GABA<sub>A</sub> signaling as well as anti-

inflammatory signaling. Previous work shows that treatment with the GABA<sub>A</sub>R agonist, muscimol rescued the myelination phenotype in the pIKO males along with the associated ASD-like behavior [73]. However, the current work shows there is also clearly a contribution of ALLO loss to inflammatory signaling. In order to tease apart the effect of both of these pathways perhaps investigation into other cell types such as Purkinje cells would be helpful. As the major GABAergic cells in the cerebellum, Purkinje cells may exhibit functional changes following ALLO loss that may contribute to myelination defects [158, 159]. Studies have shown that neuronal activity has the ability to regulate myelination such that block of synaptic transmission impairs myelination in vivo [283, 284]. By selectively manipulating Purkinje cell function and monitoring the impact of myelination and behavior may help to delineate why muscimol was so effective in rescuing behavior and how to differentiate the GABAergic effects from the anti-inflammatory ones.

In the complex system of regulating sex-based vulnerabilities for neurodevelopmental disorders, identifying points of divergence is a challenge. We conclude that loss of placental ALLO may contribute to lasting sex-specific white matter defects due to altered microglial function (Fig. 15 a-e). Via a better understanding of ALLO's diverse function in the developing brain, we can better tailor its therapeutic potential to protect babies following obstetric complications.

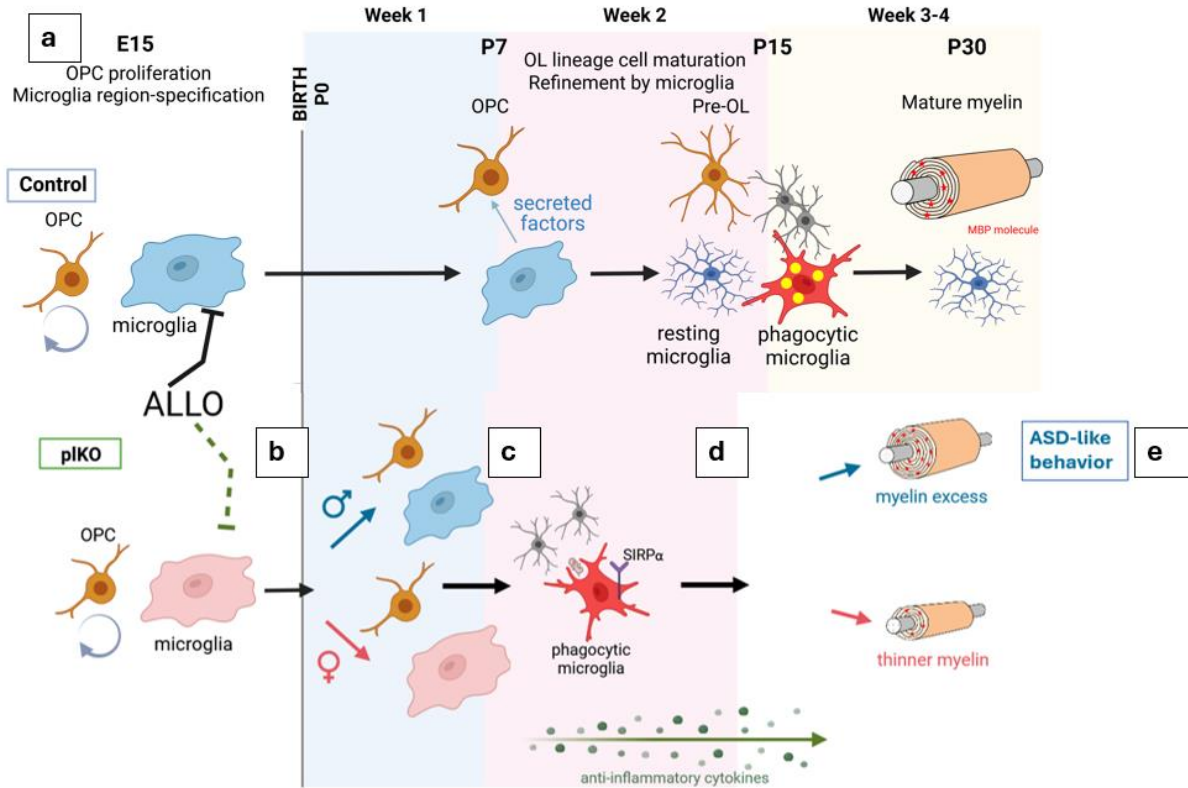


**Figure 15. Schematic of how the *akr1c14<sup>cyp19a</sup>* KO diverges from normal myelin development due to microglial functional alterations.** **a.** During embryonic development, ALLO is produced during an important time for OPC proliferation and microglia region specification. Subsequently, during the first postnatal weeks the combination of microglial secreted factors and phagocytosis help to guide the process of myelination, ultimately leading to normal levels by early adulthood. **b.** Following ALLO loss, E14.5 male pIKO placentas show an inflammatory response with almost no comparable phenotype in females. **c.** By P7 there is a divergence in WM microglia number and female pIKO microglia show a transient pro-inflammatory spike but globally show a progressive anti-inflammatory signature across development. **d.** By P7 male pIKO microglia exhibit SIRP $\alpha$  based defects in phagocytosis along with less internalized myelin resulting in excess myelin in early adulthood. **e.** The combination of these sex differences across development in both inflammatory signaling and phagocytosis culminates in the presentation of ASD like behavior in males and a more protected effect in females.

## References

1. Vacher, C.M., et al., *Editorial: Advances and perspectives in neuroplacentology*. Front Endocrinol (Lausanne), 2023. **14**: p. 1206072.
2. Wardinger, J.E. and S. Ambati, *Placental insufficiency*. 2020.
3. Liu, D., et al., *Placental dysfunction: the core mechanism for poor neurodevelopmental outcomes in the offspring of preeclampsia pregnancies*. Placenta, 2022.
4. Ueda, M., et al., *Placental pathology predicts infantile neurodevelopment*. Scientific reports, 2022. **12**(1): p. 2578.
5. Su, C.-H., et al., *Correlations between serum BDNF levels and neurodevelopmental outcomes in infants of mothers with gestational diabetes*. Pediatrics & Neonatology, 2021. **62**(3): p. 298-304.
6. Hagberg, H., et al., *The role of inflammation in perinatal brain injury*. Nature Reviews Neurology, 2015. **11**(4): p. 192-208.
7. Walker, C.K., et al., *Preeclampsia, placental insufficiency, and autism spectrum disorder or developmental delay*. JAMA Pediatr, 2015. **169**(2): p. 154-62.
8. May, T., et al., *Sex differences in neurodevelopmental disorders*. Current opinion in neurology, 2019. **32**(4): p. 622-626.
9. Vacher, C.M., et al., *Placental endocrine function shapes cerebellar development and social behavior*. Nat Neurosci, 2021. **24**(10): p. 1392-1401.
10. Parthiv Haldipur, D.D., Kathleen J. Millen, *Embryology Handbook of clinical neurology*. Vol. 154. 2018.
11. Sathyanesan, A., et al., *Emerging connections between cerebellar development, behaviour and complex brain disorders*. Nature Reviews Neuroscience, 2019. **20**(5): p. 298-313.
12. Kalagiri, R.R., et al., *Inflammation in Complicated Pregnancy and Its Outcome*. Am J Perinatol, 2016. **33**(14): p. 1337-1356.
13. Paolicelli, R.C., et al., *Synaptic pruning by microglia is necessary for normal brain development*. science, 2011. **333**(6048): p. 1456-1458.
14. Lemcke, R., et al., *Molecular Consequences of Peripheral Influenza A Infection on Cell Populations in the Murine Hypothalamus*. bioRxiv, 2023: p. 2023.03. 06.530999.
15. Fricker, M., et al., *MFG-E8 mediates primary phagocytosis of viable neurons during neuroinflammation*. Journal of Neuroscience, 2012. **32**(8): p. 2657-2666.
16. Hughes, A.N. and B. Appel, *Microglia phagocytose myelin sheaths to modify developmental myelination*. Nat Neurosci, 2020. **23**(9): p. 1055-1066.
17. Pang, Y., et al., *Differential roles of astrocyte and microglia in supporting oligodendrocyte development and myelination in vitro*. Brain Behav, 2013. **3**(5): p. 503-14.
18. Nemes-Baran, A.D., D.R. White, and T.M. DeSilva, *Fractalkine-Dependent Microglial Pruning of Viable Oligodendrocyte Progenitor Cells Regulates Myelination*. Cell Rep, 2020. **32**(7): p. 108047.
19. Rees, S., R. Harding, and D. Walker, *The biological basis of injury and neuroprotection in the fetal and neonatal brain*. International Journal of Developmental Neuroscience, 2011. **29**(6): p. 551-563.

20. Woods, L., V. Perez-Garcia, and M. Hemberger, *Regulation of placental development and its impact on fetal growth—new insights from mouse models*. *Frontiers in endocrinology*, 2018. **9**: p. 570.
21. Malassiné, A., J.L. Frendo, and D. Evain-Brion, *A comparison of placental development and endocrine functions between the human and mouse model*. *Human reproduction update*, 2003. **9**(6): p. 531-539.
22. Hemberger, M., C.W. Hanna, and W. Dean, *Mechanisms of early placental development in mouse and humans*. *Nature Reviews Genetics*, 2020. **21**(1): p. 27-43.
23. Rai, A. and J.C. Cross, *Development of the hemochorial maternal vascular spaces in the placenta through endothelial and vasculogenic mimicry*. *Developmental biology*, 2014. **387**(2): p. 131-141.
24. Kratimenos, P. and A.A. Penn, *Placental programming of neuropsychiatric disease*. *Pediatric research*, 2019. **86**(2): p. 157-164.
25. Gardella, B., et al., *Placental features of fetal vascular malperfusion and infant neurodevelopmental outcomes at 2 years of age in severe fetal growth restriction*. *American Journal of Obstetrics and Gynecology*, 2021. **225**(4): p. 413. e1-413. e11.
26. Ceasrine, A.M., et al., *Maternal diet disrupts the placenta–brain axis in a sex-specific manner*. *Nature Metabolism*, 2022. **4**(12): p. 1732-1745.
27. Cai, S., et al., *The Influence of Gestational Diabetes on Neurodevelopment of Children in the First Two Years of Life: A Prospective Study*. *PLoS One*, 2016. **11**(9): p. e0162113.
28. Maher, G.M., et al., *Association of Hypertensive Disorders of Pregnancy With Risk of Neurodevelopmental Disorders in Offspring: A Systematic Review and Meta-analysis*. *JAMA Psychiatry*, 2018. **75**(8): p. 809-819.
29. Woods, R.M., et al., *Maternal immune activation and role of placenta in the prenatal programming of neurodevelopmental disorders*. *Neuronal Signaling*, 2023. **7**(2).
30. Knuesel, I., et al., *Maternal immune activation and abnormal brain development across CNS disorders*. *Nature Reviews Neurology*, 2014. **10**(11): p. 643-660.
31. Bendix, I., et al., *Adverse neuropsychiatric development following perinatal brain injury: from a preclinical perspective*. *Pediatric research*, 2019. **85**(2): p. 198-215.
32. Zengeler, K.E. and J.R. Lukens, *Innate immunity at the crossroads of healthy brain maturation and neurodevelopmental disorders*. *Nature Reviews Immunology*, 2021. **21**(7): p. 454-468.
33. Hsiao, E.Y. and P.H. Patterson, *Activation of the maternal immune system induces endocrine changes in the placenta via IL-6*. *Brain Behav Immun*, 2011. **25**(4): p. 604-15.
34. Ponzio, N.M., et al., *Cytokine levels during pregnancy influence immunological profiles and neurobehavioral patterns of the offspring*. *Ann N Y Acad Sci*, 2007. **1107**: p. 118-28.
35. Carbó, N., F.J. López-Soriano, and J.M. Argilés, *Tumour necrosis factor- $\alpha$  does not cross the rat placenta*. *Cancer letters*, 1998. **128**(1): p. 101-104.
36. Zaretsky, M.V., et al., *Transfer of inflammatory cytokines across the placenta*. *Obstetrics & Gynecology*, 2004. **103**(3): p. 546-550.
37. Yen, S., *The placenta as the third brain*. *The Journal of reproductive medicine*, 1994. **39**(4): p. 277-280.
38. Corpéchet, C., et al., *Characterization and measurement of dehydroepiandrosterone sulfate in rat brain*. *Proceedings of the National Academy of Sciences*, 1981. **78**(8): p. 4704-4707.

39. Dubrovsky, B., *Neurosteroids, neuroactive steroids, and symptoms of affective disorders*. Pharmacology Biochemistry and Behavior, 2006. **84**(4): p. 644-655.
40. Mellon, S.H. and L.D. Griffin, *Neurosteroids: biochemistry and clinical significance*. Trends in endocrinology & metabolism, 2002. **13**(1): p. 35-43.
41. Reddy, D.S., *Neurosteroids: endogenous role in the human brain and therapeutic potentials*. Progress in brain research, 2010. **186**: p. 113-137.
42. Reddy, D.S. and K. Bakshi, *Neurosteroids: Biosynthesis, molecular mechanisms, and neurophysiological functions in the human brain*, in *Hormonal Signaling in Biology and Medicine*. 2020, Elsevier. p. 69-82.
43. Wang, M., *Neurosteroids and GABA-A receptor function*. Frontiers in endocrinology, 2011. **2**: p. 44.
44. Schverer, M., et al., *Neurosteroids: non-genomic pathways in neuroplasticity and involvement in neurological diseases*. Pharmacology & Therapeutics, 2018. **191**: p. 190-206.
45. Liang, J.J. and A.M. Rasmusson, *Overview of the molecular steps in steroidogenesis of the GABAergic neurosteroids allopregnanolone and pregnanolone*. Chronic Stress, 2018. **2**: p. 2470547018818555.
46. Chatuphonprasert, W., K. Jarukamjorn, and I. Ellinger, *Physiology and pathophysiology of steroid biosynthesis, transport and metabolism in the human placenta*. Frontiers in pharmacology, 2018. **9**: p. 1027.
47. Hu, Z.Y., et al., *Neurosteroids: oligodendrocyte mitochondria convert cholesterol to pregnenolone*. Proceedings of the National Academy of Sciences, 1987. **84**(23): p. 8215-8219.
48. Jung-Testas, I., et al., *Neurosteroids: biosynthesis of pregnenolone and progesterone in primary cultures of rat glial cells*. Endocrinology, 1989. **125**(4): p. 2083-91.
49. Mellon, S.H. and C.F. Deschepper, *Neurosteroid biosynthesis: genes for adrenal steroidogenic enzymes are expressed in the brain*. Brain Res, 1993. **629**(2): p. 283-92.
50. Ukena, K., et al., *Cytochrome P450 side-chain cleavage enzyme in the cerebellar Purkinje neuron and its neonatal change in rats*. Endocrinology, 1998. **139**(1): p. 137-147.
51. Melcangi, R.C., V. Magnaghi, and L. Martini, *Steroid metabolism and effects in central and peripheral glial cells*. Journal of neurobiology, 1999. **40**(4): p. 471-483.
52. Agís-Balboa, R.C., et al., *Characterization of brain neurons that express enzymes mediating neurosteroid biosynthesis*. Proceedings of the National Academy of Sciences, 2006. **103**(39): p. 14602-14607.
53. Compagnone, N.A. and S.H. Mellon, *Neurosteroids: biosynthesis and function of these novel neuromodulators*. Frontiers in neuroendocrinology, 2000. **21**(1): p. 1-56.
54. Gago, N., et al., *Progesterone and the oligodendroglial lineage: stage-dependent biosynthesis and metabolism*. Glia, 2001. **36**(3): p. 295-308.
55. Diotel, N., et al., *Steroid transport, local synthesis, and signaling within the brain: roles in neurogenesis, neuroprotection, and sexual behaviors*. Frontiers in neuroscience, 2018: p. 84.
56. McCarthy, M.M., *A lumpers versus splitters approach to sexual differentiation of the brain*. Frontiers in neuroendocrinology, 2011. **32**(2): p. 114-123.
57. Pasca, A.M. and A.A. Penn, *The placenta: The lost neuroendocrine organ*. NeoReviews, 2010. **11**(2): p. e64-e77.

58. Strauss III, J.F., F. Martinez, and M. Kiriakidou, *Placental steroid hormone synthesis: unique features and unanswered questions*. *Biology of reproduction*, 1996. **54**(2): p. 303-311.
59. Tuckey, R.C., et al., *Molten globule structure and steroidogenic activity of N-218 MLN64 in human placental mitochondria*. *Endocrinology*, 2004. **145**(4): p. 1700-1707.
60. Olvera-Sanchez, S., et al., *Mitochondrial heat shock protein participates in placental steroidogenesis*. *Placenta*, 2011. **32**(3): p. 222-229.
61. Achermann, J.C. and I.A. Hughes, *Pediatric disorders of sex development*. *Williams Textbook of Endocrinology*, 2016: p. 893-963.
62. Zhu, Q., et al., *Human placental 3 $\beta$ -hydroxysteroid dehydrogenase/steroid  $\Delta$ 5, 4-isomerase 1: identity, regulation and environmental inhibitors*. *Toxicology*, 2019. **425**: p. 152253.
63. Vu, T.T., et al., *Changes in human placental 5 $\alpha$ -reductase isoenzyme expression with advancing gestation: effects of fetal sex and glucocorticoid exposure*. *Reproduction, Fertility and Development*, 2009. **21**(4): p. 599-607.
64. Sheehan, P.M., et al., *5 $\beta$ -Dihydroprogesterone and steroid 5 $\beta$ -reductase decrease in association with human parturition at term*. *Molecular human reproduction*, 2005. **11**(7): p. 495-501.
65. Schumacher, M., et al., *Revisiting the roles of progesterone and allopregnanolone in the nervous system: resurgence of the progesterone receptors*. *Prog Neurobiol*, 2014. **113**: p. 6-39.
66. Hosie, A.M., et al., *Endogenous neurosteroids regulate GABAA receptors through two discrete transmembrane sites*. *Nature*, 2006. **444**(7118): p. 486-9.
67. Whiting, P.J., et al., *Molecular and functional diversity of the expanding GABA-A receptor gene family*. *Annals of the New York Academy of Sciences*, 1999. **868**(1): p. 645-653.
68. Barnard, E., et al., *International Union of Pharmacology. XV. Subtypes of  $\gamma$ -aminobutyric acidA receptors: classification on the basis of subunit structure and receptor function*. *Pharmacological reviews*, 1998. **50**(2): p. 291-314.
69. Farrant, M. and Z. Nusser, *Variations on an inhibitory theme: phasic and tonic activation of GABAA receptors*. *Nature Reviews Neuroscience*, 2005. **6**(3): p. 215-229.
70. Sieghart, W. and G. Sperk, *Subunit composition, distribution and function of GABA-A receptor subtypes*. *Current topics in medicinal chemistry*, 2002. **2**(8): p. 795-816.
71. Datta, D., D. Arion, and D.A. Lewis, *Developmental expression patterns of GABAA receptor subunits in layer 3 and 5 pyramidal cells of monkey prefrontal cortex*. *Cerebral cortex*, 2015. **25**(8): p. 2295-2305.
72. Cullinan, W.E. and T.J. Wolfe, *Chronic stress regulates levels of mRNA transcripts encoding  $\beta$  subunits of the GABAA receptor in the rat stress axis*. *Brain research*, 2000. **887**(1): p. 118-124.
73. Peng, Z., et al., *Altered expression of the  $\delta$  subunit of the GABAA receptor in a mouse model of temporal lobe epilepsy*. *Journal of Neuroscience*, 2004. **24**(39): p. 8629-8639.
74. Birzniece, V., et al., *GABAA receptor changes in acute allopregnanolone tolerance*. *European journal of pharmacology*, 2006. **535**(1-3): p. 125-134.
75. Nin, M., et al., *Antidepressant effect and changes of GABAA receptor  $\gamma$ 2 subunit mRNA after hippocampal administration of allopregnanolone in rats*. *Journal of Psychopharmacology*, 2008. **22**(5): p. 477-485.

76. Legesse, D.H., et al., *Structural insights into opposing actions of neurosteroids on GABAA receptors*. Nature Communications, 2023. **14**(1): p. 5091.
77. Lu, X., C.F. Zorumski, and S. Mennerick, *Lack of neurosteroid selectivity at  $\delta$  vs.  $\gamma$ 2-containing GABAA receptors in dentate granule neurons*. Frontiers in Molecular Neuroscience, 2020. **13**: p. 6.
78. Mihalek, R.M., et al., *Attenuated sensitivity to neuroactive steroids in  $\gamma$ -aminobutyrate type A receptor delta subunit knockout mice*. Proceedings of the National Academy of Sciences, 1999. **96**(22): p. 12905-12910.
79. Mueller, A.L., J.S. Taube, and P.A. Schwartzkroin, *Development of hyperpolarizing inhibitory postsynaptic potentials and hyperpolarizing response to gamma-aminobutyric acid in rabbit hippocampus studied in vitro*. Journal of Neuroscience, 1984. **4**(3): p. 860-867.
80. Ben-Ari, Y., *Excitatory actions of gaba during development: the nature of the nurture*. Nature Reviews Neuroscience, 2002. **3**(9): p. 728-739.
81. Payne, J.A., et al., *Cation–chloride co-transporters in neuronal communication, development and trauma*. Trends in neurosciences, 2003. **26**(4): p. 199-206.
82. Clayton, G.H., et al., *Ontogeny of cation–Cl<sup>-</sup> cotransporter expression in rat neocortex*. Developmental Brain Research, 1998. **109**(2): p. 281-292.
83. Mellon, S.H., *Neurosteroid regulation of central nervous system development*. Pharmacol Ther, 2007. **116**(1): p. 107-24.
84. Hamilton, N.B., et al., *Endogenous GABA controls oligodendrocyte lineage cell number, myelination, and CNS internode length*. Glia, 2017. **65**(2): p. 309-321.
85. Brunton, P.J., J.A. Russell, and J.J. Hirst, *Allopregnanolone in the brain: protecting pregnancy and birth outcomes*. Progress in neurobiology, 2014. **113**: p. 106-136.
86. van Tilborg, E., et al., *Origin and dynamics of oligodendrocytes in the developing brain: Implications for perinatal white matter injury*. Glia, 2018. **66**(2): p. 221-238.
87. Noorbakhsh, F., G.B. Baker, and C. Power, *Allopregnanolone and neuroinflammation: a focus on multiple sclerosis*. Frontiers in cellular neuroscience, 2014. **8**: p. 134.
88. Chen, S., et al., *Allopregnanolone promotes neuronal and oligodendrocyte differentiation in vitro and in vivo: therapeutic implication for Alzheimer's disease*. Neurotherapeutics, 2020. **17**: p. 1813-1824.
89. Rivera, C., et al., *The K<sup>+</sup>/Cl<sup>-</sup> co-transporter KCC2 renders GABA hyperpolarizing during neuronal maturation*. Nature, 1999. **397**(6716): p. 251-255.
90. Henschel, O., K.E. Gipson, and A. Bordey, *GABAA receptors, anesthetics and anticonvulsants in brain development*. CNS & Neurological Disorders-Drug Targets (Formerly Current Drug Targets-CNS & Neurological Disorders), 2008. **7**(2): p. 211-224.
91. Ghomari, A.M., et al., *Progesterone and its metabolites increase myelin basic protein expression in organotypic slice cultures of rat cerebellum*. Journal of neurochemistry, 2003. **86**(4): p. 848-859.
92. Crombie, G., et al., *Behavioural deficits induced by chronic perinatal stress is ameliorated by Xbd173 administration in male guinea pig offspring*. J Paediatr Child Health, 2018. **54**(15): p. 10.1111.
93. Shaw, J.C., et al., *Neurosteroid replacement therapy using the allopregnanolone-analogue ganaxolone following preterm birth in male guinea pigs*. Pediatric research, 2019. **85**(1): p. 86-96.

94. Chen, S., et al., *Allopregnanolone promotes regeneration and reduces  $\beta$ -amyloid burden in a preclinical model of Alzheimer's disease*. PloS one, 2011. **6**(8): p. e24293.
95. Ahmad, I., et al., *Allopregnanolone treatment, both as a single injection or repetitively, delays demyelination and enhances survival of Niemann-Pick C mice*. Journal of neuroscience research, 2005. **82**(6): p. 811-821.
96. Melcangi, R., et al., *Progesterone derivatives are able to influence peripheral myelin protein 22 and P0 gene expression: possible mechanisms of action*. Journal of neuroscience research, 1999. **56**(4): p. 349-357.
97. Melcangi, R.C., et al., *Peripheral nerves: a target for the action of neuroactive steroids*. Brain research reviews, 2005. **48**(2): p. 328-338.
98. He, J., et al., *Progesterone and allopregnanolone reduce inflammatory cytokines after traumatic brain injury*. Experimental neurology, 2004. **189**(2): p. 404-412.
99. Sayeed, I., et al., *Allopregnanolone, a progesterone metabolite, is more effective than progesterone in reducing cortical infarct volume after transient middle cerebral artery occlusion*. Annals of emergency medicine, 2006. **47**(4): p. 381-389.
100. He, J., S.W. Hoffman, and D.G. Stein, *Allopregnanolone, a progesterone metabolite, enhances behavioral recovery and decreases neuronal loss after traumatic brain injury*. Restorative neurology and neuroscience, 2004. **22**(1): p. 19-31.
101. Balan, I., et al., *Endogenous neurosteroid (3 $\alpha$ , 5 $\alpha$ ) 3-hydroxypregnan-20-one inhibits toll-like-4 receptor activation and pro-inflammatory signaling in macrophages and brain*. Scientific Reports, 2019. **9**(1): p. 1220.
102. Balan, I., et al., *Neurosteroid allopregnanolone (3 $\alpha$ , 5 $\alpha$ -THP) inhibits inflammatory signals induced by activated MyD88-dependent toll-like receptors*. Translational psychiatry, 2021. **11**(1): p. 145.
103. Balan, I., et al., *Inhibition of human macrophage activation via pregnane neurosteroid interactions with toll-like receptors: Sex differences and structural requirements*. Frontiers in Immunology, 2022. **13**: p. 940095.
104. Muller, E. and H.H. Kerschbaum, *Progesterone and its metabolites 5-dihydroprogesterone and 5-3-tetrahydroprogesterone decrease LPS-induced NO release in the murine microglial cell line, BV-2*. Neuro Endocrinol Lett, 2006. **27**(5): p. 675-8.
105. Lee, M., C. Schwab, and P.L. McGeer, *Astrocytes are GABAergic cells that modulate microglial activity*. Glia, 2011. **59**(1): p. 152-165.
106. Jolivel, V., et al., *Microglial cell morphology and phagocytic activity are critically regulated by the neurosteroid allopregnanolone: A possible role in neuroprotection*. Cells, 2021. **10**(3): p. 698.
107. Lombardo, M.V., et al., *Sex-specific impact of prenatal androgens on social brain default mode subsystems*. Molecular Psychiatry, 2020. **25**(9): p. 2175-2188.
108. Baron-Cohen, S., et al., *Foetal oestrogens and autism*. Molecular Psychiatry, 2020. **25**(11): p. 2970-2978.
109. Tsompanidis, A., et al., *Sex differences in placenta-derived markers and later autistic traits in children*. Translational Psychiatry, 2023. **13**(1): p. 256.
110. Tsompanidis, A., V. Warriar, and S. Baron-Cohen, *The genetics of autism and steroid-related traits in prenatal and postnatal life*. Frontiers in Endocrinology, 2023. **14**: p. 1126036.
111. McCarthy, M.M., et al., *Sex differences in the brain: the not so inconvenient truth*. Journal of Neuroscience, 2012. **32**(7): p. 2241-2247.

112. Becker, J.B., *Behavioral endocrinology*. 2002: Mit Press.
113. McCarthy, M.M., *How to Study the Origins of Sex Differences in Brain and Behavior*. NEW COVER TK, 2018: p. 29.
114. McEwen, B.S., et al., *Aromatization: important for sexual differentiation of the neonatal rat brain*. *Hormones and behavior*, 1977. **9**(3): p. 249-263.
115. Bowers, J.M., J. Waddell, and M.M. McCarthy, *A developmental sex difference in hippocampal neurogenesis is mediated by endogenous oestradiol*. *Biology of sex differences*, 2010. **1**: p. 1-13.
116. Fester, L., et al., *Estrogen-regulated synaptogenesis in the hippocampus: sexual dimorphism in vivo but not in vitro*. *The Journal of steroid biochemistry and molecular biology*, 2012. **131**(1-2): p. 24-29.
117. Schwarz, J.M., et al., *Estradiol induces hypothalamic dendritic spines by enhancing glutamate release: a mechanism for organizational sex differences*. *Neuron*, 2008. **58**(4): p. 584-598.
118. Dean, S.L. and M.M. McCarthy, *Steroids, sex and the cerebellar cortex: implications for human disease*. *The cerebellum*, 2008. **7**: p. 38-47.
119. Revuelta, M., et al., *Glial factors regulating white matter development and pathologies of the cerebellum*. *Neurochemical Research*, 2020. **45**: p. 643-655.
120. Sasahara, K., et al., *Mode of action and functional significance of estrogen-inducing dendritic growth, spinogenesis, and synaptogenesis in the developing Purkinje cell*. *Journal of Neuroscience*, 2007. **27**(28): p. 7408-7417.
121. Abi Ghanem, C., et al., *Long-lasting masculinizing effects of postnatal androgens on myelin governed by the brain androgen receptor*. *PLoS genetics*, 2017. **13**(11): p. e1007049.
122. Tapia-Gonzalez, S., et al., *Selective oestrogen receptor (ER) modulators reduce microglia reactivity in vivo after peripheral inflammation: potential role of microglial ERs*. 2008.
123. Penalzoza, C., et al., *Sex of the cell dictates its response: differential gene expression and sensitivity to cell death inducing stress in male and female cells*. *The FASEB Journal*, 2009. **23**(6): p. 1869.
124. Olney, K.C., et al., *Sex differences in early and term placenta are conserved in adult tissues*. *Biology of sex Differences*, 2022. **13**(1): p. 1-18.
125. Braun, A.E., et al., *Sex at the interface: the origin and impact of sex differences in the developing human placenta*. *Biology of sex Differences*, 2022. **13**(1): p. 50.
126. Gonzalez, T.L., et al., *Sex differences in the late first trimester human placenta transcriptome*. *Biology of Sex Differences*, 2018. **9**: p. 1-23.
127. Bale, T.L., *The placenta and neurodevelopment: sex differences in prenatal vulnerability*. *Dialogues in clinical neuroscience*, 2016. **18**(4): p. 459-464.
128. Howerton, C.L. and T.L. Bale, *Targeted placental deletion of OGT recapitulates the prenatal stress phenotype including hypothalamic mitochondrial dysfunction*. *Proceedings of the National Academy of Sciences*, 2014. **111**(26): p. 9639-9644.
129. Howerton, C.L., et al., *O-GlcNAc transferase (OGT) as a placental biomarker of maternal stress and reprogramming of CNS gene transcription in development*. *Proceedings of the National Academy of Sciences*, 2013. **110**(13): p. 5169-5174.

130. Vasistha, N.A., et al., *Maternal inflammation has a profound effect on cortical interneuron development in a stage and subtype-specific manner*. *Molecular psychiatry*, 2020. **25**(10): p. 2313-2329.
131. Favrais, G., et al., *Systemic inflammation disrupts the developmental program of white matter*. *Annals of neurology*, 2011. **70**(4): p. 550-565.
132. Prasad, J.D., et al., *Long-term coordinated microstructural disruptions of the developing neocortex and subcortical white matter after early postnatal systemic inflammation*. *Brain, Behavior, and Immunity*, 2021. **94**: p. 338-356.
133. Matcovitch-Natan, O., et al., *Microglia development follows a stepwise program to regulate brain homeostasis*. *Science*, 2016. **353**(6301): p. aad8670.
134. Villa, A., et al., *Sex-specific features of microglia from adult mice*. *Cell reports*, 2018. **23**(12): p. 3501-3511.
135. Lenz, K.M., et al., *Microglia are essential to masculinization of brain and behavior*. *J Neurosci*, 2013. **33**(7): p. 2761-72.
136. Schwarz, J.M., P.W. Sholar, and S.D. Bilbo, *Sex differences in microglial colonization of the developing rat brain*. *Journal of neurochemistry*, 2012. **120**(6): p. 948-963.
137. Hanamsagar, R. and S.D. Bilbo, *Sex differences in neurodevelopmental and neurodegenerative disorders: Focus on microglial function and neuroinflammation during development*. *J Steroid Biochem Mol Biol*, 2016. **160**: p. 127-33.
138. Nelson, L.H., S. Warden, and K.M. Lenz, *Sex differences in microglial phagocytosis in the neonatal hippocampus*. *Brain, behavior, and immunity*, 2017. **64**: p. 11-22.
139. Yanguas-Casas, N., et al., *Sex differences in the phagocytic and migratory activity of microglia and their impairment by palmitic acid*. *Glia*, 2018. **66**(3): p. 522-537.
140. Santos, E.N. and R.D. Fields, *Regulation of myelination by microglia*. *Science Advances*, 2021. **7**(50): p. eabk1131.
141. Kent, S.A. and V.E. Miron, *Microglia regulation of central nervous system myelin health and regeneration*. *Nature Reviews Immunology*, 2023: p. 1-15.
142. Nicholas, R.S., M.G. Wing, and A. Compston, *Nonactivated microglia promote oligodendrocyte precursor survival and maturation through the transcription factor NF-kappa B*. *Eur J Neurosci*, 2001. **13**(5): p. 959-67.
143. Barres, B.A., et al., *Multiple extracellular signals are required for long-term oligodendrocyte survival*. *Development*, 1993. **118**(1): p. 283-95.
144. Shigemoto-Mogami, Y., et al., *Microglia enhance neurogenesis and oligodendrogenesis in the early postnatal subventricular zone*. *J Neurosci*, 2014. **34**(6): p. 2231-43.
145. Grabert, K., et al., *Microglial brain region-dependent diversity and selective regional sensitivities to aging*. *Nat Neurosci*, 2016. **19**(3): p. 504-16.
146. Wlodarczyk, A., et al., *A novel microglial subset plays a key role in myelinogenesis in developing brain*. *EMBO J*, 2017. **36**(22): p. 3292-3308.
147. Kessaris, N., et al., *Competing waves of oligodendrocytes in the forebrain and postnatal elimination of an embryonic lineage*. *Nat Neurosci*, 2006. **9**(2): p. 173-9.
148. Li, Q., et al., *Developmental Heterogeneity of Microglia and Brain Myeloid Cells Revealed by Deep Single-Cell RNA Sequencing*. *Neuron*, 2019. **101**(2): p. 207-223 e10.
149. McNamara, N.B., et al., *Microglia regulate central nervous system myelin growth and integrity*. *Nature*, 2023. **613**(7942): p. 120-129.

150. Gitik, M., et al., *Myelin down-regulates myelin phagocytosis by microglia and macrophages through interactions between CD47 on myelin and SIRPalpha (signal regulatory protein-alpha) on phagocytes*. J Neuroinflammation, 2011. **8**: p. 24.
151. Lampron, A., et al., *Inefficient clearance of myelin debris by microglia impairs remyelinating processes*. J Exp Med, 2015. **212**(4): p. 481-95.
152. Poliani, P.L., et al., *TREM2 sustains microglial expansion during aging and response to demyelination*. J Clin Invest, 2015. **125**(5): p. 2161-70.
153. Healy, L.M., et al., *MerTK-mediated regulation of myelin phagocytosis by macrophages generated from patients with MS*. Neurol Neuroimmunol Neuroinflamm, 2017. **4**(6): p. e402.
154. Healy, L.M., et al., *MerTK Is a Functional Regulator of Myelin Phagocytosis by Human Myeloid Cells*. J Immunol, 2016. **196**(8): p. 3375-84.
155. Wu, Y., et al., *Microglial lysosome dysfunction contributes to white matter pathology and TDP-43 proteinopathy in GRN-associated FTD*. Cell Rep, 2021. **36**(8): p. 109581.
156. Tanaka, Y., et al., *Possible involvement of lysosomal dysfunction in pathological changes of the brain in aged progranulin-deficient mice*. Acta Neuropathol Commun, 2014. **2**: p. 78.
157. Pritzker, L.B., et al., *Deimination of myelin basic protein. 1. Effect of deimination of arginyl residues of myelin basic protein on its structure and susceptibility to digestion by cathepsin D*. Biochemistry, 2000. **39**(18): p. 5374-81.
158. Iskusnykh, I.Y. and V.V. Chizhikov, *Cerebellar development after preterm birth*. Frontiers in Cell and Developmental Biology, 2022. **10**: p. 1068288.
159. van Essen, M.J., et al., *Deconstructing cerebellar development cell by cell*. PLoS Genetics, 2020. **16**(4): p. e1008630.
160. Butts, T., M.J. Green, and R.J. Wingate, *Development of the cerebellum: simple steps to make a 'little brain'*. Development, 2014. **141**(21): p. 4031-4041.
161. Luciani, L., *Il cervelletto; nuovi studi di fisiologia normale e patologica*. Vol. 20. 1891: Le Monnier.
162. Löwenthal, M. and V.A.H. Horsley, *On the relations between the cerebellar and other centres (namely cerebral and spinal) with especial reference to the action of antagonistic muscles.(Preliminary account.)*. Proceedings of the Royal Society of London, 1897. **61**(369-377): p. 20-25.
163. Buckner, R.L., *The cerebellum and cognitive function: 25 years of insight from anatomy and neuroimaging*. Neuron, 2013. **80**(3): p. 807-815.
164. Schmahmann, J.D., *The cerebellum and cognition*. Neuroscience letters, 2019. **688**: p. 62-75.
165. Sillitoe, R.V. and A.L. Joyner, *Morphology, molecular codes, and circuitry produce the three-dimensional complexity of the cerebellum*. Annu. Rev. Cell Dev. Biol., 2007. **23**: p. 549-577.
166. Joyner, A.L., A. Liu, and S. Millet, *Otx2, Gbx2 and Fgf8 interact to position and maintain a mid-hindbrain organizer*. Current opinion in cell biology, 2000. **12**(6): p. 736-741.
167. Wang, V.Y., M.F. Rose, and H.Y. Zoghbi, *Math1 expression redefines the rhombic lip derivatives and reveals novel lineages within the brainstem and cerebellum*. Neuron, 2005. **48**(1): p. 31-43.

168. Machold, R. and G. Fishell, *Math1 is expressed in temporally discrete pools of cerebellar rhombic-lip neural progenitors*. Neuron, 2005. **48**(1): p. 17-24.
169. Hoshino, M., et al., *Ptf1a, a bHLH transcriptional gene, defines GABAergic neuronal fates in cerebellum*. Neuron, 2005. **47**(2): p. 201-213.
170. Pascual, M., et al., *Cerebellar GABAergic progenitors adopt an external granule cell-like phenotype in the absence of Ptf1a transcription factor expression*. Proceedings of the National Academy of Sciences, 2007. **104**(12): p. 5193-5198.
171. Lowenstein, E.D., K. Cui, and L.R. Hernandez-Miranda, *Regulation of early cerebellar development*. The FEBS Journal, 2023. **290**(11): p. 2786-2804.
172. Dastjerdi, F., G. Consalez, and R. Hawkes, *Pattern formation during development of the embryonic cerebellum*. Frontiers in neuroanatomy, 2012. **6**: p. 10.
173. Fleming, J.T., et al., *The Purkinje neuron acts as a central regulator of spatially and functionally distinct cerebellar precursors*. Developmental cell, 2013. **27**(3): p. 278-292.
174. Hashimoto, R., et al., *Origins of oligodendrocytes in the cerebellum, whose development is controlled by the transcription factor, Sox9*. Mechanisms of development, 2016. **140**: p. 25-40.
175. Jakab, R.L., J.K. Wong, and S.M. Belcher, *Estrogen receptor  $\beta$  immunoreactivity in differentiating cells of the developing rat cerebellum*. Journal of Comparative Neurology, 2001. **430**(3): p. 396-409.
176. Ikeda, Y. and A. Nagai, *Differential expression of the estrogen receptors alpha and beta during postnatal development of the rat cerebellum*. Brain research, 2006. **1083**(1): p. 39-49.
177. Lavaque, E., et al., *Sex differences, developmental changes, response to injury and cAMP regulation of the mRNA levels of steroidogenic acute regulatory protein, cytochrome p450scc, and aromatase in the olivocerebellar system*. Journal of neurobiology, 2006. **66**(3): p. 308-318.
178. Dean, S.L., et al., *Prostaglandin E2 stimulates estradiol synthesis in the cerebellum postnatally with associated effects on Purkinje neuron dendritic arbor and electrophysiological properties*. Endocrinology, 2012. **153**(11): p. 5415-5427.
179. Hoffman, J.F., C.L. Wright, and M.M. McCarthy, *A critical period in Purkinje cell development is mediated by local estradiol synthesis, disrupted by inflammation, and has enduring consequences only for males*. Journal of Neuroscience, 2016. **36**(39): p. 10039-10049.
180. Perez-Pouchoulen, M., et al., *Regulatory control of microglial phagocytosis by estradiol and prostaglandin E2 in the developing rat cerebellum*. The Cerebellum, 2019. **18**: p. 882-895.
181. Gomez Perdiguero, E., et al., *Tissue-resident macrophages originate from yolk-sac-derived erythro-myeloid progenitors*. Nature, 2015. **518**(7540): p. 547-551.
182. Kierdorf, K., et al., *Microglia emerge from erythromyeloid precursors via Pu. 1-and Irf8-dependent pathways*. Nature neuroscience, 2013. **16**(3): p. 273-280.
183. Nikodemova, M., et al., *Microglial numbers attain adult levels after undergoing a rapid decrease in cell number in the third postnatal week*. Journal of neuroimmunology, 2015. **278**: p. 280-288.
184. Lawson, L.J., et al., *Heterogeneity in the distribution and morphology of microglia in the normal adult mouse brain*. Neuroscience, 1990. **39**(1): p. 151-70.

185. Vela, J.M., et al., *Morphology and distribution of microglial cells in the young and adult mouse cerebellum*. J Comp Neurol, 1995. **361**(4): p. 602-16.
186. Stowell, R.D., et al., *Cerebellar microglia are dynamically unique and survey Purkinje neurons in vivo*. Dev Neurobiol, 2018. **78**(6): p. 627-644.
187. Ayata, P., et al., *Epigenetic regulation of brain region-specific microglia clearance activity*. Nat Neurosci, 2018. **21**(8): p. 1049-1060.
188. Stoessel, M.B. and A.K. Majewska, *Little cells of the little brain: microglia in cerebellar development and function*. Trends in neurosciences, 2021. **44**(7): p. 564-578.
189. Groteklaes, A., et al., *Developmental maturation of the cerebellar white matter—an instructive environment for cerebellar inhibitory interneurons*. The Cerebellum, 2020. **19**: p. 286-308.
190. Nandi, S., et al., *The CSF-1 receptor ligands IL-34 and CSF-1 exhibit distinct developmental brain expression patterns and regulate neural progenitor cell maintenance and maturation*. Dev Biol, 2012. **367**(2): p. 100-13.
191. Kana, V., et al., *CSF-1 controls cerebellar microglia and is required for motor function and social interaction*. Journal of Experimental Medicine, 2019. **216**(10): p. 2265-2281.
192. Irwin, R.W. and R.D. Brinton, *Allopregnanolone as regenerative therapeutic for Alzheimer's disease: translational development and clinical promise*. Prog Neurobiol, 2014. **113**: p. 40-55.
193. Ngo, D.H. and T.S. Vo, *An Updated Review on Pharmaceutical Properties of Gamma-Aminobutyric Acid*. Molecules, 2019. **24**(15).
194. Zhu, X., et al., *A role of endogenous progesterone in stroke cerebroprotection revealed by the neural-specific deletion of its intracellular receptors*. Journal of Neuroscience, 2017. **37**(45): p. 10998-11020.
195. Liere, P., et al., *Novel lipoidal derivatives of pregnenolone and dehydroepiandrosterone and absence of their sulfated counterparts in rodent brain*. Journal of lipid research, 2004. **45**(12): p. 2287-2302.
196. Kechin, A., et al., *cutPrimers: a new tool for accurate cutting of primers from reads of targeted next generation sequencing*. Journal of Computational Biology, 2017. **24**(11): p. 1138-1143.
197. Goldstein, L.D., et al., *Prediction and quantification of splice events from RNA-seq data*. PloS one, 2016. **11**(5): p. e0156132.
198. Anders, S., P.T. Pyl, and W. Huber, *HTSeq—a Python framework to work with high-throughput sequencing data*. bioinformatics, 2015. **31**(2): p. 166-169.
199. Sun, J., et al., *TCC: an R package for comparing tag count data with robust normalization strategies*. BMC bioinformatics, 2013. **14**(1): p. 1-14.
200. Krämer, A., et al., *Causal analysis approaches in ingenuity pathway analysis*. Bioinformatics, 2014. **30**(4): p. 523-530.
201. Hicks, S.C. and R.A. Irizarry, *Quantro: a data-driven approach to guide the choice of an appropriate normalization method*. Genome biology, 2015. **16**: p. 1-8.
202. Hicks, S.C., et al., *Smooth quantile normalization*. Biostatistics, 2018. **19**(2): p. 185-198.
203. Ritchie, M.E., et al., *limma powers differential expression analyses for RNA-sequencing and microarray studies*. Nucleic acids research, 2015. **43**(7): p. e47-e47.
204. Law, C.W., et al., *voom: Precision weights unlock linear model analysis tools for RNA-seq read counts*. Genome biology, 2014. **15**(2): p. 1-17.

205. Smyth, G.K., J. Michaud, and H.S. Scott, *Use of within-array replicate spots for assessing differential expression in microarray experiments*. *Bioinformatics*, 2005. **21**(9): p. 2067-75.
206. Livak, K.J. and T.D. Schmittgen, *Analysis of relative gene expression data using real-time quantitative PCR and the 2(-Delta Delta C(T)) Method*. *Methods*, 2001. **25**(4): p. 402-8.
207. Bohlen, C.J., F.C. Bennett, and M.L. Bennett, *Isolation and Culture of Microglia*. *Curr Protoc Immunol*, 2019. **125**(1): p. e70.
208. Egashira, N., et al., *Impaired social interaction and reduced anxiety-related behavior in vasopressin V1a receptor knockout mice*. *Behav Brain Res*, 2007. **178**(1): p. 123-7.
209. Gyertyán, I., *Analysis of the marble burying response: marbles serve to measure digging rather than evoke burying*. *Behav Pharmacol*, 1995. **6**(1): p. 24-31.
210. Nadler, J.J., et al., *Automated apparatus for quantitation of social approach behaviors in mice*. *Genes Brain Behav*, 2004. **3**(5): p. 303-14.
211. Silverman, J.L., et al., *Behavioural phenotyping assays for mouse models of autism*. *Nature Reviews Neuroscience*, 2010. **11**(7): p. 490-502.
212. El-Kordi, A., et al., *Development of an autism severity score for mice using Nlgn4 null mutants as a construct-valid model of heritable monogenic autism*. *Behavioural brain research*, 2013. **251**: p. 41-49.
213. Belelli, D., et al., *Realising the therapeutic potential of neuroactive steroid modulators of the GABAA receptor*. *Neurobiology of Stress*, 2020. **12**: p. 100207.
214. Schumacher, M., et al., *Revisiting the roles of progesterone and allopregnanolone in the nervous system: resurgence of the progesterone receptors*. *Progress in neurobiology*, 2014. **113**: p. 6-39.
215. Zimmerberg, B., S.H. Rackow, and K.P. George-Friedman, *Sex-dependent behavioral effects of the neurosteroid allopregnanolone (3 $\alpha$ , 5 $\alpha$ -THP) in neonatal and adult rats after postnatal stress*. *Pharmacology Biochemistry and Behavior*, 1999. **64**(4): p. 717-724.
216. Kelley, M.H., et al., *Sex difference in sensitivity to allopregnanolone neuroprotection in mice correlates with effect on spontaneous inhibitory post synaptic currents*. *Neuropharmacology*, 2011. **61**(4): p. 724-729.
217. Wenzel, P.L. and G. Leone, *Expression of Cre recombinase in early diploid trophoblast cells of the mouse placenta*. *genesis*, 2007. **45**(3): p. 129-134.
218. Marques, S., et al., *Oligodendrocyte heterogeneity in the mouse juvenile and adult central nervous system*. *Science*, 2016. **352**(6291): p. 1326-1329.
219. Thakurela, S., et al., *The transcriptome of mouse central nervous system myelin*. *Scientific Reports*, 2016. **6**(1): p. 25828.
220. Baumann, N. and D. Pham-Dinh, *Biology of oligodendrocyte and myelin in the mammalian central nervous system*. *Physiological reviews*, 2001. **81**(2): p. 871-927.
221. Chen, V.S., et al., *Histology atlas of the developing prenatal and postnatal mouse central nervous system, with emphasis on prenatal days E7. 5 to E18. 5*. *Toxicologic pathology*, 2017. **45**(6): p. 705-744.
222. Zonouzi, M., et al., *GABAergic regulation of cerebellar NG2 cell development is altered in perinatal white matter injury*. *Nature neuroscience*, 2015. **18**(5): p. 674-682.

223. Stoodley, C.J., et al., *Altered cerebellar connectivity in autism and cerebellar-mediated rescue of autism-related behaviors in mice*. *Nature neuroscience*, 2017. **20**(12): p. 1744-1751.
224. Wang, S.S.-H., A.D. Kloth, and A. Badura, *The cerebellum, sensitive periods, and autism*. *Neuron*, 2014. **83**(3): p. 518-532.
225. Courchesne, E., et al., *Unusual brain growth patterns in early life in patients with autistic disorder: an MRI study*. *Neurology*, 2001. **57**(2): p. 245-54.
226. Zeidán-Chuliá, F., et al., *Up-regulation of oligodendrocyte lineage markers in the cerebellum of autistic patients: evidence from network analysis of gene expression*. *Molecular neurobiology*, 2016. **53**: p. 4019-4025.
227. Premoli, M., et al., *Specific profile of ultrasonic communication in a mouse model of neurodevelopmental disorders*. *Scientific Reports*, 2019. **9**(1): p. 15912.
228. Kim, H., C.-S. Lim, and B.-K. Kaang, *Neuronal mechanisms and circuits underlying repetitive behaviors in mouse models of autism spectrum disorder*. *Behavioral and Brain Functions*, 2016. **12**(1): p. 1-13.
229. Lugo, J.N., et al., *Deletion of PTEN produces autism-like behavioral deficits and alterations in synaptic proteins*. *Frontiers in molecular neuroscience*, 2014. **7**: p. 27.
230. Fraser, M.M., et al., *Phosphatase and tensin homolog, deleted on chromosome 10 deficiency in brain causes defects in synaptic structure, transmission and plasticity, and myelination abnormalities*. *Neuroscience*, 2008. **151**(2): p. 476-488.
231. Pacey, L.K., et al., *Delayed myelination in a mouse model of fragile X syndrome*. *Human molecular genetics*, 2013. **22**(19): p. 3920-3930.
232. Rothwell, P.E., et al., *Autism-associated neuroligin-3 mutations commonly impair striatal circuits to boost repetitive behaviors*. *Cell*, 2014. **158**(1): p. 198-212.
233. Agrawal, S., et al., *Prevalence of autism spectrum disorder in preterm infants: a meta-analysis*. *Pediatrics*, 2018. **142**(3).
234. Guennoun, R., *Progesterone in the brain: hormone, neurosteroid and neuroprotectant*. *International journal of molecular sciences*, 2020. **21**(15): p. 5271.
235. Pang, Y., J. Dong, and P. Thomas, *Characterization, neurosteroid binding and brain distribution of human membrane progesterone receptors  $\delta$  and  $\epsilon$  (mPR $\delta$  and mPR $\epsilon$ ) and mPR $\delta$  involvement in neurosteroid inhibition of apoptosis*. *Endocrinology*, 2013. **154**(1): p. 283-295.
236. Thomas, P. and Y. Pang, *Anti-apoptotic actions of allopregnanolone and ganaxolone mediated through membrane progesterone receptors (PAQRs) in neuronal cells*. *Frontiers in endocrinology*, 2020. **11**: p. 417.
237. Hertig, A., et al., *Steroid profiling in preeclamptic women: evidence for aromatase deficiency*. *American journal of obstetrics and gynecology*, 2010. **203**(5): p. 477. e1-477. e9.
238. Becker, E.B. and C.J. Stoodley, *Autism spectrum disorder and the cerebellum*. *International review of neurobiology*, 2013. **113**: p. 1-34.
239. Fatemi, S.H., et al., *Consensus paper: pathological role of the cerebellum in autism*. *The Cerebellum*, 2012. **11**: p. 777-807.
240. Rogers, T.D., et al., *Is autism a disease of the cerebellum? An integration of clinical and pre-clinical research*. *Frontiers in systems neuroscience*, 2013. **7**: p. 15.

241. Stoodley, C.J. and J.D. Schmahmann, *Evidence for topographic organization in the cerebellum of motor control versus cognitive and affective processing*. Cortex, 2010. **46**(7): p. 831-44.
242. McCarthy, M.M., *Sex differences in the developing brain as a source of inherent risk*. Dialogues in clinical neuroscience, 2016. **18**(4): p. 361-372.
243. Fitzgerald, K.A., et al., *Mal (MyD88-adaptor-like) is required for Toll-like receptor-4 signal transduction*. Nature, 2001. **413**(6851): p. 78-83.
244. Gay, N.J., et al., *Assembly and localization of Toll-like receptor signalling complexes*. Nat Rev Immunol, 2014. **14**(8): p. 546-58.
245. He, J., et al., *Progesterone and allopregnanolone reduce inflammatory cytokines after traumatic brain injury*. Exp Neurol, 2004. **189**(2): p. 404-12.
246. Liao, G., et al., *Allopregnanolone treatment delays cholesterol accumulation and reduces autophagic/lysosomal dysfunction and inflammation in Npc1<sup>-/-</sup> mouse brain*. Brain Res, 2009. **1270**: p. 140-51.
247. Yilmaz, C., et al., *Neurosteroids as regulators of neuroinflammation*. Front Neuroendocrinol, 2019. **55**: p. 100788.
248. Rupprecht, R., et al., *Steroid receptor-mediated effects of neuroactive steroids: characterization of structure-activity relationship*. Eur J Pharmacol, 1996. **303**(3): p. 227-34.
249. Hirst, J.J., et al., *Stress in pregnancy activates neurosteroid production in the fetal brain*. Neuroendocrinology, 2006. **84**(4): p. 264-74.
250. Westcott, K.T., et al., *Brain allopregnanolone in the fetal and postnatal rat in response to uteroplacental insufficiency*. Neuroendocrinology, 2008. **88**(4): p. 287-92.
251. Wenzel, P.L. and G. Leone, *Expression of Cre recombinase in early diploid trophoblast cells of the mouse placenta*. Genesis, 2007. **45**(3): p. 129-34.
252. Bakalar, D., et al., *Lack of placental neurosteroid alters cortical development and female somatosensory function*. Front Endocrinol (Lausanne), 2022. **13**: p. 972033.
253. Gitik, M., et al., *Phagocytic receptors activate and immune inhibitory receptor SIRP $\alpha$  inhibits phagocytosis through paxillin and cofilin*. Frontiers in cellular neuroscience, 2014. **8**: p. 104.
254. Müller, C., et al., *Making myelin basic protein -from mRNA transport to localized translation*. Front Cell Neurosci, 2013. **7**: p. 169.
255. Cabrales, P., *RRx-001 Acts as a Dual Small Molecule Checkpoint Inhibitor by Downregulating CD47 on Cancer Cells and SIRP- $\alpha$  on Monocytes/Macrophages*. Transl Oncol, 2019. **12**(4): p. 626-632.
256. Woodling, N.S., et al., *Suppression of Alzheimer-associated inflammation by microglial prostaglandin-E2 EP4 receptor signaling*. J Neurosci, 2014. **34**(17): p. 5882-94.
257. Mor, G., et al., *Inflammation and pregnancy: the role of the immune system at the implantation site*. Annals of the new York Academy of Sciences, 2011. **1221**(1): p. 80-87.
258. Hussain, T., et al., *Understanding the immune system in fetal protection and maternal infections during pregnancy*. Journal of Immunology Research, 2022. **2022**.
259. Afkham, A., et al., *Toll-like receptors signaling network in pre-eclampsia: An updated review*. J Cell Physiol, 2019. **234**(3): p. 2229-2240.
260. Aldo, P.B., et al., *A novel three-dimensional in vitro system to study trophoblast-endothelium cell interactions*. Am J Reprod Immunol, 2007. **58**(2): p. 98-110.

261. Goldenberg, R.L., J.C. Hauth, and W.W. Andrews, *Intrauterine infection and preterm delivery*. N Engl J Med, 2000. **342**(20): p. 1500-7.
262. Rodrigues-Duarte, L., et al., *Fetal and Maternal Innate Immunity Receptors Have Opposing Effects on the Severity of Experimental Malaria in Pregnancy: Beneficial Roles for Fetus-Derived Toll-Like Receptor 4 and Type I Interferon Receptor 1*. Infect Immun, 2018. **86**(5).
263. Goines, P.E., et al., *Increased midgestational IFN-gamma, IL-4 and IL-5 in women bearing a child with autism: A case-control study*. Mol Autism, 2011. **2**: p. 13.
264. Gumusoglu, S.B., et al., *Chronic maternal interleukin-17 and autism-related cortical gene expression, neurobiology, and behavior*. Neuropsychopharmacology, 2020. **45**(6): p. 1008-1017.
265. Smith, S.E., et al., *Maternal immune activation alters fetal brain development through interleukin-6*. J Neurosci, 2007. **27**(40): p. 10695-702.
266. Werling, D.M., *The role of sex-differential biology in risk for autism spectrum disorder*. Biol Sex Differ, 2016. **7**: p. 58.
267. Hagemeyer, N., et al., *Microglia contribute to normal myelinogenesis and to oligodendrocyte progenitor maintenance during adulthood*. Acta Neuropathol, 2017. **134**(3): p. 441-458.
268. Logtenberg, M.E., F.A. Scheeren, and T.N. Schumacher, *The CD47-SIRP $\alpha$  immune checkpoint*. Immunity, 2020. **52**(5): p. 742-752.
269. VanRyzin, J.W., L.A. Pickett, and M.M. McCarthy, *Microglia: Driving critical periods and sexual differentiation of the brain*. Dev Neurobiol, 2018. **78**(6): p. 580-592.
270. Cainelli, E., F. Arrigoni, and L. Vedovelli, *White matter injury and neurodevelopmental disabilities: A cross-disease (dis) connection*. Progress in neurobiology, 2020. **193**: p. 101845.
271. Back, S.A. and P.A. Rosenberg, *Pathophysiology of glia in perinatal white matter injury*. Glia, 2014. **62**(11): p. 1790-1815.
272. Westcott, K.T., et al., *Brain allopregnanolone in the fetal and postnatal rat in response to uteroplacental insufficiency*. Neuroendocrinology, 2008. **88**(4): p. 287-292.
273. Hirst, J.J., et al., *Neuroactive steroids in pregnancy: key regulatory and protective roles in the foetal brain*. J Steroid Biochem Mol Biol, 2014. **139**: p. 144-53.
274. Kawasaki, T. and T. Kawai, *Toll-like receptor signaling pathways*. Front Immunol, 2014. **5**: p. 461.
275. Grassin-Delyle, S., et al., *The Role of Toll-Like Receptors in the Production of Cytokines by Human Lung Macrophages*. J Innate Immun, 2020. **12**(1): p. 63-73.
276. Michaelis, K.A., et al., *Persistent Toll-like receptor 7 stimulation induces behavioral and molecular innate immune tolerance*. Brain, behavior, and immunity, 2019. **82**: p. 338-353.
277. Cho, K.H., et al., *Protective effects of delayed intraventricular TLR7 agonist administration on cerebral white and gray matter following asphyxia in the preterm fetal sheep*. Scientific reports, 2019. **9**(1): p. 9562.
278. Missig, G., et al., *Sex-dependent neurobiological features of prenatal immune activation via TLR7*. Molecular Psychiatry, 2020. **25**(10): p. 2330-2341.
279. Makinson, R., et al., *Intrauterine inflammation induces sex-specific effects on neuroinflammation, white matter, and behavior*. Brain, behavior, and immunity, 2017. **66**: p. 277-288.

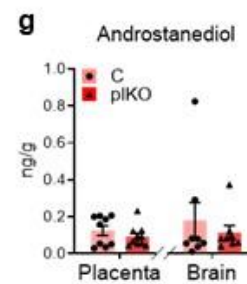
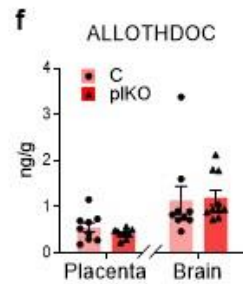
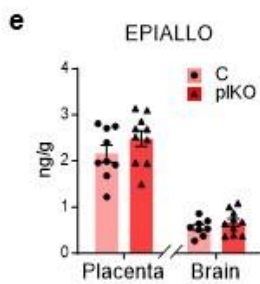
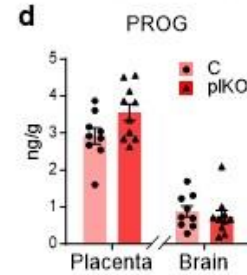
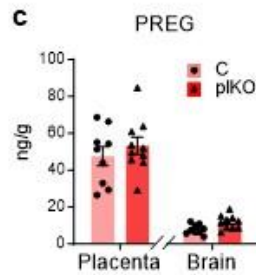
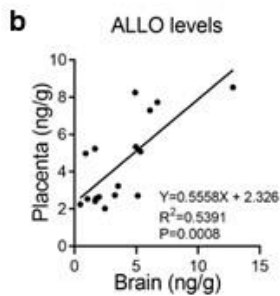
280. Bénardais, K., et al., *Long-term impact of neonatal inflammation on demyelination and remyelination in the central nervous system*. *Glia*, 2014. **62**(10): p. 1659-1670.
281. VanRyzin, J.W., et al., *Microglial phagocytosis of newborn cells is induced by endocannabinoids and sculpts sex differences in juvenile rat social play*. *Neuron*, 2019. **102**(2): p. 435-449. e6.
282. Lehrman, E.K., et al., *CD47 Protects Synapses from Excess Microglia-Mediated Pruning during Development*. *Neuron*, 2018. **100**(1): p. 120-134.e6.
283. Hines, J.H., et al., *Neuronal activity biases axon selection for myelination in vivo*. *Nature neuroscience*, 2015. **18**(5): p. 683-689.
284. Mensch, S., et al., *Synaptic vesicle release regulates myelin sheath number of individual oligodendrocytes in vivo*. *Nature neuroscience*, 2015. **18**(5): p. 628-630.

# Appendix A: Chemical validation of the pIKO model by mass spectrometry

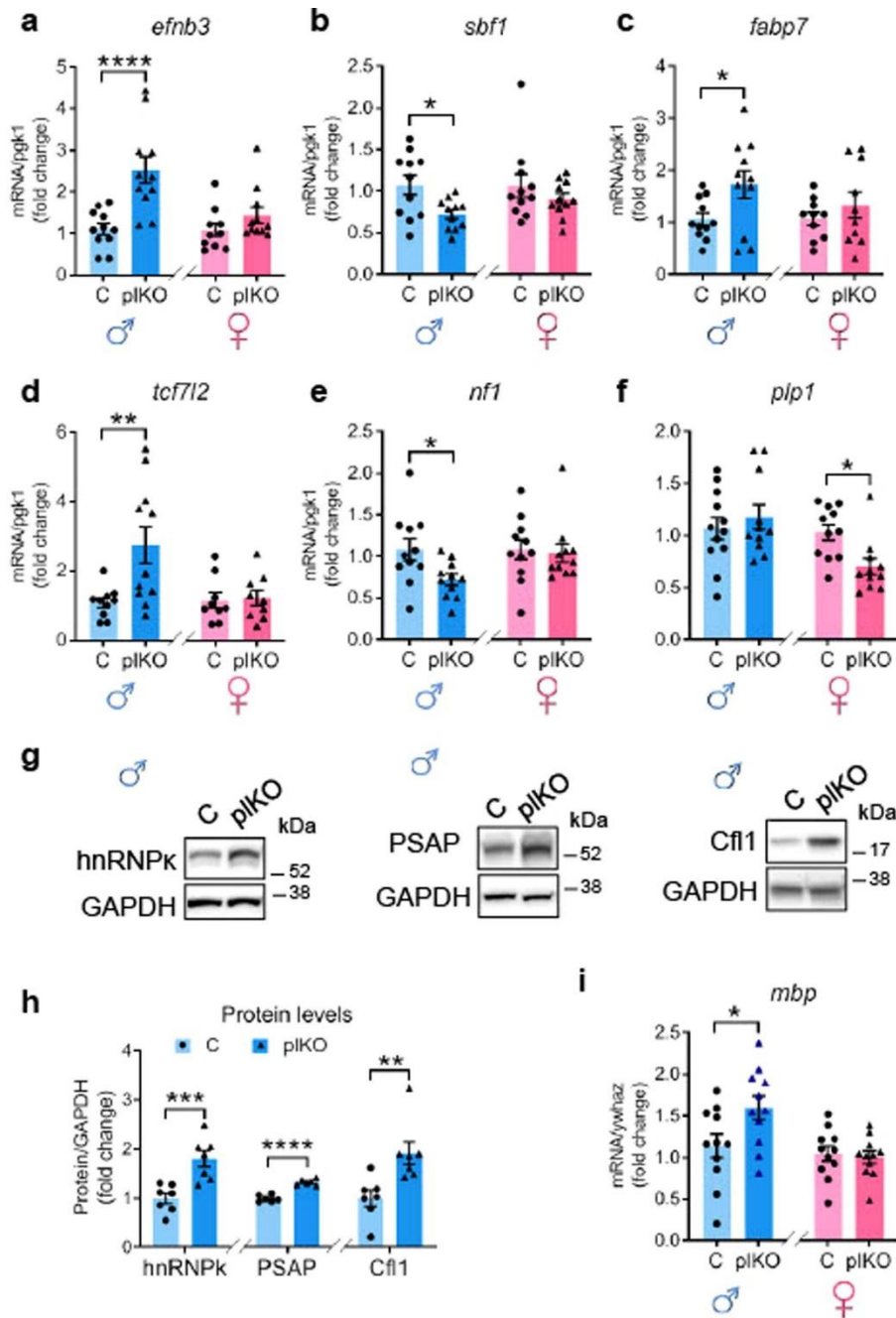
a, Table of placental steroid levels and subsequent p values. b, Linear regression of ALLO levels in placenta and brain, all sexes and genotypes included. ALLO levels in placenta and brain show a positive correlation ( $p = 0.0008$ ;  $n = 18$ ). c-g, Mass spectrometry data in placenta and brain at E17.5. Data is presented as means  $\pm$  SEM ( $n = 9$  C and 10 pIKO). Two-way ANOVA with Sidak's multiple comparison test. Sex mixed as no sex effect was evidenced. ALLO, allopregnanolone; EPIALLO, epiallopregnanolone; PREG, pregnenolone; PROG, progesterone; ALLOTHDOC, allotetrahydrodeoxycorticosterone.

**a**

Embryonic day Placental steroid (ng/g)	C		pIKO		Genotype effect: p value	Sex effect p value
	Males	Females	Males	Females		
<b>E12.5</b>						
FREG	124.04±12.86	175.72±10.08	133.62±28.3	164.94±32.96	0.9796	0.0827
PROG	17.24±3.84	25.9±15.48	9.87±1.43	14.68±3.18	0.2717	0.4213
ALLO	22.51±1.95	21.47±4.3	14.68±2.72	13.87±2.09	<b>0.0176</b>	0.7546
EPIALLO	15.23±2.73	18.58±7.11	12.61±1.33	14.39±1.22	0.3968	0.5212
ALLOTHDOC	0.31±0.03	0.32±0.04	0.26±0.07	0.29±0.06	0.4351	0.6805
Androstenediol	0.52±0.15	0.92±0.25	0.45±0.15	0.47±0.17	0.1869	0.2832
ALLO/FROG (ratio)	1.51±0.25	1.89±0.58	1.59±0.28	1.13±0.26	0.37	0.9172
ALLOTHDOC/FROG (ratio)	0.023±0.008	0.035±0.013	0.0283±0.005	0.023±0.006	0.5621	0.5587
<b>E14.5</b>						
FREG	62.21±10.36	77.99±3.05	55.95±12.69	60.81±4.19	0.1914	0.2471
PROG	4.15±0.93	4.28±0.39	5.1±0.44	4.97±0.51	0.1958	>0.9999
ALLO	15.62±3.89	13.9±0.36	<b>6.99±0.91<sup>***</sup></b>	<b>7.15±0.65<sup>***</sup></b>	<b>0.0008</b>	0.8889
EPIALLO	3.99±0.98	3.6±0.2	3.6±0.42	3.70±0.53	0.8147	0.8173
ALLOTHDOC	0.41±0.06	0.37±0.03	<b>0.17±0.01<sup>***</sup></b>	<b>0.2±0.03<sup>**</sup></b>	<b>&lt;0.0001</b>	0.8444
Androstenediol	0.56±0.18	0.56±0.11	0.32±0.26	0.5±0.13	0.4167	0.6512
ALLO/FROG (ratio)	3.82±0.73	3.37±0.34	<b>1.38±0.16<sup>***</sup></b>	<b>1.49±0.19<sup>**</sup></b>	<b>0.0001</b>	0.8887
ALLOTHDOC/FROG (ratio)	0.112±0.022	0.089±0.013	<b>0.035±0.004<sup>***</sup></b>	<b>0.041±0.004<sup>**</sup></b>	<b>0.0002</b>	0.5791
<b>E17.5</b>						
FREG	48.95±6.91	45.93±7.8.9	52.66±3.14	53.74±9.28	0.4457	0.8966
PROG	3.07±0.21	2.73±0.43	3.47±0.33	3.64±0.35	0.0651	0.7906
ALLO	6.53±1.06	5.2±1.5	<b>3.44±0.69<sup>**</sup></b>	3.72±0.62	<b>0.0331</b>	0.5977
EPIALLO	2.35±0.17	1.92±0.33	2.66±0.22	2.29±0.25	0.188	0.1074
ALLOTHDOC	0.66±0.15	0.43±0.11	0.48±0.03	0.36±0.04	0.2388	0.0947
Androstenediol	0.16±0.03	0.08±0.03	0.11±0.03	0.07±0.01	0.3712	0.0732
ALLO/FROG (ratio)	2.16±0.39	1.82±0.33	<b>0.98±0.16<sup>***</sup></b>	1.07±0.23	<b>0.0048</b>	0.6735
ALLOTHDOC/FROG (ratio)	0.218±0.054	0.197±0.065	0.144±0.013	0.103±0.017	0.0939	0.527



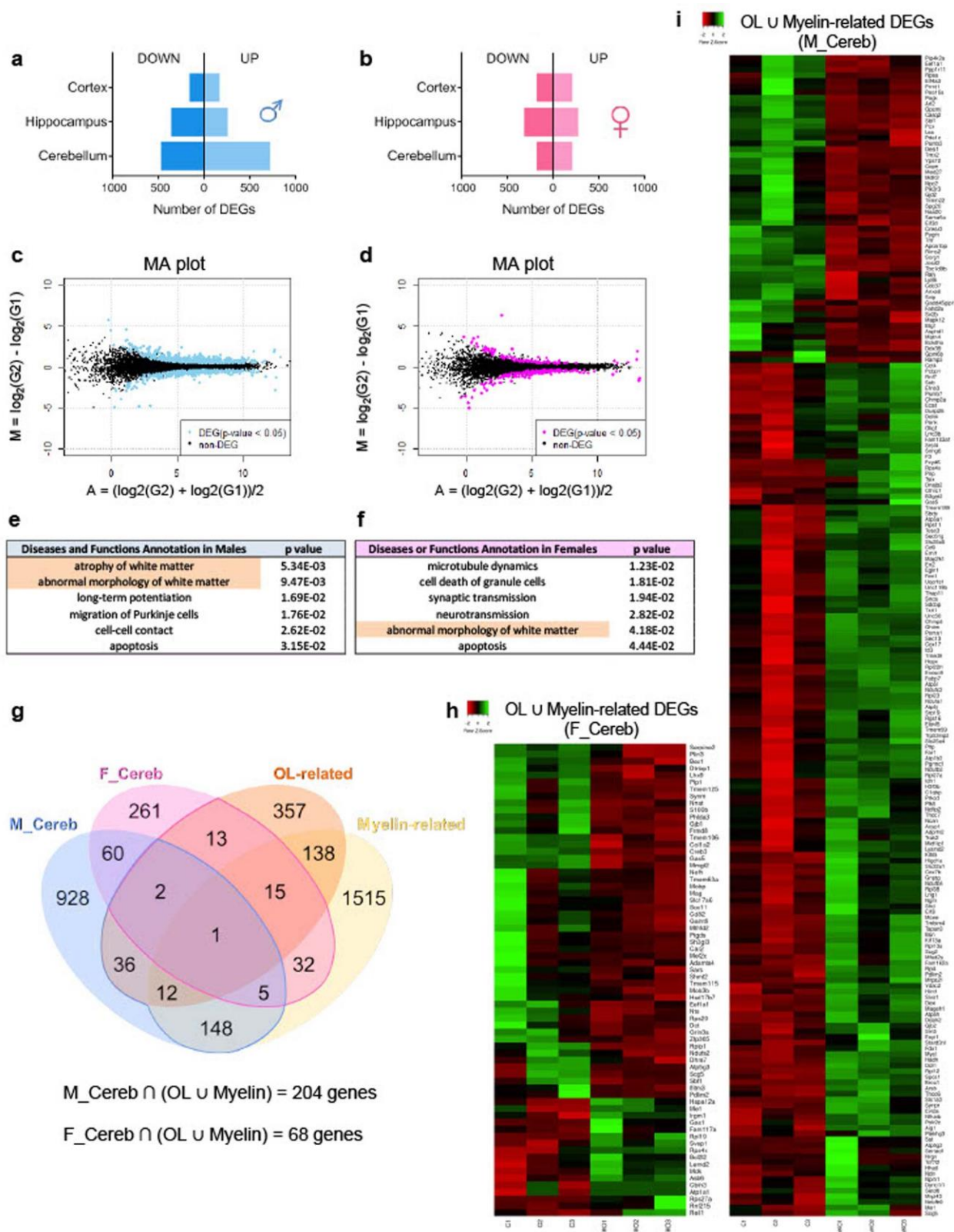
## Appendix B: Molecular validation of the RNA sequencing cutoffs.



Changes in mRNA (a-f) or protein (g-h) contents of selected cerebellar dysregulated genes after normalization. a, *efnb3*, ephrinB3 (RNAseq rank #26/1192 in males; up-regulated;  $q = 0.018$ ;  $p = 3.41E-05$ ). b, *sbf1*, SET Binding Factor 1 (RNAseq rank #82/1192 in males; down-regulated;  $q = 0.067$ ;  $p = 0.00039$ ). c, *fabp7*, Fatty Acid Binding Protein 7 (RNAseq rank #84/1192 in males; up-regulated;  $q = 0.0725$ ;  $p = 0.00043$ ). d, *tcf7l2*, transcription factor 7 like 2 (RNAseq rank #795/1192; up-regulated;  $q = 0.514$ ;  $p = 0.029$ ). e, *nf1*, Neurofibromin 1 (RNAseq rank #1189/1192

in males; down-regulated;  $q = 0.59$ ;  $p = 0.0499$ ). f, plp1, Proteolipid Protein 1 (RNAseq rank #64/389 in females; down-regulated;  $q = 1$ ;  $p = 0.0054$ ). Normalized qRT-PCR data (to pgk1) is presented as mean fold changes  $\pm$  SEM,  $n = 10$  samples/group.). Two-way ANOVA with Sidak's multiple comparison test (a-f). \* $p < 0.05$ , \*\* $p < 0.01$ , \*\*\*\* $p < 0.0001$ . g-h, Cerebellum protein contents determined by Western blot in males, and normalized to GAPDH levels. hnRNP $\kappa$ /Cfl1:  $n = 7$  C and 7 pIKO; PSAP:  $n = 6$  C and 6 pIKO. Multiple unpaired t tests with Holm-Sidak multiple comparison test (\*\* $p < 0.01$ , \*\*\* $p < 0.005$ , \*\*\*\* $p < 0.0001$ ). PSAP, prosaposin (RNAseq rank #950/1192 in males; up-regulated;  $q = 0.5329$ ;  $p = 0.0359$ ). Cfl1, cofilin-1 (RNAseq rank #27/1192 in males; up-regulated;  $q = 0.0192$ ;  $p = 4.03E-05$ ). hnRNP $\kappa$ , heterogeneous nuclear ribonucleoprotein  $\kappa$  (rank #787; up-regulated;  $q = 0.509$ ;  $p = 0.0284$ ). i, mbp, myelin basic protein. Normalized qRT-PCR data (to ywhaz, Tyrosine 3-Monooxygenase/Tryptophan 5-Monooxygenase Activation Protein Zeta). Two-way ANOVA with Sidak's multiple comparison test ( $n = 11$  C and 11 pIKO; \* $p < 0.05$ ). See Extended Data Table 1 sheets 1 and 2 for list of ranked DEGs.

**Appendix C: Long-term impact of placental ALLO insufficiency on  
brain transcriptome: highlight on the myelin-associated genes in the  
cerebellum**



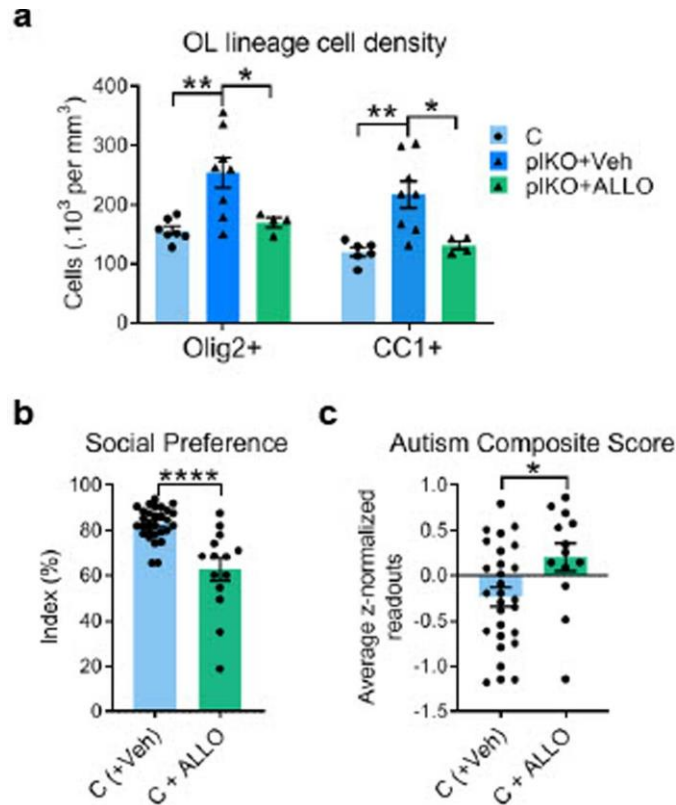
a-b, Number of differentially expressed genes (DEGs) that are up- or down-regulated in the cerebral cortex, hippocampus and cerebellum of pIKO vs C mice at P30 in males (blue) and

females (pink). The majority of DEGs were found in the male cerebellum. c-d, MA plots for the cerebellar RNAseq analysis of pIKO vs C mice at P30. M, log ratio; A, mean average. DEGs are represented as colored dots (blue for males and pink for females). e-f, Top significant diseases and functions IPA annotations. g, Venn diagrams showing the overlaps between cerebellar DEGs in the pIKO males (M\_Cereb) and females (F\_Cereb), and oligodendrocyte (OL) and myelin transcriptomes. [213, 214]h-i, Heatmaps of OL-and myelin-related cerebellar DEGs in C and pIKO samples. Genes and samples were hierarchically clustered based on Pearson distance of z-score data and average linkage. n = 3 independent samples/group [218, 219]

## Appendix D: Appendix D: List of Donors

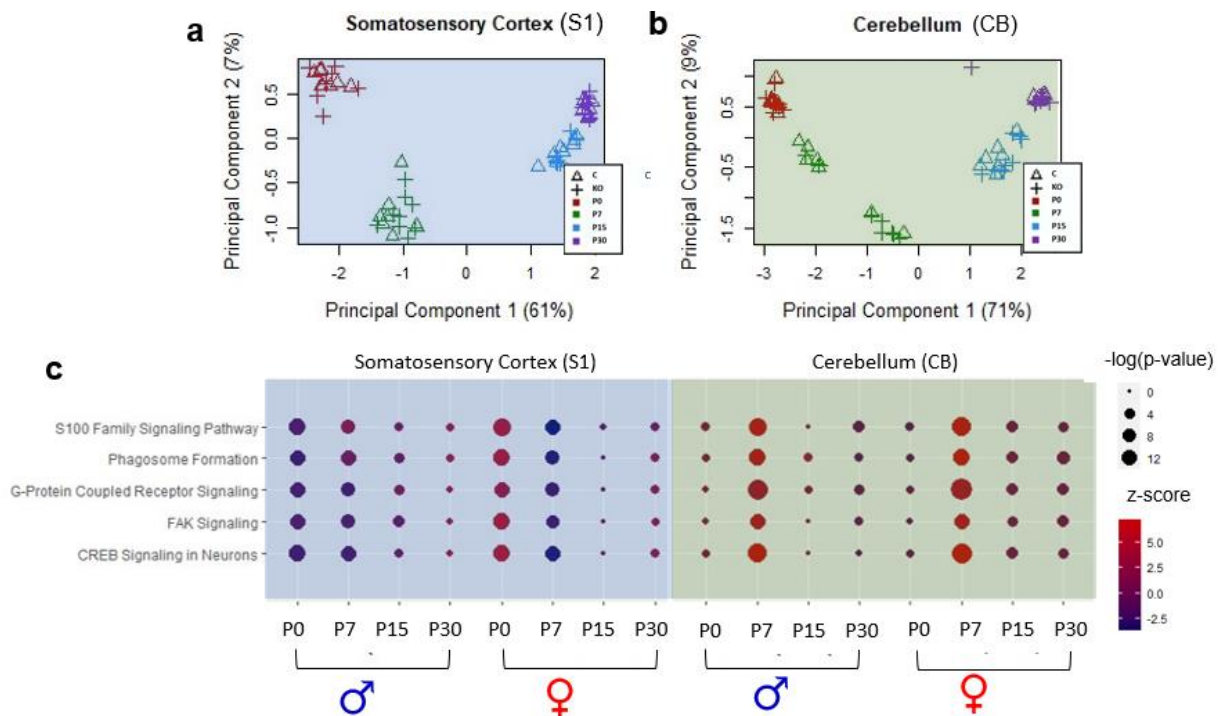
UMBN	Group	Sex	GA at birth (wks)	Age at death (d)	Age at death (wks)	Corrected age (wks)	PMI	RIN	Brain weight (g)	Race	Cause of Death
1325	Preterm	F	25	182	26.0	11.0	18	-	-	-	Sudden Unexplained Death in Infancy
1487	Preterm	F	29	64	9.1	-1.9	24	-	-	Black	Prematurity with complications
4353	Term	M	40	34	4.9	4.9	5	9	-	Black	Probable overlay
4355	Term	M	38	81	11.6	9.6	22	8.2	633	Caucasian	SUID, Prone Sleep position and excessive bedding
4364	Preterm	M	27	145	20.7	7.7	23	7.6	-	-	Prematurity, Pneumonia
4373	Preterm	F	34	100	14.3	8.3	13	7.2	570	Caucasian	Methicillin susceptible Staphylococcus
4375	Term	F	40	2	0.3	0.3	26	8.9	400	Caucasian	Positional asphyxia
4381	Term	F	40	91	13.0	13.0	18	6.9	680	-	Probable Asphyxia
4383	Term	F	40	76	10.9	10.9	8	8	625	Black	Probable overlay
4389	Preterm	F	34	79	11.3	5.3	27	8.5	516	Black	Positional Asphyxia
4391	Term	M	40	27	3.9	3.9	13	9.5	450	Caucasian	Asphyxia due to co-sleeping
4400	Term	M	40	86	12.3	12.3	13	7.5	602	Caucasian	Positional Asphyxia
4402	Term	M	39	66	9.4	8.4		6.7	555	Black	Co-Sleeping
4412	Term	M	40	66	9.4	9.4	21	-	684	Black	Sudden Unexplained Infant Death
4414	Term	F	37	38	5.4	2.4	5	8.2	456	Caucasian	Sudden Unexpected Infant Death with Co-sleeping
4416	Preterm	F	26	142	20.3	6.3	27	3.1	-	-	Asphyxia, Prematurity
4417	Preterm	M	28	71	10.1	-1.9	45	8.5	392	Black	Undetermined, Hepatic Stenosis, Prematurity
4420	Term	M	40	63	9.0	9.0	36	8.9	550	Caucasian	Positional asphyxia
5658	Term	M	38	41	5.9	3.9	32	-	550	-	Sudden Unexplained Death in Infancy
5708	Preterm	F	29	156	22.3	11.3	31	-	-	-	Viral syndrome with focal acute pneumonia
5716	Preterm	M	29	96	13.7	2.7	27	-	-	-	Sudden Unexplained Death in Infancy
5754	Preterm	M	33	149	21.3	14.3	13	4.6	-	-	Sudden Unexplained Death in Infancy
5843	Preterm	M	34	99	14.1	8.1	33	8.3	-	-	Unknown
5886	Term	M	40	46	6.6	6.6	27	8.9	590	Black	Sudden Unexplained Death in Infancy

## Appendix E: Cerebellar WM and behavioral impairments in male pIKO mice can be prevented by pharmacological treatments at E15.5.



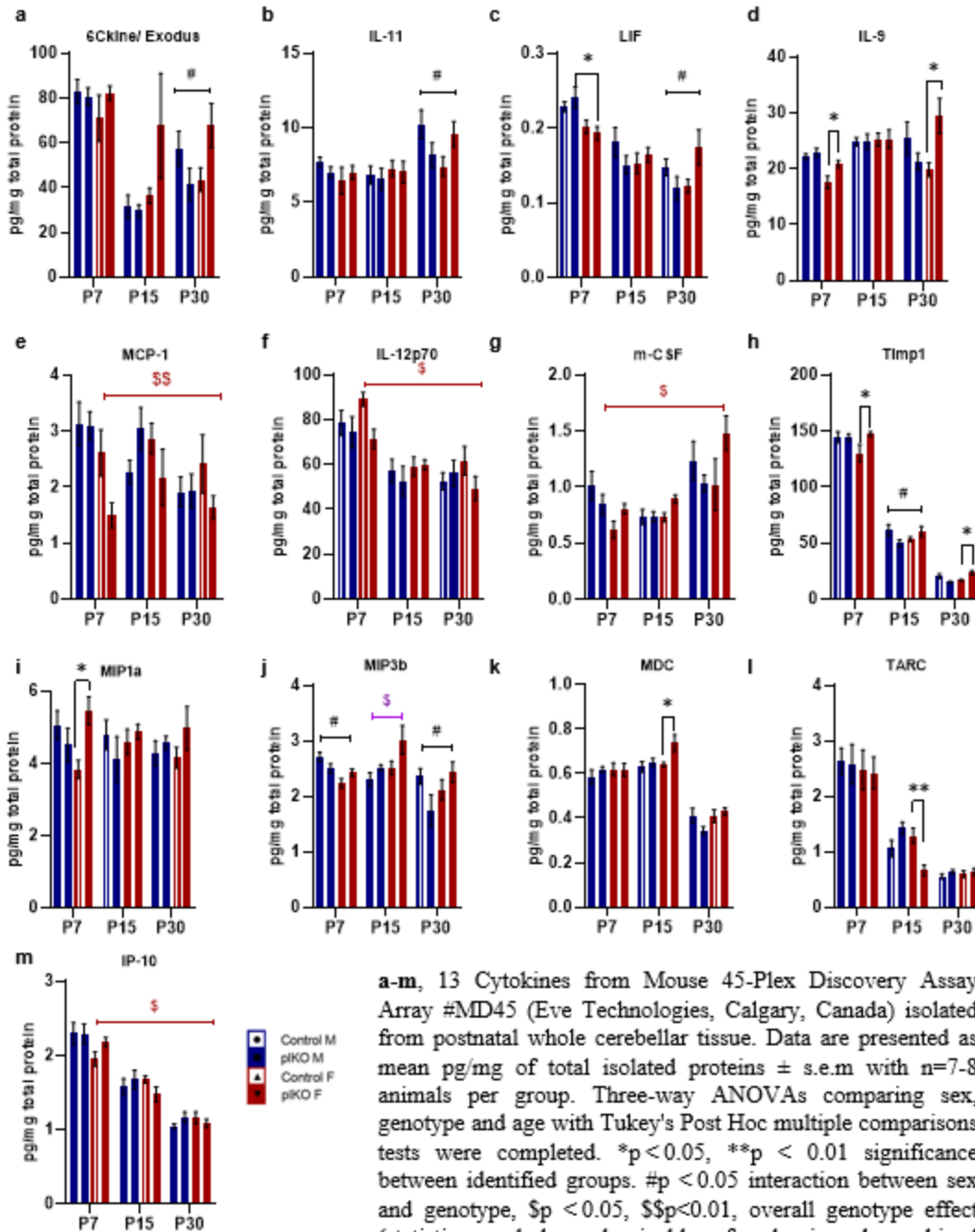
a, Quantification of Olig2+ and CC1+ cell densities in the male cerebellar WM (n = 7 C, 8 pIKO+Veh and 4 pIKO+ALLO). Data presented as means  $\pm$  SEM. Two-way ANOVA with Sidak's multiple comparisons test (\* $p < 0.05$ ; \*\* $p < 0.01$ ). Olig2+ = C vs pIKO+Veh:  $p = 0.0024$ ; C vs pIKO+ALLO:  $p = 0.9982$ ; pIKO+Veh vs pIKO+ALLO:  $p = 0.041$ . CC1+ : C vs pIKO+Veh:  $p = 0.0014$ ; C vs pIKO+ALLO:  $p = 0.9995$ ; pIKO+Veh vs pIKO+ALLO:  $p = 0.0354$ . b, 3-chamber sociability test. Data is presented as means  $\pm$  SEM. Two-tailed unpaired Student's t test with Welch's correction (\*\*\*\* $p < 0.001$ ). n = 29 C(+Veh) and 14 C + ALLO ( $p < 0.0001$ ). c, ASD composite severity score. Data presented as means  $\pm$  SEM. Two-tailed unpaired Student's t test with Welch's correction (\* $p < 0.05$ ). n = 28 C(+Veh) and 13 C + ALLO ( $p = 0.0261$ ).

## Appendix F: The plKO brain transcriptome landscape shows dysregulated inflammation-related pathways across postnatal development



**a-b**, Principal component analysis for postnatal RNAseq analysis in the somatosensory cortex (s1) and cerebellum at P0 (red), P7 (green), P15(blue), and P30 (purple). **c**, Top canonical pathways from IPA comparison analysis of all regions organized by z-score and  $-\log(p\text{-value})$ . n=4 independent samples per group.

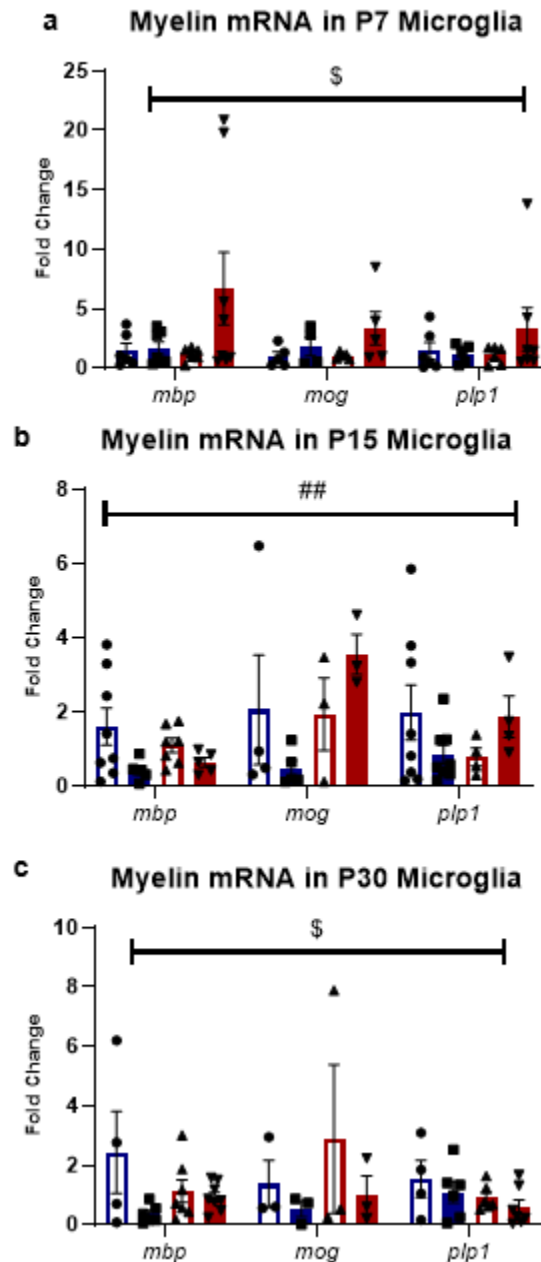
**Appendix G: pIKO cytokine panels show sex-specific developmental trajectories**



**a-m**, 13 Cytokines from Mouse 45-Plex Discovery Assay Array #MD45 (Eve Technologies, Calgary, Canada) isolated from postnatal whole cerebellar tissue. Data are presented as mean pg/mg of total isolated proteins  $\pm$  s.e.m with  $n=7-8$  animals per group. Three-way ANOVAs comparing sex, genotype and age with Tukey's Post Hoc multiple comparisons tests were completed. \* $p < 0.05$ , \*\* $p < 0.01$  significance between identified groups. # $p < 0.05$  interaction between sex and genotype, \$ $p < 0.05$ , \$\$ $p < 0.01$ , overall genotype effect (statistics symbols: males in blue, females in red, combined sexes in purple).

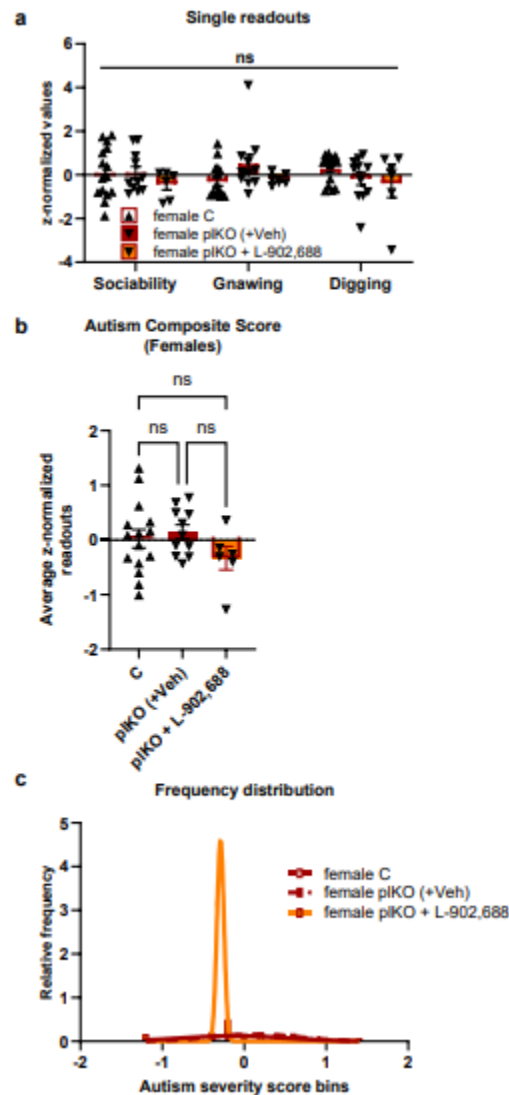


**Appendix I: The contents in myelin-enriched transcripts are altered  
in the plKO microglia in a sex-linked manner.**



**a-c**, RT-qPCR data for myelin-related mRNA (*mbp*, *mog*, *plp1*) in sorted microglia at P7 (a), P15 (b), and P30 (c). Data are presented as mean fold change  $\pm$  s.e.m. Three-way ANOVAs were completed with Tukey's Post Hoc multiple comparisons tests.  $n=5-10$  independent samples per group, \$ $p < 0.05$  genotype effect, ## $p < 0.01$  interaction between genotype and sex.

## Appendix J: EP4 agonist treatment does not alter female behaviors



a, z-standardized single significant behavior readouts that are integrated into the autism composite score in females at P30 following 6-day injection series of PGE2 agonist, L-902688 (1 mg/kg/day; s.c.). Data are presented as mean  $\pm$  s.e.m. Two-way ANOVA with Tukey multiple comparison tests. b, ASD composite severity score in females at P30 following 6-day injection series of PGE2 agonist, L-902688 (1 mg/kg/day; s.c.). Data are presented as mean  $\pm$  s.e.m. Two-way ANOVA with Sidak's multiple comparison tests. c, Relative frequency distribution of autism composite score bins at P30 following 6-day injection series of PGE2 agonist, L-902688 (1 mg/kg/day; s.c.). Data are presented as mean  $\pm$  s.e.m. In group "pIKO (+Veh)", mixed populations from non-injected and saline-injected animals are pooled as they show no

significant behavioral differences. Control and plKO group scores were published in Vacher, et al. 2021. n=6-15 animals per group.